

UNIVERSITY OF CALIFORNIA
IRVINE

Dissolution or Growth of Soluble Spherical Oscillating Bubbles

by

Marios Miki Fyrillas

A dissertation submitted in partial fulfillment of the requirements for the degree of

Doctor of Philosophy

in

Engineering

Dissertation Committee:

Professor Andrew J. Szeri, Chair

Professor Donald K. Edwards

Professor Dimitri Papamoschou

Professor Edriss Titi

2006

The dissertation of Marios Miki Fyrillas is approved,
and is acceptable in quality and form for
publication on microfilm:

Committee Chair

University of California, Irvine

2006

To my Country,
and to my Family.

Everything should be made as simple as possible, but not simpler.

– Albert Einstein

Ἄνδρῶν ἐπιφανῶν, πᾶσα γῆ τάφος.

– Θουκυδίδης

Contents

List of Figures	vi
Nomenclature	vii
Acknowledgements	ix
Curriculum Vitae	xi
Abstract	xiii
Chapter 1 Introduction	1
1.1 Literature Review	1
1.2 Bubble dynamics	7
1.3 Organization of Thesis	9
Chapter 2 Classical Problem of Rectified Diffusion	10
2.1 Formulation	10
2.1.1 Lagrangian formulation	13
2.1.2 Splitting of the problem	14
2.2 The oscillatory problem	17
2.3 The smooth problem	20
2.4 Comparison with previous formulations	24
2.5 Numerical results	25
2.5.1 Nonlinear bubble dynamics	27
2.5.2 Threshold criterion	28
2.5.3 Rate of growth of bubbles away from threshold conditions	31
2.6 Conclusions	34
Chapter 3 Effect of Surfactants on Bubble Growth Rates	36
3.1 Formulation	36
3.2 Oscillatory problem	38
3.2.1 Zeroth order oscillatory problem	40
3.2.2 First order oscillatory problem	41
3.3 The smooth problem	42
3.4 Effect of surfactants on a still bubble	45
3.5 Interfacial Resistance	45
3.6 Theoretical predictions of bubble growth rates	47
3.7 Conclusions	57

Chapter 4	Surfactant Transport Problem	59
4.1	Formulation	59
4.2	Analysis	62
4.2.1	Oscillatory Problem	63
4.2.2	Smooth Problem	64
4.2.3	Surface Excess	65
4.3	Results and Discussion	67
4.3.1	A still vs an oscillating bubble	67
4.3.2	Equation of State	70
4.3.3	Bubble growth rates	71
4.4	Conclusions	71
Chapter 5	Conclusions	73
5.1	Summary of Work	73
5.2	Future Work	75
References		77
Appendix A	Transients in the oscillatory problem	81
Appendix B	Transients in the smooth problem	83
Appendix C	Polytropic vs non-polytropic bubble models	85
Appendix D	Splitting	91
Appendix E	Expansions for G and Ψ_e	93

List of Figures

2.1	The asymptotic concentration profile for the oscillatory problem.	19
2.2	The gradient of the concentration field on the bubble surface and the boundary condition for the concentration field versus the nonlinear time $\hat{\tau}$	20
2.3	The asymptotic concentration profile for the smooth problem.	23
2.4	The ratio of the threshold pressure amplitude for rectified diffusion to the steady part of the background pressure versus equilibrium bubble radius.	29
2.5	The ratio of the threshold pressure amplitude for rectified diffusion to the steady part of the background pressure versus equilibrium bubble radius for different far-field concentrations of gas in the liquid.	29
2.6	The rate of bubble growth in μm per minute versus equilibrium bubble radius in μm	31
2.7	A bifurcation diagram or response curve. On the vertical axis, as a measure of the solution, we take the maximum bubble radius in μm over the period of oscillation.	32
2.8	Time traces of the bubble response at various points along the branch indicated in figure 2.7.	33
3.1	Interfacial resistance versus surfactant surface concentration.	48
3.2	The rate of bubble growth versus dimensionless pressure amplitude for a bubble of radius $20 \mu\text{m}$	52
3.3	The rate of bubble growth versus dimensionless pressure amplitude for a bubble of radius $40 \mu\text{m}$	53
3.4	The rate of bubble growth versus dimensionless pressure amplitude for a a bubble of radius $60 \mu\text{m}$	54
3.5	The effect of the initial concentration of surfactants on bubble growth rates.	55
3.6	The rate of bubble growth versus the exponent α	56
3.7	The term $x^2 R_I - \langle x^2 R_I \rangle_{\hat{\tau}}$ versus time for two different values of the exponent α	56
4.1	The dimensionless excess amount of surfactant versus dimensionless concentration at infinity for a bubble of radius $20 \mu\text{m}$	69
C.1	A plot of the ratio of the threshold pressure amplitude for rectified diffusion to the steady part of the background pressure versus equilibrium bubble radius.	86
C.2	The rate of bubble growth versus equilibrium bubble radius.	87
C.3	An expanded view of the bifurcation diagram of figure 2.7.	88

Nomenclature

Roman Symbols

a	Initial bubble radius.
A	Parameter that measures the non-ideality of the interface.
A_f	Affinity of surfactant.
C	$\tilde{C} - C_\infty$.
\tilde{C}	Mass fraction of gas dissolved in the liquid.
C_∞	Mass fraction of gas at infinity.
C_{sb}	p_{Gi}/k .
D	Diffusivity of the gas in the liquid.
D_s	Diffusivity of the surfactant in the liquid.
k	Henry's constant.
k_i	Forward rate constant in the kinetic rate expression.
K_a	Adsorption coefficient.
m_G	Mass of the gas in the bubble.
M	Molecular weight of the gas.
p_G	Partial pressure of the gas in the liquid.
p_{Gi}	Initial pressure of the gas in the bubble.
p_s	Pressure in the liquid.
p_v	Vapor pressure in the bubble.
\mathcal{P}	Péclet number for the gas transport problem.
\mathcal{P}_f	Péclet number for the surfactant transport problem.
r	Radial coordinate.
R	Bubble radius (function of time).
R_G	Universal gas constant.
\tilde{R}_I	Interfacial resistance.
R_I	Dimensionless interfacial resistance.
Re	Reynold's number.
s	Stretched lagrangian coordinate.
t	Time.
T	Period of bubble oscillation.
T_∞	Temperature of the fluid.
We	Weber number.
x	Dimensionless bubble radius (function of time).
x_{min}	Value of x at the minimum.

Greek Symbols

γ	Interfacial tension.
η	Polytropic exponent.
λ	Long time scale.
μ	Viscosity of the liquid.
ξ	Dimensionless radial coordinate.
ρ	Density of the liquid.
ρ	Mass of surfactant per unit volume.
ρ_∞	Concentration of surfactant at infinity.
ρ^s	Surface-excess mass density of the surfactant.
ρ_∞^s	Surface-excess saturation density.
σ	Lagrangian coordinate.
τ	Dimensionless time.
$\hat{\tau}$	Nonlinear time.
Ψ	Dimensionless surfactant bulk concentration.
Ψ^s	Dimensionless surfactant surface concentration.
Ω_0	Natural frequency of bubble oscillations.

Diacritics

–	Asymptotic limit in time.
---	---------------------------

Brackets

$\langle f(\tau) \rangle_\tau$	Average of f with respect to the time τ over one period of bubble oscillation.
$\langle f(\hat{\tau}) \rangle_{\hat{\tau}}$	Average of f with respect to the time $\hat{\tau}$ over one period of bubble oscillation.

Superscripts

0	Zeroth order quantity.
1	First order quantity.
*	Dimensionless quantity.

Subscripts

<i>osc</i>	Oscillatory.
<i>sm</i>	Smooth.

Acknowledgements

“The reason I have seen as far as I did, is because I stood on the shoulders of Giants”. For Newton, those Giants were Kepler and Copernicus. In my case they were, my advisor, Professor Andrew Szeri, and my Parents. Their guidance and trust helped me develop both as a researcher and a man.

I would like to extend my appreciation to the members of my committee, Professors Donald K. Edwards, Dimitri Papamoscou and Edriss Titi, for their participation and contribution to this work. Their comments led to greater insight in the mathematics and physics of my work.

In my years of study I realized that common sense leads to ingenuity. Since “Common sense is the collection of prejudices acquired by age eighteen”, I would like to extend a special thanks to my elementary and high school teachers (Mr. Papantoniou, Mr. Papavasilis, Mr. Pashias, Mr. Constantinidis, Mr. Charitou and more) who always made sure that I was thinking harder than what I thought I could.

I have been extremely fortunate to share offices with some intelligent and knowledgeable people. I would like to thank Jean-Pierre, Albino, David, Vi, Ryan, and Perry, who were ready to provide me with help, whenever I needed it. I would like to extend a very special thanks to a very special friend and colleague, Kiko Nomura. She brought “Turbulence” and “Chaos” in my life, and her “pasta” problem provided me with “food” for thought.

“A picture is one thousand words”, and an equation is one thousand pictures. I would like to thank Professor Titi and his group, especially Shandy, Shannon and Hung, who provided me with stimulation and challenge the last two years through the applied mathematics classes and seminars.

I would like to thank the Greek and Greek-Cypriot community of Irvine for helping me forget about school when I was away from school, even if I did not want to. A special thanks to Costas, whose guidance helped me out in a lot of difficult occasions. The Costas I am talking about knows who he is! The other twelve were a pain in the neck! A “special” thanks to my friends back home, especially my cousin Maria, who made sure that I did not do any research during the summer.

I gratefully acknowledge the support I received from the Office of Naval Research and the Mechanical and Aerospace Engineering department. Money makes the world go round ... and bubbles grow.

Finally, I would like to thank my Family for supporting and believing in me in every occasion and at all costs. My Brother, who is a great guy; my Father, who had he had the opportunity would have been a great scientist; my Grandmother, whose wish was for her grandson to become a “Doctor”; and my Mother, whose love, strength, energy, and stubbornness, made me who I am.

Curriculum Vitae

Education

9/87-6/90 B.S. Mechanical Engineering
Imperial College - London, England

9/90-12/91 M.S. Mechanical Engineering
University of California - Irvine, Irvine, CA

Research Experience

9/90-12/91 Department of Mechanical and Aerospace Engineering,
University of California - Irvine, Irvine, CA
Advisor: Prof. R. Rangel
Topic: Kelvin-Helmholtz instability.

12/91-9/92 Department of Civil Engineering,
University of California - Irvine, Irvine, CA
Advisor: Prof. C. Chrysikopoulos
Topic: Mass transport through porous media.

9/92-present Department of Mechanical and Aerospace Engineering,
University of California - Irvine, Irvine, CA
Advisor: Prof. A. Szeri
Topic: Mass transfer across dynamic interfaces.

Teaching Experience

9/89-12/93 University of California - Irvine, Irvine, CA
Classes: Introduction to Thermodynamics (ME91),
Introduction to Fluid Dynamics (ME130A),
Heat Transfer (ME120),
Numerical Methods (ME185),
Engineering Analysis (ME200B).

Publications

1. C. V. CHRYSIKOPOULOS, E. A. VOUDRIAS AND M. M. FYRILLAS 1994 Modeling of contaminant transport resulting from dissolution of nonaqueous phase liquid pools in saturated porous media *Transport in Porous Media* **16**, 125-145.
2. M. M. FYRILLAS AND A. J. SZERI 1994 Dissolution or growth of soluble, spherical, oscillating bubbles *Journal of Fluid Mechanics* **277**, 381-407.
3. M. M. FYRILLAS AND A. J. SZERI 1995 Dissolution or growth of soluble, spherical, oscillating bubbles: the effect of surfactants *Journal of Fluid Mechanics* **289**, 295-314.

Conferences

1. Conference Presentation: The battle between convection and diffusion associated with dissolving, oscillating bubbles *9th Annual University of California Conference on Nonlinear Science* UCLA, February 20-21, 1993.
2. Conference Presentation: Dissolution or growth of soluble, spherical, oscillating bubbles *46th Annual Meeting of the Division of Fluid Dynamics of the American Physical Society* Albuquerque, November 21-23, 1993.
3. Conference Presentation: Dissolution or growth of soluble, spherical, oscillating bubbles. The effect of surfactants *47th Annual Meeting of the Division of Fluid Dynamics of the American Physical Society* Atlanta, November 20-22, 1994.

Abstract of the Dissertation

Dissolution or Growth of Soluble Spherical Oscillating Bubbles

by

Marios Miki Fyrillas

Doctor of Philosophy in Engineering

University of California, Irvine, 2006

Professor Andrew J. Szeri

The gas and surfactant transport associated with an oscillating gas bubble embedded in an infinite liquid is studied theoretically by taking advantage of the large Péclet number (\mathcal{P}) characterizing these problems. Furthermore, expressions obtained for the bubble growth rates are then compared with experimental results and observations.

For the gas transport problem two cases are considered which differ in the boundary condition on the bubble surface: (i) the case of a clean bubble where the concentration on the bubble surface is related to the bubble internal pressure by Henry's law, and (ii) the case of a bubble contaminated with surfactants where a mass flux boundary condition is used. In both cases, it is the dissolved gas transport in the liquid that is the rate-limiting step. The convection-diffusion equation governing transport of dissolved gas in the liquid is written in Lagrangian coordinates to account for the moving domain. The boundary condition is split into a constant and an oscillating part, yielding the *smooth* and the *oscillatory* problems which are treated using singular perturbation techniques. To leading order, the clean and the surfactant-covered surface problems give the same result. Continuing to higher order it is shown that the latter depends on $R_I \mathcal{P}^{-1/2}$, where R_I is the (dimensionless) interfacial resistance associated with the presence of surfactants. Owing to the fact that the magnitude of R_I is approximately the same as the magnitude of $\mathcal{P}^{1/2}$ at conditions of practical interest,

surfactants are shown to have a very significant effect on bubble growth rates, which agrees with experimental observations by Crum [12, 13]. Depending on the relationship between the interfacial resistance and surface concentration, surfactants might favor or inhibit bubble growth rates.

The surfactant transport problem is treated in a similar way. We were able to obtain expressions for: (i) the dynamic surface concentration of surfactant and (ii) the surface equation of state, asymptotically in time. The surfactant is nearly insoluble and the dynamic surface concentration satisfies the corresponding adsorption isotherm in an average sense. For dilute solutions, the excess amount is higher on an oscillating bubble than on a still bubble which agrees with numerical results by Nadim [37]. In contrast, oscillations lower the saturation limit of the interface which is controlled by the minimum bubble radius.

Chapter 1

Introduction

1.1 Literature Review

A bubble that would ordinarily dissolve in a liquid may increase in mass, rather than dissolve, if it undergoes volume oscillations in response to some perturbation. Previous analyses of the problem of the mass transport associated with an oscillating bubble have focused on the phenomenon of rectified diffusion, first identified by Blake [4]. In rectified diffusion, the normal process of dissolution of a gas bubble in a liquid may be reversed by sufficiently intense volume oscillations; hence a bubble which pulsates owing to the influence of an acoustic pressure field may grow if the amplitude of the pressure oscillations exceeds a certain *threshold* value.

In engineering applications, the equations of rectified diffusion were used successfully to investigate the growth of microbubbles in biological media [36], to explain the appearance of gas bubbles in insonified guinea pigs [14], and to predict the bubble growth rate associated with low frequency sonar propagation in the ocean [15]. In these studies, conditions that lead to bubble growth might prove hazardous to humans and marine mammals that are exposed to the sound wave. Rectified diffusion was also used by Apfel [1] in synthesizing cavitation prediction charts for water. More recently, engineers at Westinghouse Hanford were working on developing a sonic agitator that is going to prevent the buildup of hydrogen gases in a nuclear waste storage tank [52].

Past analyses of the mass transport across the dynamic interface associated with a bubble undergoing spherical oscillations have been restricted to infinitesimal radial oscillations of the bubble, or to threshold conditions where there is no net transport, or to both of these limitations. The reason for the restriction to the equilibrium problem of threshold conditions is that it was not known how to formulate the problem for the concentration field away from threshold conditions. The theoretical difficulty hinges on determination of the motion of the net flux of dissolved gas either away from a dissolving bubble or toward a growing bubble. In the latter case the zone of liquid in which the gas concentration is lowered as a consequence of net bubble growth has been referred to as the depletion layer by several authors. An additional challenging problem is to develop a rigorous means by which to deduce the influence of convection associated with the bubble volume oscillations on the diffusion of the net flux of dissolved gas.

A detailed review of the past work in this area and other areas relevant to bubble dynamics was conducted by Plesset & Prosperetti [40].

The phenomenon of rectified diffusion, was first identified by Blake [4], who estimated the net inflow of dissolved gas using a quasi-static solution of the diffusion problem in the liquid. Hsieh & Plesset [27] studied the problem by assuming that the forcing acoustic pressure field, the bubble radius, and the concentration of gas in the liquid at the surface of the bubble all have (small amplitude) sinusoidal dependence on time. Eller & Flynn [20] removed the restriction to small sinusoidal oscillations in favor of a restriction to high frequency oscillations and performed a boundary layer analysis in Lagrangian coordinates first introduced by Plesset & Zwick [41]. This form of approximation is known as the thin diffusion layer approximation; it is uniformly valid in time only at threshold conditions. In other words, no provision is made for net flux of dissolved gas toward or away from the bubble.

In two papers Skinner [46, 47] treated the mass transport problem of an oscillating bubble using an ingenious decomposition of the concentration field. In the first paper, Skinner computed the forcing pressure threshold for rectified diffusion associated with a

bubble undergoing small amplitude sinusoidal radial oscillations. The equilibrium concentration field was computed via a double perturbation scheme that assumed (i) that the oscillations are small, and (ii) that the concentration gradients in the liquid are negligible outside a thin layer.

In the second paper, Skinner studied the problem of mass transport associated with an oscillating bubble away from threshold conditions. Two separate boundary layers in the concentration field near the bubble surface were identified. The first (thinner) layer is associated with the time-dependent concentration of gas in the liquid at the surface of the bubble that arises according to Henry's law. The second (thicker) layer is associated with net flux of dissolved gas in the liquid. The two layers were handled by decomposing the concentration field into two parts. Skinner used the solution for the concentration field to examine the rate of growth of the average radius of a bubble undergoing small amplitude sinusoidal oscillations.

More recently, Crum [11] reports an extension to the threshold theory of Eller & Flynn, and experimental results of bubble growth rates away from threshold that far exceed the theoretical predictions of Eller & Flynn (or related theories). In addition, Crum finds that the addition of surface active material to the bubble has an effect on bubble growth rates that is dramatically greater than can be accounted for by a simple modification of surface tension in the theory. Also observed were significant departures from the theoretical thresholds at super or sub-saturated conditions in the far field.

Crum & Hansen [13] and Church [10] compare the various results for threshold acoustic pressure amplitude for growth of gas bubbles by rectified diffusion. Crum & Hansen generalize the analysis of Eller & Flynn to include more accurate perturbation results for the radial oscillations and damping. Church demonstrates graphically the sensitive dependence of the phenomenon of rectified diffusion on gas concentration in the far field.

Numerical solutions of the convection-diffusion equation for the dissolved gas in the liquid are reported by Kamath & Prosperetti [31]. These authors report that away from saturation conditions, the theory of Eller & Flynn tends to over-predict the threshold driving

pressure amplitude for rectified diffusion, and under-predict the growth rates of bubbles at conditions that exceed threshold.

Finally, another possible approach to this class of problems is represented by the recent work of Fannjiang & Papanicolaou [22] and references therein. These authors develop a general framework for homogenization of convection-diffusion equations valid for small diffusivities and for steady, spatially-periodic flow fields in infinite domains. However, the mass transport problem of interest here includes an unsteady, spatially inhomogeneous (but not spatially-periodic) velocity field and an extremely problematic boundary condition.

In summary, there appears to be an adequate theory for threshold conditions in a saturated liquid, but very little progress has been made on the non-equilibrium problem of nonlinear bubble growth or dissolution away from threshold conditions. The principal practical deficiency of the theory is the under-prediction of bubble growth rates at conditions that exceed threshold, especially for bubbles intentionally contaminated with surface active materials as mentioned in Crum [13, 12]. Even in the absence of consideration of the effects of surfactants, the growth or dissolution of nonlinearly oscillating bubbles has not been addressed owing to the difficulties mentioned above, *i.e.* a rigorous formulation of convection-enhanced diffusion.

In the absence of surfactant contamination, rectified diffusion is a direct consequence of Henry's law which states that the gas concentration on the bubble interface is proportional to the gas pressure inside the bubble. When a bubble undergoing volume oscillations is in the collapsed phase, the internal gas pressure is high –this leads to a flow of gas out of the bubble through the interface. When the bubble is in the expanded phase, the internal pressure is low and the bubble gains gas from the surrounding liquid through the dynamic interface. However, these two phenomena are not in balance due to the changing bubble surface area; bubble growth is favored because in the expanded phase the surface area is much larger and the mass concentration boundary layer is much thinner than in the collapsed phase.

When there is, in addition, interfacial resistance associated with the presence of surfactant, the imbalance that leads to rectified diffusion may be enhanced. Because the surface area of the bubble changes by a large amount over a typical bubble oscillation, the surface concentration of surfactant molecules is highly variable. When the bubble is contracted, and there is a tendency of the bubble to lose gas, the interfacial resistance is high as a consequence of high surface concentration of surfactant. In contrast, the interfacial resistance is low when the bubble is expanded and the tendency is to gain dissolved gas from the surrounding liquid.

Actually, associated with the presence of surfactants at a gas-liquid interface are two effects: (i) most importantly, surfactants present a barrier to mass transport, and (ii) surfactants reduce the surface tension [5], reflected in a minor change in the dynamics of bubble oscillations. Although it is generally accepted that certain monolayers have been shown through experiment to inhibit mass transport through an interface [2], the understanding of this phenomenon is somewhat limited. Theoretical efforts include the work of Whitaker & Pigford [55], who assumed an interface of zero thickness but with finite capacity for the solute and an adsorption/desorption process at the interface. Nguyen Ly, Carbonell & McCoy [39] considered an interfacial region of finite thickness with capacity for the dissolved gases greater than the solubility in water but with much reduced diffusivity. Plevan & Quinn [42] developed an interfacial resistance model which has received some theoretical justification from Borwankar & Wasan [6]. The latter authors do not rule out, however, the validity of the other models. Their justification is the leading order solution to the microscopic equations of mass transport of Brenner & Leal [7].

Experimental determination of interfacial resistance to gas transport is complicated by the need to isolate interfacial resistance from the overall resistance to transport. Thus, the monolayer resistance must be determined by comparison of two measurements; one performed on the system with the monolayer present and one performed on the system without the monolayer. A detailed review of the evaporation of liquids and transport of gases in the presence of monolayers is given by Barnes [2]. There is a paucity of data that relate interfacial resistance to surface concentration of surfactant molecules. One exception

is the work of Caskey & Barlage [8, 9]. In the first paper [8] the authors report results of dynamic surface tension versus surface concentration for several surfactants; in the second paper [9] are the results of interfacial resistance versus surface concentration for the same surfactants. In reporting the predictions of the theory we shall develop, we make use of the interfacial resistances determined by Caskey & Barlage. Using these experimental results we can specify the dependence of the interfacial resistance on the surface concentration of surfactant. Determining an explicit expression for the latter would require solution of the mass transport problem for a surfactant outside a spherically oscillating bubble.

A surfactant molecule consists of a hydrophobic and a hydrophilic portion; as a consequence gas-liquid interfaces are ideal for surfactant molecules which tend to accumulate on them. This adsorption process introduces a discontinuity to the macroscopic concentration field, and the classical transport equation needs to be supplemented by appropriate equations to quantify the excess quantity. Namely, we introduce (i) an appropriate equation to characterize the “jump” in the surfactant surface concentration, known as the surface excess balance equation, and (ii) a bulk interphase partition relation that describes the equilibrium between the bulk and surface excess [17]. In the case of a fixed domain (in our case for a still bubble) the bulk problem can be eliminated by the use of Laplace transforms, and an integral equation for the surface excess can be obtained. This technique was used by several investigators and outlined by Borwankar & Wasan [5]. However, for the case of an oscillating bubble one has to restrict to limiting cases. The case of small oscillations was treated originally by Gottier *et al.* [25]. Johnson & Stebe [28] improved their analysis to obtain information about the sorption kinetics of surfactants and to measure surface tension and dilatational viscosity using the phase lag and amplitude ratio between the gas pressure and bubble radius. Recently, some numerical results were performed for small-amplitude axisymmetric bubble oscillations and large-amplitude nonlinear spherical oscillations by Nadim [37]. Although his analysis does not suffer from any limitations, the numerical solution gives only a qualitative description of the adsorption process and quantitative results are restricted to specific numerical values of the relevant dimensionless parameters. He observed (i) that the amount of surfactants on an oscillating bubble can be

thirty percent higher than the initial equilibrium value and (ii) that damping due to surface dilatational viscosity can be comparable to that due to other effects.

Relevant to surfactant transport associated with an oscillating bubble is transport associated with surface dilatation. In both cases the moving interface sets up convection currents that must be accounted for in the diffusion equation. Van Voorst Vader *et al.* [54] studied the case of an expanding interface whereas Joos and Van Uffelen [29, 53] studied a contracting interface. They both concluded that for constant dilatation rates, surface tension achieves a steady state, and their results showed good agreement with experiments. Van Uffelen and Joos [53], however, point out that for fast rates of compression or fairly insoluble surfactants, the monolayer collapses near some critical value of the surface excess concentration. In other words, diffusion is unable to remove surfactant molecules at a sufficient rate to prevent destruction of the monolayer.

1.2 Bubble dynamics

An important topic that constitutes an integral part of this work is the model for bubble dynamics. However, in the analysis presented in the following chapters we treat the bubble oscillation as a known but arbitrary function of time which can be obtained by integration of the bubble dynamical equations. No assumptions were made on the oscillation except that it is a periodic function of time and purely radial.

The problem of expansion or contraction of a gas bubble was first treated by Rayleigh [45]. He assumed that the motion of the bubble surface, assumed to be spherical, produces a purely radial flow through the action of pressure forces. In such a motion the velocity can be related to a potential, and, upon applying Bernoulli's equation, the differential equation governing bubble dynamics can be obtained

$$\frac{p(R, t) - p(\infty)}{\rho} = R\ddot{R} + \frac{3}{2}\dot{R}^2,$$

known as the Rayleigh-Plesset equation. Here $p(R)$ is the pressure just outside the bubble surface and $p(\infty)$ the pressure at infinity. The pressure $p(R)$ is connected to the pressure

acting on the inner side of the bubble surface ($p_i(t)$) by the condition on the normal stresses

$$p_i(R, t) = p(R, t) + 2\gamma/R + 4\mu\dot{R}/R,$$

where γ is the surface tension and μ liquid viscosity. Here, and in the analysis that follows, it is assumed that the vapor pressure inside the bubble is much smaller than the gas pressure, as follows from Raoult's law, and can be omitted.

What is left is to obtain an expression for $p_i(R, t)$. The simplest assumption is that the gas in the bubble behaves polytropically and assume a value for the polytropic exponent η . Two limiting cases are (i) isothermal behavior *i.e.* $\eta = 1$ or (ii) adiabatic behavior, *i.e.* $\eta = c_p/c_v$. The former is applicable when the thermal diffusion length (defined as the square root of the ratio between thermal diffusivity χ_G and frequency of bubble oscillations ω) is large compared to the initial bubble radius (a) and the latter when $(\chi_G/\omega)^{1/2} \ll a$. An exact evaluation of the polytropic exponent however would require the solution of the conservation equations of mass, momentum and energy in the bubble as mentioned by Prosperetti [43]. Kamath & Prosperetti [30] relaxed the polytropic assumption and allowed for a spatially varying temperature field inside the bubble. Now, the energy equation inside the bubble can no longer be eliminated and has to be solved simultaneously with the bubble dynamical equations. Although polytropic and non-polytropic models agree quite well away from resonances, the former seems to exaggerate their importance dramatically as shown in appendix C.

To account for the effects of liquid compressibility, the equations of mass and momentum are expanded in a formal series in the Mach number assuming isentropic motion in the liquid and purely radial motion [43]. Radial oscillations can be justified provided that the wavelength of the applied sound field (c/ω) is much larger than the bubble radius. Here c is the speed of sound in the liquid. If the bubble radius is comparable with c/ω then different sections of the bubble would be exposed to different pressure and the bubble would undergo shape oscillations.

1.3 Organization of Thesis

The overall objective of this work is to obtain expressions for the growth rate of oscillating gas bubbles and obtain information on the effect of oscillations and surfactants on the growth rates. Taking advantage of the small diffusion characterizing the transport of gases in liquids we were able to solve the problem asymptotically in time using singular perturbation techniques.

The format of the thesis is as follows. In Chapter 2 we treat the problem of a single bubble oscillating in a liquid of arbitrary saturation. Chapter 3 deals with the effect of insoluble surfactants on bubble growth rates whereas in Chapter 4 we extend these results to soluble surfactants. Finally, a summary of the main conclusions and recommendations for future work are given in Chapter 5.

Chapter 2

Classical Problem of Rectified Diffusion

In this chapter we treat the problem of a single bubble oscillating in a liquid of arbitrary saturation, *i.e.* away from threshold conditions. We focus on developing the mathematical techniques required to solve convection-diffusion equations outside an oscillating bubble together with complicated unsteady boundary conditions at the interface.

2.1 Formulation

In this section we formulate the mass transport problem and concentrate on the practical problem of large Péclet number. The differential equation governing the convection and diffusion of a dissolved gas in a liquid is the equation of continuity for a component A in a binary mixture. This can be simplified assuming constant mass density and constant binary diffusion coefficient to

$$\frac{\partial C_A}{\partial t} + \mathbf{u} \cdot \nabla C_A = D \nabla^2 C_A, \quad (2.1)$$

where C_A is the mass (or molar) concentration or mass (or mole) fraction of A, \mathbf{u} is the mass average velocity and D is the diffusivity of the gas in the liquid. This simplified problem is usually used for diffusion in dilute liquid solutions at constant pressure and temperature [3]. The mass transport problem in the gas phase, *i.e.* inside the bubble, does not play a significant role in the diffusion process since the diffusion coefficient in gases is much higher than in liquids. Hence the diffusion process is controlled by the liquid phase, and the mass fraction of gas inside the bubble can be assumed uniform.

In the case under consideration, due to the radial oscillations of the bubble, we can assume spherical symmetry, and equation (2.1) simplifies to

$$\frac{\partial \tilde{C}}{\partial t} + \frac{R^2(t)\dot{R}(t)}{r^2} \frac{\partial \tilde{C}}{\partial r} = \frac{D}{r^2} \frac{\partial}{\partial r} \left(r^2 \frac{\partial \tilde{C}}{\partial r} \right), \quad (2.2)$$

where \tilde{C} is the mass fraction of gas dissolved in the liquid, $R^2(t)\dot{R}(t)/r^2$ is the radial velocity field in the liquid associated with the bubble oscillations obtained by solving the mass conservation equation in the liquid. Note that the bubble radius R is treated as an arbitrary function of time t .

The dynamical equation for bubble oscillations is a non-linear differential equation, such as the Rayleigh-Plesset equation, with derivation reviewed by Prosperetti [43]:

$$R\ddot{R} + \frac{3}{2}\dot{R}^2 = \frac{1}{\rho} \left(p_{Gi} \left(\frac{a}{R} \right)^{3\eta} + p_v(T_\infty) - p_s(t) - \frac{2\gamma}{R} - \frac{4\mu\dot{R}}{R} \right). \quad (2.3)$$

Although the results we develop in the present work apply irrespective of exactly which bubble dynamical equations are used, we have written the Rayleigh-Plesset equation in order to fix ideas and to aid in non-dimensionalization. Here and in what follows, ρ is the density of the liquid, m_G is the mass of the gas in the bubble, M is the molecular weight of the gas, R_G is the universal gas constant, T_∞ is the temperature of the fluid, p_v is the vapor pressure, p_s is the pressure in the liquid, γ is the interfacial tension and μ is the viscosity of the liquid. The polytropic exponent η varies between the extremes of unity for an isothermal bubble and the ratio of specific heats c_p/c_v for an adiabatic bubble.

The boundary condition at the bubble surface is developed by application of Henry's law, which relates the concentration of a gas in a liquid to the partial pressure of the gas above the liquid; hence

$$\tilde{C}(r = R(t), t) = \frac{p_G}{k}.$$

Here, p_G is the partial pressure of the gas and k is the constant of Henry's law. For oscillations of a gas bubble with initial pressure equal to p_{Gi} , the surface boundary condition may be written

$$\tilde{C}(r = R(t), t) = \frac{p_{Gi}}{k} p_G^*(t), \quad (2.4)$$

where $p_G^*(t)$ is dimensionless. The bubble is assumed to be created in a fluid which initially has a uniform concentration of the gas C_∞ . Hence the initial condition and the far-field conditions are

$$\tilde{C}(r, t = 0) = \tilde{C}(r \rightarrow \infty, t) = C_\infty. \quad (2.5)$$

The rate of transport of gas across the bubble interface is

$$\frac{dm_G}{dt} = 4\pi R^2 D \rho \frac{\partial \tilde{C}(r = R(t), t)}{\partial r}.$$

The problem may be non-dimensionalized with respect to the following natural scales. As a length scale, we take a , the radius of the undisturbed bubble. The time scale is Ω_0^{-1} , which is the inverse of the natural frequency of radial oscillations of the bubble about the undisturbed state. The pressure is made dimensionless using the pressure scale $\frac{1}{2}\rho a^2 \Omega_0^2$. This leads to dimensionless parameters corresponding to the gas pressure in the undisturbed bubble,

$$p_{Gi}^* = \frac{3m_G R_G T_\infty}{2\pi M \rho a^5 \Omega_0^2} = \frac{2p_{Gi}}{\rho a^2 \Omega_0^2},$$

the Weber number We ,

$$We = \frac{2\rho(a\Omega_0)^2 a}{\gamma},$$

the Reynolds number Re ,

$$Re = \frac{\rho(a\Omega_0)a}{\mu},$$

and the dimensionless forcing pressure

$$p^*(\tau) = \frac{p_s(\tau\Omega_0^{-1}) - p_v(T_\infty)}{\frac{1}{2}\rho a^2 \Omega_0^2}.$$

The convection-diffusion equation (2.1) is non-dimensionalized to read

$$\frac{\partial C}{\partial \tau} + \frac{x^2(\tau)x_\tau(\tau)}{\xi^2} \frac{\partial C}{\partial \xi} = \frac{1}{\mathcal{P}} \frac{1}{\xi^2} \frac{\partial}{\partial \xi} \left(\xi^2 \frac{\partial C}{\partial \xi} \right), \quad (2.6)$$

where ξ is the dimensionless radial coordinate, $x(\tau)$ is the dimensionless bubble radius, and the Péclet number is $\mathcal{P} = a^2 \Omega_0 / D$. Next we non-dimensionalize the Henry's law boundary condition (2.4) to read

$$C(\xi = x(\tau), \tau) = \frac{p_{Gi}^*}{k^*} p_G^*(\tau) - C_\infty.$$

The dimensionless Henry's law constant is $k^* = 2k/\rho(a\Omega_0)^2$. Note that we have subtracted the concentration at infinity from the concentration field, *i.e.* $C = \tilde{C} - C_\infty$. Hence the initial and far-field conditions (2.5) become

$$C(\xi, \tau = 0) = C(\xi \rightarrow \infty, \tau) = 0.$$

Finally, for a motionless bubble, we have

$$p_{Gi}^* = p_0^* + \frac{8}{We},$$

from which we obtain an alternate expression of the boundary condition at the bubble surface

$$C(\xi = x(\tau), \tau) = \frac{p_0^*}{k^*} \left(1 + \frac{8}{p_0^* We} \right) p_G^*(\tau) - C_\infty. \quad (2.7)$$

The saturation concentration in the liquid separated from gas at pressure p_0^* by a plane boundary is $C_{sp} = p_0^*/k^*$. The saturation concentration in the liquid separated from gas within a spherical bubble of dimensionless radius $x = 1$ is

$$C_{sb} = C_{sp} \left(1 + \frac{8}{p_0^* We} \right) = \frac{p_{Gi}^*}{k^*}.$$

2.1.1 Lagrangian formulation

The principal analytical difficulties presented by the governing equations are the following. First, the boundary condition at the surface of the bubble (2.7) is applied at a time-dependent value of the radial coordinate $\xi = x(\tau)$; hence the problem is one with a moving boundary. Moreover, the boundary condition applied at the moving boundary is unsteady. The second observation is that the spatially inhomogeneous convection velocity can change sign, and is a nonlinear function of the bubble radius which evolves according to its own (nonlinear) ordinary differential equation. It is not possible to judge whether the convection tends to drive dissolved gas toward or away from the bubble. The goal of the present analysis is to refrain from specification of the bubble oscillation during development of the general theory in order that the concentration field and enhancement of transport may be studied for bubble oscillations that are as general as possible.

The first analytical difficulty, namely the moving boundary, can be eliminated by transforming the problem into Lagrangian coordinates; this is suggested by the observation that the bubble surface is a material surface. We assume the fluid outside the bubble is incompressible (at least for the purposes of solution of the convection-diffusion equation). Volume conservation and the particle paths one can obtain from the velocity field imply that the coordinate $\sigma = \frac{1}{3}(\xi^3 - x^3(\tau))$ has a constant value for a particle of fixed identity. In what follows, we shall work in the Lagrangian coordinates (σ, τ) rather than in the Eulerian coordinates (ξ, τ) .

Equation (2.6) for the concentration field takes the form

$$\frac{\partial C}{\partial \tau} = \frac{1}{\mathcal{P}} \frac{\partial}{\partial \sigma} \left(\left(3\sigma + x^3(\tau) \right)^{(4/3)} \frac{\partial C}{\partial \sigma} \right), \quad (2.8)$$

with boundary and initial conditions

$$C(\sigma = 0, \tau) = C_{sb} p_G^*(\tau) - C_\infty, \quad (2.9)$$

$$C(\sigma, \tau = 0) = C(\sigma \rightarrow \infty, \tau) = 0.$$

The equations now describe a field in a domain with a fixed boundary at the bubble surface.

In dimensionless, Lagrangian variables, the rate of transport is given by

$$\frac{dm_G^*}{d\tau} = \frac{3}{\mathcal{P}} x^4 \frac{\partial C(\sigma = 0, \tau)}{\partial \sigma} \quad (2.10)$$

where m_G^* is m_G divided by the mass of liquid displaced by the undisturbed bubble.

2.1.2 Splitting of the problem

In the limit of infinite \mathcal{P} , the concentration field is simply determined by the initial condition and the motion of the fluid particles outside the bubble; this is a consequence of the fact that (2.8) has the solution $C(\sigma)$ in that limit. However, the solution for large but finite \mathcal{P} is not a smooth perturbation of the solution for infinite \mathcal{P} but a singular one. Physically the reasons for this are as follows. When $\mathcal{P} = \infty$, the concentration field is a material field with C constant for each material point of fluid outside the bubble. When

$1 \ll \mathcal{P} < \infty$, however, the existence of diffusion means that C changes slowly for a material point of fluid in response to the gradient in C with neighboring material points. Of course, the gradient in C with neighboring material points alternately steepens and shallows over a cycle of bubble oscillation. Hence there are two time-scales that are important in the problem; the indications are that a multiple-scales approach will be profitable. We refer the interested reader to the recent book by Hinch [26] for an insightful discussion of this reasoning.

Another analytical difficulty is the time dependent boundary condition (2.9). At large \mathcal{P} , the concentration field will be characterized by oscillatory behavior close to the bubble surface, due to the Henry's law boundary condition, and by slow diffusion further away from the bubble. To solve for the concentration field, it is profitable to split the problem into two parts. One part, the oscillatory problem, corresponds to the oscillatory part of the boundary condition, but as we shall see this part contributes nothing to the mass transport, asymptotically in time. The second part, the smooth problem, represents the constant part of the boundary condition which produces the same effect on the concentration in the far field as the full, time dependent boundary condition. This constant boundary condition is not arbitrary but actually emerges from the solution of the oscillatory problem.

To begin the splitting, we define the average with respect to a convenient new non-linear time $\hat{\tau}$

$$\hat{\tau}(\tau) \equiv \int_0^\tau x^4(\theta) d\theta; \quad (2.11)$$

the average is

$$\langle f(\sigma, \tau) \rangle_{\hat{\tau}} \equiv \frac{1}{\hat{\tau}(T)} \int_0^{\hat{\tau}(T)} f(\sigma, \hat{\tau}) d\hat{\tau} = \frac{1}{\int_0^T x^4(\tau) d\tau} \int_0^T f(\sigma, \tau) x^4(\tau) d\tau,$$

where T is the dimensionless period of bubble oscillation. This somewhat peculiar averaging scheme will soon emerge as a clear manifestation of the spherical nature of the problem.

Using this average, we split the boundary condition at the surface of the bubble (2.9) as follows

$$C(\sigma = 0, \tau) = C_{sb} p_G^*(\tau) - C_\infty = C_{sb} \langle p_G^*(\tau) \rangle_{\hat{\tau}} - C_\infty + C_{sb} [p_G^*(\tau) - \langle p_G^*(\tau) \rangle_{\hat{\tau}}],$$

where the oscillating part is associated with the oscillatory problem and the constant part with the smooth problem. The *oscillatory problem* is therefore

$$\frac{\partial C_{osc}}{\partial \tau} = \frac{1}{\mathcal{P}} \frac{\partial}{\partial \sigma} \left(\left(3\sigma + x^3(\tau) \right)^{(4/3)} \frac{\partial C_{osc}}{\partial \sigma} \right), \quad (2.12)$$

with boundary and initial conditions

$$C_{osc}(\sigma = 0, \tau) = C_{sb} [p_G^*(\tau) - \langle p_G^*(\tau) \rangle_{\hat{\tau}}], \quad (2.13)$$

$$C_{osc}(\sigma, \tau = 0) = C_{osc}(\sigma \rightarrow \infty, \tau) = 0.$$

The *smooth problem* is defined by

$$\frac{\partial C_{sm}}{\partial \tau} = \frac{1}{\mathcal{P}} \frac{\partial}{\partial \sigma} \left(\left(3\sigma + x^3(\tau) \right)^{(4/3)} \frac{\partial C_{sm}}{\partial \sigma} \right), \quad (2.14)$$

with boundary and initial conditions

$$C_{sm}(\sigma = 0, \tau) = C_{sb} \langle p_G^*(\tau) \rangle_{\hat{\tau}} - C_{\infty}, \quad (2.15)$$

$$C_{sm}(\sigma, \tau = 0) = C_{sm}(\sigma \rightarrow \infty, \tau) = 0.$$

The sum of the solutions to the oscillatory and smooth problems is the solution to the full problem, *i.e.* $C(\sigma, \tau) = C_{osc}(\sigma, \tau) + C_{sm}(\sigma, \tau)$. From equation (2.14) and boundary condition (2.15), it is straightforward to realize that (2.15) equal to zero gives the threshold criterion for rectified diffusion. We return to this point shortly.

The splitting just described closely parallels what one might do to solve for the motion in a fluid above an infinite flat plate that is moved horizontally in an impulsive fashion. Suppose that the plate is moved in an oscillatory manner with some nonzero mean velocity. As a consequence of the linear nature of the Navier-Stokes equations when restricted to the case of parallel flow in a domain of infinite extent, the problem is easily split in two. In one problem (Stokes' first problem [49]) the flat plate moves at a uniform speed. In the second problem (Stokes' second problem) the flat plate oscillates with zero mean. In both cases the motion of the fluid is most easily understood by the diffusion of vorticity created by the no-slip boundary condition on the solid wall. We refer the interested reader to Kundu [33] or to Leal [35] for a discussion of these points. The main difference between Stokes' problems and the convection-diffusion problem pursued here is that we must resort to singular perturbation analyses in both the oscillatory and smooth problems.

2.2 The oscillatory problem

Solution of the oscillatory problem provides the rationale for the non-intuitive averaging procedure used to split the problem in the previous section, as well as the threshold condition for rectified diffusion. However, the oscillatory solution contributes virtually nothing to the mass transport across the bubble surface even at conditions far removed from threshold. To solve the oscillatory problem, we re-scale the spatial coordinate σ by the square-root of the Péclet number. Hence we define $s = \mathcal{P}^{1/2}\sigma$. The oscillatory equation (2.12) becomes

$$\frac{\partial C_{osc}}{\partial \tau} = \frac{\partial}{\partial s} \left(\left(3 \frac{s}{\mathcal{P}^{1/2}} + x^3(\tau) \right)^{(4/3)} \frac{\partial C_{osc}}{\partial s} \right).$$

In the limit of large \mathcal{P} , this equation simplifies; to leading order, we have

$$\frac{\partial C_{osc}^0}{\partial \tau} = x^4(\tau) \frac{\partial^2 C_{osc}^0}{\partial s^2}, \quad (2.16)$$

where C_{osc}^0 is the leading term in an expansion of the form

$$C_{osc}\left(\frac{s}{\mathcal{P}^{1/2}}, \tau\right) = C_{osc}^0(s, \tau) + \frac{1}{\mathcal{P}^{1/2}} C_{osc}^1(s, \tau) + \dots$$

The leading order problem may be solved by rescaling time as in (2.11) in order to transform to a canonical parabolic equation. This yields

$$\frac{\partial C_{osc}^0}{\partial \hat{\tau}} = \frac{\partial^2 C_{osc}^0}{\partial s^2}.$$

Hence, after application of techniques from singular perturbation theory and a nonlinear transformation of time, the leading order solution of the oscillatory problem is identical to Stokes' second problem of flow near an oscillating flat plate. Eller & Flynn [20] work out the details of the transient solution for the concentration field as an initial step in their analysis. However, they use a different boundary condition as we describe in section 2.4 below.

We compute the asymptotic solution \bar{C}_{osc}^0 (indicated by an overbar) via a Fourier series approach, as follows. First, the boundary condition (2.13) is expanded as a Fourier series in the nonlinear time $\hat{\tau}$:

$$\bar{C}_{osc}^0(s=0, \hat{\tau}) = C_{sb} [p_G^*(\tau) - \langle p_G^*(\tau) \rangle_{\hat{\tau}}]$$

$$= \sum_{m=1}^{\infty} [a_m \cos(\omega_m \hat{\tau}) + b_m \sin(\omega_m \hat{\tau})], \quad (2.17)$$

where

$$\omega_m = \frac{2m\pi}{\hat{\tau}(T)}.$$

It is of critical importance to note that there is no mean term in the Fourier expansion of the boundary condition in the nonlinear time by construction, because (2.13) implies

$$a_0 = \frac{1}{\hat{\tau}(T)} \int_0^{\hat{\tau}(T)} C_{osc}^0(s=0, \hat{\tau}) d\hat{\tau} = 0.$$

Next, we assume a (real) solution of the form

$$\bar{C}_{osc}^0(s, \hat{\tau}) = \sum_{m=-\infty, m \neq 0}^{\infty} A_m(s) \exp[\omega_m i \hat{\tau}].$$

Term-by-term, one can solve to obtain the asymptotic concentration field for the oscillatory problem

$$\begin{aligned} \bar{C}_{osc}^0(s, \tau) = & \sum_{m=1}^{\infty} \exp\left[-\left(\frac{\omega_m}{2}\right)^{1/2} s\right] \times \\ & \left\{ a_m \cos\left[\omega_m \hat{\tau} - \left(\frac{\omega_m}{2}\right)^{1/2} s\right] + b_m \sin\left[\omega_m \hat{\tau} - \left(\frac{\omega_m}{2}\right)^{1/2} s\right] \right\}. \end{aligned} \quad (2.18)$$

Each mode is heavily damped with distance s away from the bubble. For example, the amplitude of mode m is reduced to one percent when $s = 6.5/(\omega_m)^{(1/2)}$, *i.e.* when $\sigma = 6.5/(\mathcal{P} \omega_m)^{(1/2)}$. Hence by requiring the mean term to be zero, the effect of the oscillatory boundary condition is localized to a small boundary layer region close to the bubble. In order to expose the dependence of the boundary layer thickness on the driving frequency we express ω_m and s in the original variables:

$$\left(\frac{\omega_m}{2}\right)^{1/2} s \equiv \left(\frac{m\pi a^2 \Omega}{D} \frac{1}{\frac{1}{T} \int_0^T x^4(\theta) d\theta} \right)^{1/2} \sigma,$$

where Ω is the driving frequency. The average of x^4 (known as the fourth moment) is large for oscillations that linger at large x . The parameters that tend to increase the boundary layer thickness are low frequency, small bubbles, large diffusion coefficient and nonlinear bubble oscillations. In figure 2.1 we show the asymptotic solution of the oscillatory problem of the concentration field for $\mathcal{P} = 1000$ and $x(\tau) = 1 + 0.1 \sin(2\pi\tau)$.

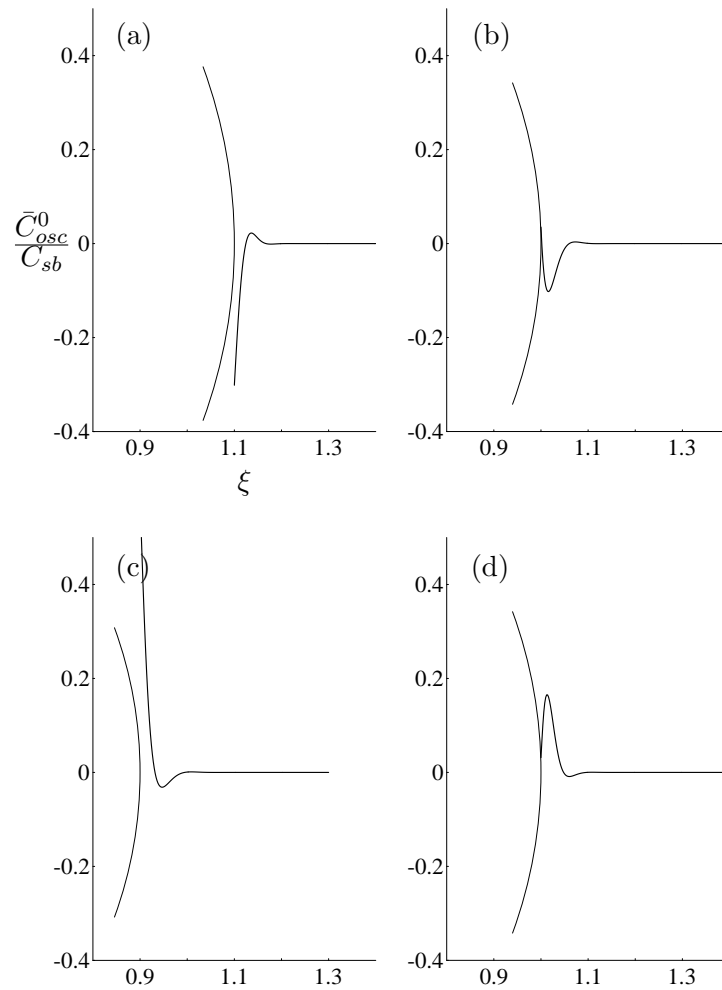


Figure 2.1: The asymptotic concentration profile for the oscillatory problem for $\mathcal{P} = 1000$, $x(\tau) = 1 + 0.1 \sin(2\pi\tau)$ and $p_G^*(\tau) = x^{-4.2}(\tau)$ at (a) $\tau = T/4$, (b) $\tau = T/2$, (c) $\tau = 3T/4$ and (d) $\tau = T$. The plots show \bar{C}_{osc}^0/C_{sb} versus the dimensionless Eulerian radial coordinate ξ . The circular arc shows the position of the bubble surface.

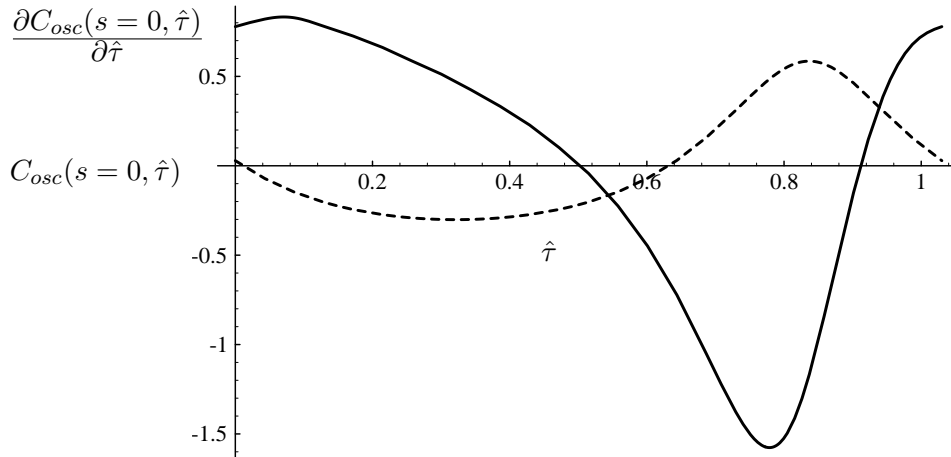


Figure 2.2: The gradient of the concentration field on the bubble surface (solid curve) and the boundary condition for the concentration field (dashed curve) versus the nonlinear time $\hat{\tau}$. The bubble oscillation and the boundary condition are the same as in figure 2.1. Note that $\hat{\tau}(0.5) = 0.643$.

The rate of mass transport (2.10) expressed in the nonlinear time $\hat{\tau}$ and scaled spatial coordinate s is

$$\frac{dm_{G_{osc}}^*}{d\hat{\tau}} = \frac{3}{\mathcal{P}^{1/2}} \frac{\partial C_{osc}(s=0, \hat{\tau})}{\partial s}.$$

In figure 2.2 we show, for comparison, the asymptotic rate of mass transport (solid curve) and the boundary condition for the concentration field (dashed curve) versus the nonlinear time $\hat{\tau}$. Note that their phase difference is not π , as one might expect, but $3\pi/4$. With the use of the asymptotic solution (2.18), it is a simple matter to determine that the associated mass transport over one period is zero. In Appendix A, we show that the asymptotic solution is reached very rapidly in a few periods of the bubble oscillation. Hence the mass transport associated with the transient in the oscillatory problem is negligible.

2.3 The smooth problem

It is in solving the smooth problem that we must develop a means by which to handle both convection-enhanced diffusion and the depletion layer associated with bubbles

that grow by rectified diffusion. The smooth problem is characterized by slow convection-enhanced diffusion and by a steady boundary condition. Therefore, we introduce a second time scale $\lambda \equiv \tau/\mathcal{P} = tD/a^2$, which captures the slow diffusive behavior. Furthermore, we define for future use a second (conventional) time average with respect to τ over one period of bubble oscillation,

$$\langle f(\sigma, \tau) \rangle_\tau \equiv \frac{1}{T} \int_0^T f(\sigma, \tau) d\tau. \quad (2.19)$$

Next we expand

$$C_{sm}(\sigma, \tau) = C_{sm}^0(\sigma, \lambda, \tau) + \frac{1}{\mathcal{P}} C_{sm}^1(\sigma, \lambda, \tau) + \dots$$

Then, to zeroth order in the small parameter \mathcal{P}^{-1} , we have the system

$$\frac{\partial C_{sm}^0}{\partial \tau} = 0, \quad (2.20)$$

with boundary and initial conditions

$$C_{sm}^0(\sigma = 0, \lambda, \tau) = C_{sb} \langle p_G^*(\tau) \rangle_{\hat{\tau}} - C_\infty,$$

$$C_{sm}^0(\sigma, \lambda = 0, \tau = 0) = C_{sm}^0(\sigma \rightarrow \infty, \lambda, \tau) = 0.$$

The solution to the zeroth order problem (2.20) is simply $C_{sm}^0(\sigma, \lambda, \tau) = C_{sm}^0(\sigma, \lambda)$. However C_{sm}^0 is further determined by the first order problem:

$$\frac{\partial C_{sm}^1}{\partial \tau} = -\frac{\partial C_{sm}^0}{\partial \lambda} + \frac{\partial}{\partial \sigma} \left((3\sigma + x^3(\tau))^{(4/3)} \frac{\partial C_{sm}^0}{\partial \sigma} \right), \quad (2.21)$$

with boundary and initial conditions

$$C_{sm}^1(\sigma = 0, \lambda, \tau) = C_{sm}^1(\sigma, \lambda = 0, \tau = 0) = C_{sm}^1(\sigma \rightarrow \infty, \lambda, \tau) = 0.$$

We must ensure that there is no secular behavior, lest the expansion become disordered as τ increases. Hence we force the right-hand-side of the first order problem (2.21) to have zero τ -average (defined in (2.19)); this leads to a second equation for C_{sm}^0

$$\frac{\partial C_{sm}^0}{\partial \lambda} = \frac{\partial}{\partial \sigma} \left(\left\langle (3\sigma + x^3(\tau))^{(4/3)} \right\rangle_\tau \frac{\partial C_{sm}^0}{\partial \sigma} \right), \quad (2.22)$$

as a consequence of the critical simplification $C_{sm}^0(\sigma, \lambda, \tau) = C_{sm}^0(\sigma, \lambda)$. It is interesting to note that of the two time averages we have defined, $\langle \cdot \rangle_{\hat{\tau}}$ and $\langle \cdot \rangle_\tau$, each has a strong

physical motivation. The time average with respect to the nonlinear time has the property of extracting mean behavior in Lagrangian spherical coordinates, whereas only the true time average can be used to distinguish secular behavior.

The smooth problem has a very straightforward asymptotic solution $\bar{C}_{sm}^0(\sigma)$ (indicated by an overbar) in the limit $\lambda \rightarrow \infty$, obtained as follows. We set $\partial/\partial\lambda \equiv 0$ and integrate once with respect to σ . This yields

$$\frac{b}{\langle (3\sigma + x^3(\tau))^{(4/3)} \rangle_\tau} = \frac{d\bar{C}_{sm}^0}{d\sigma},$$

where b is a constant to be determined. A definite integration from zero to ∞ yields

$$b \int_0^\infty \frac{d\sigma}{\langle (3\sigma + x^3(\tau))^{(4/3)} \rangle_\tau} = \bar{C}_{sm}^0(\sigma \rightarrow \infty) - \bar{C}_{sm}^0(\sigma = 0) = C_\infty - C_{sb} \langle p_G^*(\tau) \rangle_{\hat{\tau}}.$$

Therefore, the asymptotic solution to the smooth problem is

$$\bar{C}_{sm}^0(\sigma) = (C_{sb} \langle p_G^*(\tau) \rangle_{\hat{\tau}} - C_\infty) \left[1 - \frac{\int_0^\sigma \frac{d\sigma'}{\langle (3\sigma' + x^3(\tau))^{(4/3)} \rangle_\tau}}{\int_0^\infty \frac{d\sigma}{\langle (3\sigma + x^3(\tau))^{(4/3)} \rangle_\tau}} \right]. \quad (2.23)$$

We emphasize that this solution is valid, asymptotically in time, for any nonlinear periodic bubble oscillation. In figure 2.3 we show plots of the asymptotic, smooth concentration profile at various instants of time for $x(\tau) = 1 + 0.8 \sin(2\pi\tau)$ and $p_G^*(\tau) = x^{-3.6}(\tau)$. In addition, $b = 0$ emerges clearly as the threshold condition for rectified diffusion.

The rate of mass transport (2.10) associated with the zeroth order approximation of the smooth problem is

$$\frac{dm_{G_{sm}}^*}{d\lambda} = 3 \langle x^4(\tau) \rangle_\tau \frac{\partial C_{sm}^0(\sigma = 0, \lambda)}{\partial \sigma}.$$

The asymptotic solution (2.23) gives an expression for the rate of mass transport

$$\frac{d\bar{m}_{G_{sm}}^*(\lambda)}{d\lambda} = -3 \frac{[C_{sb} \langle p_G^*(\tau) \rangle_{\hat{\tau}} - C_\infty]}{\int_0^\infty \frac{d\sigma}{\langle (3\sigma + x^3(\tau))^{(4/3)} \rangle_\tau}}, \quad (2.24)$$

which is valid for any nonlinear periodic bubble oscillation. Because the denominator of equation (2.24) is always positive, the threshold for rectified diffusion is

$$C_{sb} \langle p_G^*(\tau) \rangle_{\hat{\tau}} - C_\infty = 0. \quad (2.25)$$

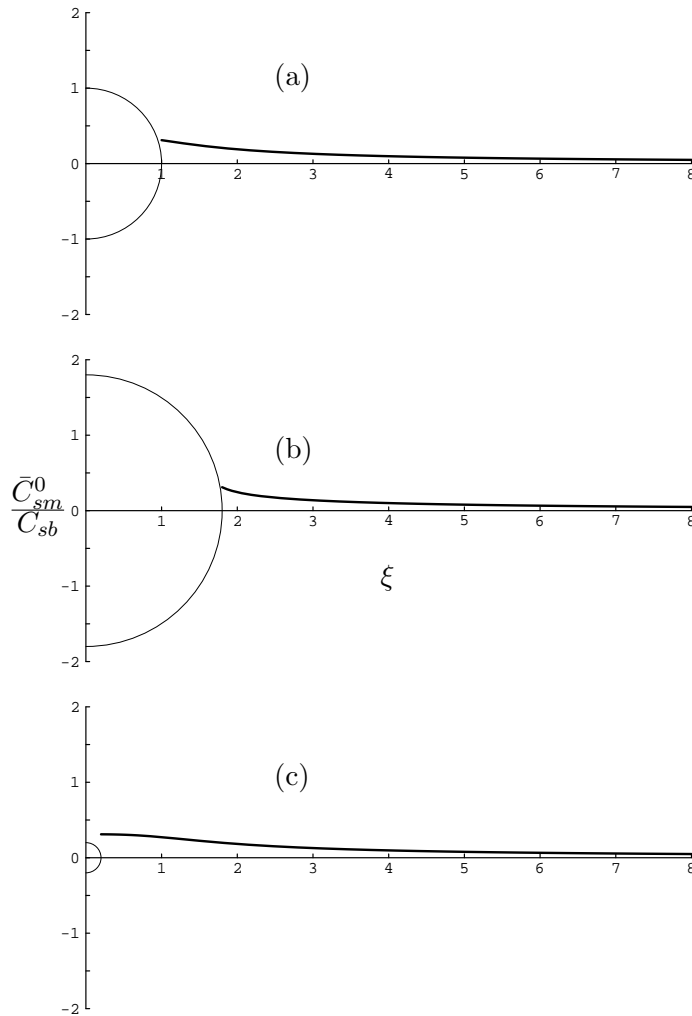


Figure 2.3: The asymptotic concentration profile for the smooth problem for the bubble oscillation $x(\tau) = 1 + 0.8 \sin(2\pi\tau)$ and $p_G^*(\tau) = x^{-3.6}(\tau)$ at (a) $\tau = 0$, (b) $\tau = T/4$, and (c) $\tau = T/2$. The plots show \bar{C}_{sm}^0/C_{sb} versus the dimensionless Eulerian radial coordinate ξ for the case $C_\infty = 0$. The circular arc shows the position of the bubble surface.

This relation agrees with the criterion developed by Eller & Flynn [20]. The growth rate of bubbles away from threshold conditions is close to the result of Eller & Flynn, except for large-amplitude oscillations.

The rate of mass transport associated with the transient in the smooth problem can be computed analytically only under the assumption of small oscillations, as discussed in Appendix B. The mass transport associated with the transient solution of the smooth problem is quite significant at the initial stages. It reaches its asymptotic limit for $\lambda \approx 10$; this corresponds to $t \approx 10a^2/D$ if expressed in dimensional variables. For example, outside a bubble of radius $35 \mu\text{m}$, the rate of mass transport reaches its asymptotic value by $t = 5$ seconds. This is still a short time when compared to the experiments of Crum [11] of 500 seconds duration.

2.4 Comparison with previous formulations

Now that we have completed our mathematical analysis, it is useful to return to the work of previous researchers in this area. We shall focus on the analysis of Eller & Flynn [20], as it is the basis for much of the theoretical work concerning rectified diffusion, including Eller [18], Eller [19], Crum [11], Crum & Hansen [13], and Church [10]. In each of these works, the underlying assumption is made that diffusion is of importance only in a thin layer near the surface of the bubble.

The thin-diffusion-layer approximation is exactly the same as the boundary layer analysis we undertook to solve the oscillatory problem, with one exception. In the oscillatory problem, the boundary condition has zero average $\langle \cdot \rangle_{\hat{\tau}}$; this ensures that the oscillatory concentration field differs from zero only in a thin layer of thickness $O(\mathcal{P}^{-1/2})$ near the bubble surface. This is the reason, in our solution of the oscillatory problem, why the Fourier expansion of the boundary condition (2.17) has zero $\hat{\tau}$ -mean.

In contrast, Eller & Flynn consider what we have called the oscillatory problem, but they apply the full boundary condition, *i.e.* including the $\hat{\tau}$ -average term in the Fourier

expansion. In fact, when Eller & Flynn take their “high-frequency limit”, they simply replace the boundary condition by its $\hat{\tau}$ -average! In other words, the high-frequency limit of Eller & Flynn is to solve what we call the oscillatory problem by applying what we use as the boundary condition of the smooth problem. This procedure, pursued by Eller & Flynn (and by others mentioned above), is valid only for short times, as pointed out in section 5 of their paper. The reason is that after some time has passed, the smooth boundary condition leads to a diffusion layer with thickness that grows like $\hat{\tau}^{1/2}$. Therefore the underlying assumption in the analysis eventually ceases to be valid. In the present work, we have defined unambiguously the splitting of the problem so that (i) the oscillating part of the boundary condition contributes (almost) nothing to the transport of gas and leads to a concentration field that differs from zero only in a thin layer of liquid near the bubble surface, for all time, and (ii) the steady part of the boundary condition is handled in a way that is uniformly valid in time and accounts for convection-enhanced diffusion.

2.5 Numerical results

Now we turn to numerical evaluation of the analytic expressions of (i) the threshold criterion for rectified diffusion and (ii) the rate of growth or dissolution of bubbles away from threshold conditions. A complete calculation of the rate of growth or dissolution of bubbles away from threshold conditions would, of course, have to account for slow changes in the periodic response of the bubble associated with its changing mass. However, close examination of the experimental results of Crum [11] reveals that the rate of growth or dissolution is very nearly constant over several million periods of bubble oscillations. An exception occurs when Crum observes the emergence of obvious surface waves on larger (*e.g.* strongly forced $50\ \mu\text{m}$) bubbles. This situation is clearly not addressed by the theory we have outlined. In summary, it would appear to be sufficient simply to examine the rate of growth of bubbles of various amplitudes under differing conditions.

The problem of computing the periodic response of a bubble to periodic variations in the background pressure has been approached via full numerical solution by Eller & Flynn

[20], by Eller [18], and more recently by Church [10] and Gaitan, *et al.* [24] using several different methods. In all works except that of Eller [18], the authors first computed then discarded the initial transient in order to obtain the asymptotic, periodic solution. The same is true in other areas of bubble research; Lauterborn [34] also computed then discarded initial transients to obtain frequency-response curves for periodically driven bubbles. This proves to be an expensive undertaking, particularly when one wants to examine changes in the bubble oscillations over regions of multi-dimensional parameter space. Eller [18] used a laborious shooting method to determine the initial conditions that lead to a periodic oscillation for a given set of parameter values. However, like the discarding of initial transients, this procedure also provides no information regarding why the oscillations change as one alters the parameter.

In view of these difficulties, many authors have assumed a (small amplitude sinusoidal) form of the radius as a function of time and used this as a basis for computing the required averages. These works include those of Hsieh & Plesset [27], Eller [18], Eller [19], Crum [11], Crum & Hansen [13], and Nagiev & Khabeev [38]. For small amplitudes of pressure variation about the mean, these methods are satisfactory, provided one is careful to avoid resonances.

We depart from previous work in what follows by using a new technique to compute asymptotic periodic bubble oscillations of arbitrary amplitude numerically, without proceeding through the transient. In order to accomplish this, we use a continuation algorithm to find the periodic bubble oscillation that is a global attractor at a new parameter value, by starting with an initial guess that is the converged solution at a nearby parameter value. The first task is to recast the system as an autonomous system of ordinary differential equations. This is easily done if one writes an auxiliary differential equation which has the periodic forcing as its global attractor. Then one simply couples the bubble oscillation to the driver. A suitable nonlinear driver sub-system is

$$\begin{aligned} \dot{x}_3 &= x_3 + \theta x_4 - x_3 (x_3^2 + x_4^2) \\ \dot{x}_4 &= -\theta x_3 + x_4 - x_4 (x_3^2 + x_4^2), \end{aligned}$$

which has the asymptotic solution $x_3 = \sin(\theta t)$, $x_4 = \cos(\theta t)$; the periodic driver motion is a normally-hyperbolic limit cycle. Therefore, the stability of the periodic bubble oscillation will be characterized by the eigenvalues of the associated fixed point of the Poincaré (or period) map that derive from the bubble sub-system.

The numerical method we use is AUTO (Doedel [16]). The differential equations (in time) are discretized using an extremely efficient adaptive collocation procedure. In practice, this provides a very accurate and quick way to generate asymptotic periodic bubble oscillations directly as one varies a parameter. We remark that the method only works in the presence of damping in the problem, which makes the periodic solution an attractor, in the bubble sub-system. To begin the method, we simply set the parameter that controls the coupling between the driver and bubble sub-systems to zero. Hence the initial solution is just the (steady) equilibrium in the bubble sub-system $x(\tau) = 1$, and the periodic driving motion in the driver sub-system. Thereafter, changing the coupling parameter from zero results in a smooth development of the asymptotic bubble oscillation in response to the driving. Moreover, continuation is possible in any of the many parameters of the problem, *e.g.* equilibrium bubble radius, amplitude of the driving pressure oscillations, interfacial tension, liquid saturation, *etc.* Readers well-versed in nonlinear dynamics will note that the method we have outlined will detect a period-doubling bifurcation to a solution of the form $x(\tau) = x(\tau + 2T) \neq x(\tau + T)$. These solutions, which may occur at higher amplitudes of the forcing, are known to be of importance; see Lauterborn [34], Smereka, *et al.* [48] and Kamath & Prosperetti [30] for a discussion and examples. Note, however, that the quasi-periodic or chaotic motions described by these authors, as well as by Szeri & Leal [51], cannot be approached by the technique just described.

2.5.1 Nonlinear bubble dynamics

The method just outlined may be applied directly to any suitable model of bubble dynamics. In view of the expected importance of resonances, as shown by the numerical results of Church [10], and as a consequence of known inaccuracies of polytropic models near resonances, we make use of a more sophisticated non-polytropic bubble model. This model,

like the polytropic models, assumes that the pressure field within the bubble is uniform. However a spatially non-uniform temperature field is allowed. This requires solution of the energy equation for the gas within the bubble, which is a partial differential equation. We shall use the four-term Galerkin formulation of Kamath & Prosperetti [30]. Hence, to the bubble sub-system and driver sub-system, we append four ordinary differential equations for the amplitude coefficients of the Galerkin expansion of the temperature field. The pressure inside the bubble is given explicitly by an equation based on constant mass of gas within the bubble. These equations are given in the appendix of the paper by Kamath & Prosperetti [30]. The bubble sub-system consists of a second order ordinary differential equation which we transform into a first order system, and use the same scales as before to non-dimensionalize; this yields,

$$\frac{dx_1}{d\tau} = x_2$$

and

$$\frac{dx_2}{d\tau} = \left[3 x_2^2 \left(\frac{x_2}{3 c^*} - 1 \right) + \left(1 + \frac{x_2}{c^*} \right) (p_B^* - p^*) + \frac{x_1}{c^*} \left(\frac{8 x_2}{We x_1^2} + \frac{8 x_2^2}{Re x_1^2} - p_{Gi}^* \frac{dp_G^*(\tau)}{d\tau} \right) \right] \times \left[2 \left(1 - \frac{x_2}{c^*} \right) x_1 + \frac{8}{Re c^*} \right]^{-1},$$

where

$$p_B^* = p_{Gi}^* p_G^*(\tau) - \frac{8}{We x_1} - \frac{8 x_2}{Re x_1}$$

$$p^* = p_\infty^* \left[1 - \frac{p_A^* (1/\Omega_0 [\tau + x_1/c^*])}{p_\infty^*} \right],$$

and the dimensionless sound speed is $c^* = c/(a\Omega_0)$.

2.5.2 Threshold criterion

In figures 2.4 and 2.5 we show plots of the threshold criterion for rectified diffusion (2.25), together with some experimental points, due to Eller [18] and Crum [11] respectively.

The physical parameters are the threshold ratio of the amplitude of pressure oscillations with respect to the background pressure versus the equilibrium bubble radius. The curves in the figures are computed as follows. We begin the continuation algorithm at the

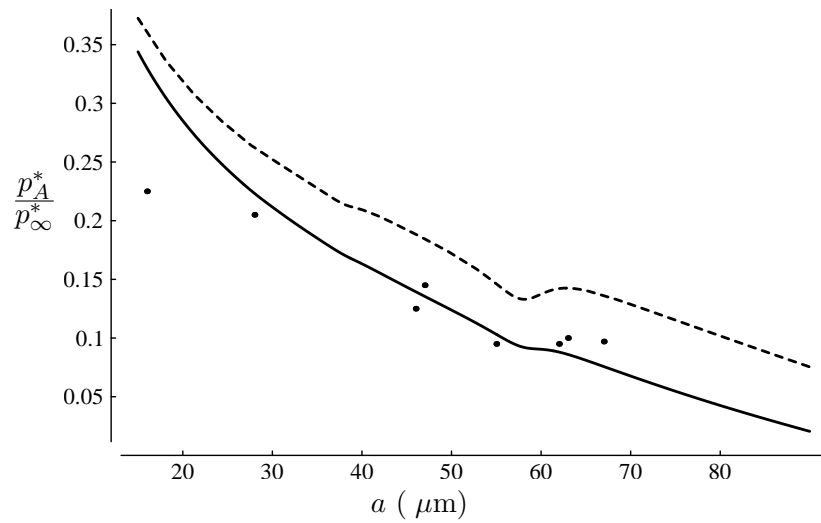


Figure 2.4: The ratio of the threshold pressure amplitude for rectified diffusion to the steady part of the background pressure versus equilibrium bubble radius. The bubbles are driven at a frequency of 26.6 kHz, and the interfacial tension is 73 dynes cm^{-1} . The dashed curve is (2.25) for saturated liquid (as reported by Eller [18]), the solid curve is (2.25) for a saturation of 101.5 % (a correction suggested by Church [10]), the points are the experimental data of Eller [18].

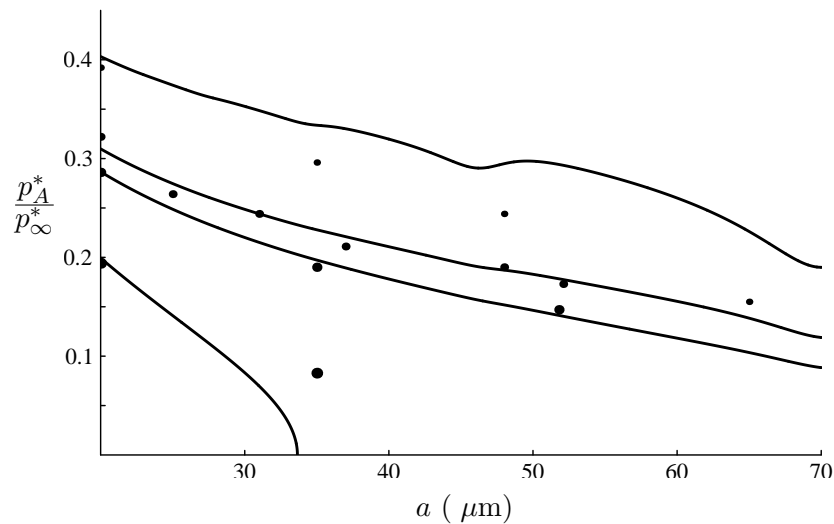


Figure 2.5: The ratio of the threshold pressure amplitude for rectified diffusion to the steady part of the background pressure versus equilibrium bubble radius for different far-field concentrations of gas in the liquid. The solid curves are (2.25), with $C_{sp}/C_\infty = 0.95$ (uppermost), 1.00, 1.01, and 1.04 (bottom). The points are the experimental data of Crum [11] at the same conditions. The bubbles are driven at a frequency of 22.1 kHz and the interfacial tension is 68 dynes cm^{-1} .

trivial (normally-hyperbolic) periodic attractor in which the driver sub-system is completely decoupled from the bubble sub-system. Thereafter, the coupling parameter, which corresponds physically to the amplitude of background pressure variations, is increased slowly from zero. While this is happening, we monitor the value of the *threshold function*, the left-hand-side of (2.25). As the pressure amplitude increases, yielding bubble oscillations of larger and larger amplitude, the threshold function smoothly passes through zero. We capture the exact value of the pressure amplitude at which the threshold function yields zero. In this way the threshold pressure amplitude is obtained for a bubble of a single equilibrium radius, without computing any transients.

From this first point, we use continuation to trace out the remainder of the threshold curve by switching tactics. The parameter corresponding to the value of the threshold function is held constant, while continuation in a takes place. An additional free parameter is required; this is met by the amplitude of pressure variations. As one can see from figures 2.4 and 2.5, the threshold pressure amplitude generally decreases with increasing equilibrium bubble radius.

Note that even with the improvements of the theory we have put forward, including a much more sophisticated means for determination of nonlinear bubble oscillations, the problem remains that the threshold condition is accurate only near saturation. In other words, the threshold amplitude of background oscillations is in error, compared with the experiments shown in figures 2.4 and 2.5, at over-and under-saturated conditions. At saturations of 1 and 1.01, the threshold results agree quite well with the experimental data of Crum. The agreement between theory and the experimental data of Eller [18], shown in figure 2.4, is not as good unless one takes as 101.5 % as the saturation of the liquid. This correction is suggested by Church [10]. While the errors may in part be due to experimental difficulties, these results may also indicate the need to account for the physical effects of surfactants on the gas transport across the dynamic interface.

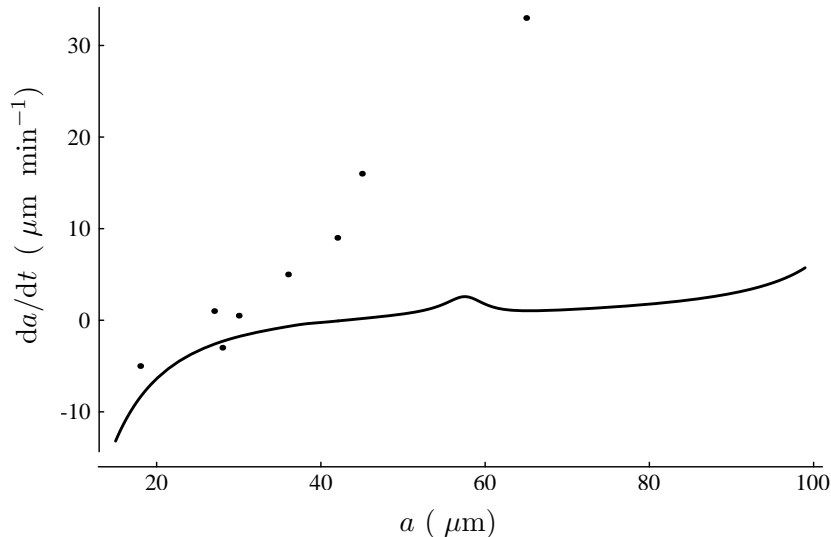


Figure 2.6: The rate of bubble growth in μm per minute versus equilibrium bubble radius in μm . The bubbles are forced at a pressure amplitude of 0.2 bar. The solid curve corresponds to (2.26), the points correspond to the experimental data of Eller [18]. The diffusivity of the gas in the liquid is $2.0 \times 10^{-5} \text{ cm}^2 \text{ sec}^{-1}$. The bubbles are driven at a frequency of 26.6 kHz, and the interfacial tension is 73 dynes cm^{-1} .

2.5.3 Rate of growth of bubbles away from threshold conditions

Finally, we turn to an investigation of the rate of growth of bubbles away from threshold conditions. Following Eller [18], the rate of growth of the equilibrium bubble radius is related to the mass transfer (given by (2.24)) as follows

$$\begin{aligned} \frac{da}{dt} &= a \Omega_0 \frac{R_G T_\infty \rho}{3 M p_0 \mathcal{P}} \left(1 + \frac{16}{3 We p_0^*}\right)^{-1} \frac{dm_{Gsm}^*}{d\lambda} \\ &= a \Omega_0 \frac{R_G T_\infty \rho}{M p_0 \mathcal{P}} \left(1 + \frac{16}{3 We p_0^*}\right)^{-1} \frac{(C_\infty - C_{sb} \langle p_G^*(\tau) \rangle_{\hat{\tau}})}{\int_0^\infty \frac{d\sigma}{\langle (3\sigma + x^3(\tau))^{(4/3)} \rangle_\tau}}. \end{aligned} \quad (2.26)$$

In figure 2.6 we show a plot of the rate of bubble growth versus equilibrium bubble radius, for bubbles forced by a background pressure field oscillating at an amplitude of 0.2 bar. Also included in the figure are the experimental points of Eller [18]. The general trend is for larger bubbles (in terms of equilibrium radius) to grow faster.

The slight bump at a just less than $60 \mu\text{m}$ corresponds to a resonance in the bubble dynamical equations. This may be seen in the bubble response curve in figure 2.7. As the

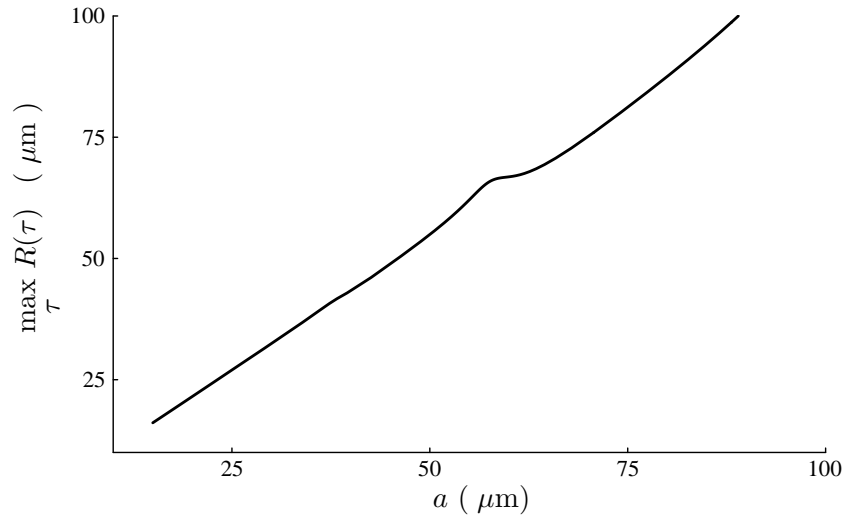


Figure 2.7: A bifurcation diagram or response curve. On the vertical axis, as a measure of the solution, we take the maximum bubble radius in μm over the period of oscillation. On the horizontal axis is the equilibrium bubble radius. The bubble oscillations are everywhere stable. The bubbles are driven at a frequency of 26.6 kHz, and the interfacial tension is 73 dynes cm^{-1} .

measure of the solution on the vertical axis, we have taken the maximum bubble radius over the periodic attractor. On the horizontal axis is the equilibrium bubble radius. For reference, in figure 2.8 we show several bubble time traces for various equilibrium bubble radii in figure 2.7.

One can observe that the bubble growth rates predicted theoretically by the methods outlined above, and plotted as the solid curve in figure 2.6, are of the same order as the experimental results. The predictions are quite good for smaller bubbles, but for larger bubbles the growth rates are quite seriously under-predicted. Contrary to the polytropic model (Appendix C) the effect of resonances is ruled out as the reason for the poor agreement between theory and experiment. It would appear that the speculations of Crum [11] and Church [10] on the importance of surfactants even in relatively clean laboratory situations cannot be overlooked in a complete description of the phenomenon of rectified diffusion.

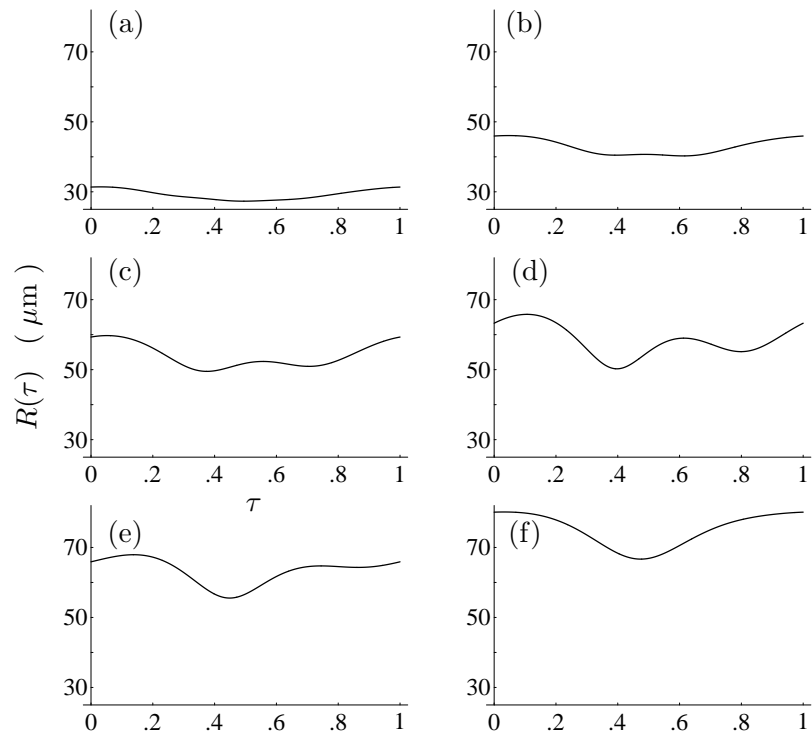


Figure 2.8: Time traces of the bubble response at various points along the branch indicated in figure 2.7. The plots show the bubble radius in μm versus dimensionless time. The equilibrium radii are (a) 32, (b) 48, (c) 53.4, (d) 57.4, (e) 62.9, and (f) 70 μm .

2.6 Conclusions

We have presented a new formulation and solution of the problem of mass transport across the dynamic interface of a soluble spherical gas bubble undergoing volume oscillations in a liquid. The validity of the methods employed depends on the Péclet number being large, for then the time scale associated with diffusion of dissolved gas through the liquid is very much longer than the time scale associated with convection of dissolved gas by the radial velocity in the liquid arising from bubble oscillations. This approach is a departure from previous theoretical analyses of the problem, in which either infinitesimal bubble oscillations or threshold conditions (or both) were assumed. The principal theoretical barriers overcome in this work are (i) how to formulate the problem for the depletion layer outside a bubble that is growing via rectified diffusion (or the excess layer outside a dissolving bubble), (ii) how to handle convection-enhanced diffusion of dissolved gas in the liquid, where the motion is driven by the bubble oscillations, and (iii) how to formulate a problem for the time-dependent part of the Henry's law boundary condition that yields a solution that differs from zero only in a thin layer of liquid near the surface of the bubble, for all time.

To accomplish these advances, we split the convection-diffusion problem into two parts: the oscillatory problem and the smooth problem. The splitting corresponds in a certain sense, to Stokes' first problem of the impulsive motion of an infinite flat plate and to Stokes' second problem of an oscillating infinite flat plate. The solutions to the oscillatory and smooth problems are valid everywhere in the liquid. The solution of the oscillatory problem is characterized by a boundary layer in the concentration field of thickness controlled by the Péclet number. The oscillatory concentration field accounts for the unsteady part of the boundary condition, but quickly approaches zero as one moves away from the bubble. The solution of the smooth problem accounts for the steady or average part of the boundary condition, as well as the net flux of dissolved gas toward or away from the oscillating bubble. As a consequence of the small diffusivity of gases in liquids, the smooth problem is efficiently treated using the method of multiple scales in time, with evolution on a slow time scale controlled by the Péclet number superposed on motion on the fast time scale associated with bubble oscillations. Unlike the work of previous authors described above,

we need assume neither small amplitude sinusoidal oscillations nor threshold conditions to solve for the concentration field using the new formulation.

Even with the progress reported here on the formulation and solution of the problem of mass transport across a dynamic interface, it seems clear after comparison with experimental results that some physics remains unaccounted for. Although the theory and experiment agree quite well for small bubbles that grow slowly in saturated liquids, the prevalence of large growth rates for strongly forced bubbles remains elusive. It would appear that a likely candidate for the remaining physics that ought to be included in a complete theory is the modification of the gas transport across the bubble surface owing to the (ubiquitous) presence of surface active materials, which is going to be investigated in the following chapter.

Chapter 3

Effect of Surfactants on Bubble Growth Rates

The techniques developed in chapter 2 are used to solve the gas transport problem associated with an oscillating bubble contaminated with surfactants. Although the governing convection-diffusion equation is the same, the boundary condition on the bubble surface is modified, to account for the effect of surfactants, and a more delicate treatment is required.

3.1 Formulation

In this section we formulate the problem for dissolution or growth of a soluble, spherical bubble undergoing volume oscillations in response to some external forcing in a liquid contaminated with surfactants. As in section 2.1, the differential equation governing the convection and diffusion of a dissolved gas in a liquid outside a spherically symmetric bubble is, in spherical polar coordinates,

$$\frac{\partial \tilde{C}}{\partial t} + \frac{R^2(t)\dot{R}(t)}{r^2} \frac{\partial \tilde{C}}{\partial r} = \frac{D}{r^2} \frac{\partial}{\partial r} \left(r^2 \frac{\partial \tilde{C}}{\partial r} \right),$$

where \tilde{C} is the mass fraction of gas dissolved in the liquid, $R^2(t)\dot{R}(t)/r^2$ is the radial velocity field in the liquid associated with the bubble oscillations, D is the diffusivity of the gas in the liquid, and the bubble radius R is a function of time t . The radius $R(t)$ may be obtained by integration of the equations of motion of the bubble. We defer any specification of these equations to section 3.6 on numerical results, and section 2.5.1 in the previous chapter. The bubble is assumed to be created in a fluid which initially has a uniform concentration of the gas \tilde{C}_∞ . Hence the initial condition and the far-field conditions are

$$\tilde{C}(r, t = 0) = \tilde{C}(r \rightarrow \infty, t) = \tilde{C}_\infty.$$

In the clean surface problem, the boundary condition is developed by application of Henry's law which relates the concentration of a gas in a liquid to the partial pressure of the gas above the liquid. In the presence of surfactants the concentration of the interface is no longer in equilibrium. The surfactant monolayer affects the mass transfer characteristics of the interface, both at the microscopic and at the macroscopic level, a fact established by numerous experiments [39, 21, 55, 42]. The Henry's law boundary condition of the clean surface problem (boundary condition of the first kind) is replaced by a flux boundary condition of the third kind in which the nonequilibrium partitioning of the gas across the interface is the driving force behind mass transport through the surfactant monolayer. In the present analysis we employ the interfacial resistance model suggested by Plevan & Quinn [42]. This model was placed on firmer theoretical ground by Borwankar & Wasan [6] using the microscopic approach of Brenner & Leal [7]. The result is that the flux through the interface is proportional to the difference of the surface concentration and the equilibrium concentration (given by Henry's law); this is expressed mathematically as

$$D \frac{\partial \tilde{C}(r = R(t), t)}{\partial r} = \frac{1}{\tilde{R}_I} \left(\tilde{C}(r = R(t), t) - \frac{p_G(t)}{k} \right).$$

Here $p_G(t)$ is the partial pressure of the gas and k is the (equilibrium partition) constant of Henry's law. The constant of proportionality \tilde{R}_I measures the resistance of the monolayer, *i.e.* if $\tilde{R}_I \rightarrow 0$ the clean surface problem is recovered (Chapter 2). In general, \tilde{R}_I depends strongly on the concentration of surfactants on the interface; for the present we shall treat it as a general function of time, $\tilde{R}_I = \tilde{R}_I(t)$. We develop an explicit form for $\tilde{R}_I(t)$ in section 3.5 below.

As in Chapter 2 the transport problem is recast in dimensionless, Lagrangian coordinates to yield

$$\frac{\partial C}{\partial \tau} = \frac{1}{\mathcal{P}} \frac{\partial}{\partial \sigma} \left(\left(3\sigma + x^3(\tau) \right)^{(4/3)} \frac{\partial C}{\partial \sigma} \right), \quad (3.1)$$

with boundary and initial conditions

$$\frac{x^2(\tau) R_I(\tau)}{\mathcal{P}} \frac{\partial C(\sigma = 0, \tau)}{\partial \sigma} = C(\sigma = 0, \tau) - (C_{sb} p_G^*(\tau) - C_\infty), \quad (3.2)$$

$$C(\sigma, \tau = 0) = C(\sigma \rightarrow \infty, \tau) = 0.$$

The scales for nondimensionalization are a , the radius of the undisturbed bubble, and Ω_0^{-1} , the inverse natural frequency of radial oscillations of the bubble about the undisturbed state. The dimensionless parameters introduced are the Péclet number ($\mathcal{P} = a^2\Omega_0/D$), which is the ratio between the time scales for convection and diffusion; the dimensionless bubble radius $x(\tau)$; and the dimensionless interfacial resistance, $R_I(\tau) = \tilde{R}_I(t/\Omega_0) a\Omega_0$. As explained in Chapter 2, if the initial pressure inside the bubble is used to non-dimensionalize Henry's constant we get the dimensionless parameter $C_{sb} = p_{Gi}/k$, which corresponds to the saturation concentration in the liquid separated from a gas within a spherical bubble with initial pressure p_{Gi} . The dimensionless Lagrangian coordinate is

$$\sigma \equiv \frac{1}{3} \left(\frac{r^3}{a^3} - x^3(\tau) \right).$$

We have subtracted the concentration at infinity from the concentration field, *i.e.*, $C = \tilde{C} - \tilde{C}_\infty$.

3.2 Oscillatory problem

Following the analysis in Chapter 2 we shall split the problem in two, in order to handle the complicated boundary condition. We proceed to split the time-dependent boundary condition into a constant and an oscillating part, making use of the linearity of the problem for the concentration field. The constant part of the boundary condition is associated with the *smooth problem* (C_{sm}) and the oscillating part of the boundary condition with the *oscillatory problem* (C_{osc}).

Because the convection-diffusion equation for C is linear, the splitting is not unique. The splitting is defined by requiring the solution to the oscillatory problem to be different from zero only in a thin layer near the bubble surface in a way that is uniformly valid in time (see section 2.2). This was accomplished to leading order in the small parameter $\mathcal{P}^{-1/2}$. In effect, this procedure places a restriction on what part of the total boundary condition we can ascribe to the oscillatory problem, in order that it should be nonzero in only a thin layer near the bubble surface. The remainder of the boundary condition is satisfied by the

smooth solution, which is permitted to be nonzero away from the bubble surface. We treat the oscillatory problem using the method of matched asymptotic expansions. The outer approximation to the solution of the oscillatory problem is identically zero by construction if we restrict the boundary condition of the oscillatory problem in such a way as to have the outer limit of the inner approximation be zero. In this case, the inner approximation to the solution of the oscillatory problem is uniformly valid in space.

To begin the splitting, we transform the problem (3.1) into the oscillatory form using (i) the nonlinear time $\hat{\tau}$, developed by Plesset & Zwick [41] and later used by Eller & Flynn [20]:

$$\hat{\tau}(\tau) \equiv \int_0^\tau x^4(\theta) d\theta,$$

and (ii) the re-scaled Lagrangian coordinate $s = \mathcal{P}^{1/2}\sigma$. The result is:

$$\frac{\partial C_{osc}}{\partial \hat{\tau}} = \frac{\partial}{\partial s} \left(\left(\frac{3s}{x^3(\hat{\tau})\mathcal{P}^{1/2}} + 1 \right)^{(4/3)} \frac{\partial C_{osc}}{\partial s} \right). \quad (3.3)$$

Next we assume an expansion of the form

$$C_{osc} = C_{osc}^0(s, \hat{\tau}) + \frac{1}{\mathcal{P}^{1/2}} C_{osc}^1(s, \hat{\tau}) + \frac{1}{\mathcal{P}} C_{osc}^2(s, \hat{\tau}) + \dots,$$

together with a similar expansion for the smooth problem, and use the binomial theorem to expand equation (3.3) for large \mathcal{P} (small $\mathcal{P}^{-1/2}$). To zeroth and first order we have

$$\begin{aligned} \frac{\partial C_{osc}^0}{\partial \hat{\tau}} &= \frac{\partial^2 C_{osc}^0}{\partial s^2} \\ C_{osc}^0(s=0, \hat{\tau}) &= C_{sb} p_G^*(\hat{\tau}) - C_\infty - C_{sm}^0(\sigma=0, \hat{\tau}), \end{aligned} \quad (3.4)$$

and

$$\begin{aligned} \frac{\partial C_{osc}^1}{\partial \hat{\tau}} &= \frac{\partial^2 C_{osc}^1}{\partial s^2} + \frac{4}{x^3(\hat{\tau})} \frac{\partial}{\partial s} \left(s \frac{\partial C_{osc}^0}{\partial s} \right) \\ C_{osc}^1(s=0, \hat{\tau}) &= x^2(\hat{\tau}) R_I(\hat{\tau}) \frac{\partial \bar{C}_{osc}^0(s=0, \hat{\tau})}{\partial s} - C_{sm}^1(\sigma=0, \hat{\tau}), \end{aligned} \quad (3.5)$$

respectively. In (3.4) and (3.5) we have introduced the extra terms, $C_{sm}^0(\sigma=0, \hat{\tau})$ and $C_{sm}^1(\sigma=0, \hat{\tau})$ to aid in splitting the problem. Effectively, in (3.4) and (3.5) we write the boundary condition of the oscillatory problem at a given order in $\mathcal{P}^{-1/2}$ as the full boundary

condition at that order minus the boundary condition of the smooth problem at that order. $C_{sm}^0(\sigma = 0, \hat{\tau})$ and $C_{sm}^1(\sigma = 0, \hat{\tau})$ are the constant parts of the boundary condition that we shall use in order to satisfy the conditions for the splitting.

The next step is to ensure that the long-time asymptotic solutions (indicated by an overbar), \bar{C}_{osc}^0 and \bar{C}_{osc}^1 , are uniformly valid in space and do not require an outer expansion. This is achieved by forcing the “outer” limit of \bar{C}_{osc}^0 and \bar{C}_{osc}^1 , *i.e.* as $s \rightarrow \infty$, to be zero. As a result, the outer approximation for the oscillatory problem leads to a homogeneous problem with both boundary conditions and initial condition zero.

As we shall see, the oscillatory problem contributes very little to the mass transport across the bubble surface. An expression for the amount of mass transfer is

$$m_G^*(\hat{\tau}) - m_G^*(0) = \frac{1}{\mathcal{P}} \int_0^{\hat{\tau}} \frac{\partial C(\sigma = 0, \hat{\tau}')}{\partial \sigma} d\hat{\tau}',$$

where m_G^* is the mass of the gas in the bubble divided by the mass of liquid displaced by the undisturbed bubble. A more useful expression can be easily obtained from the differential equation for the concentration field (3.1) by two integrations; one in s from zero to infinity and one in $\hat{\tau}$

$$m_G^*(\hat{\tau}) - m_G^*(0) = - \int_0^{\infty} C(\sigma', \hat{\tau}) d\sigma'. \quad (3.6)$$

3.2.1 Zeroth order oscillatory problem

The zeroth order problem is presented in detail in section 2.2 where it was shown that the outer limit of the zeroth order oscillatory problem is zero, if the average of the boundary condition with respect to the time $\hat{\tau}$ is zero, *i.e.* $\langle C_{osc}^0(0, \hat{\tau}) \rangle_{\hat{\tau}} = 0$. The average $\langle \cdot \rangle_{\hat{\tau}}$ is defined by

$$\langle f(\sigma, \hat{\tau}) \rangle_{\hat{\tau}} \equiv \frac{1}{\hat{\tau}(T)} \int_0^{\hat{\tau}(T)} f(\sigma, \hat{\tau}) d\hat{\tau} = \frac{1}{\int_0^T x^4(\tau) d\tau} \int_0^T f(\sigma, \tau) x^4(\tau) d\tau,$$

where T is the dimensionless period of bubble oscillation. Hence the boundary conditions for C_{osc}^0 and C_{sm}^0 are determined from (3.4) to be

$$C_{osc}^0(s = 0, \hat{\tau}) = C_{sb} [p_G^*(\hat{\tau}) - \langle p_G^*(\hat{\tau}) \rangle_{\hat{\tau}}]$$

and

$$C_{sm}^0(\sigma = 0, \tau) = C_{sb} \langle p_G^*(\hat{\tau}) \rangle_{\hat{\tau}} - C_{\infty}, \quad (3.7)$$

respectively. The asymptotic solution \bar{C}_{osc}^0 is very quickly approached within a few periods of bubble oscillation; it is easily computed using Fourier series. The result is the same as the clean bubble problem treated in section 2.2:

$$\begin{aligned} \bar{C}_{osc}^0(s, \hat{\tau}) = & \sum_{m=1}^{\infty} \exp \left[- \left(\frac{\omega_m}{2} \right)^{1/2} s \right] \times \\ & \left\{ a_m \cos \left[\omega_m \hat{\tau} - \left(\frac{\omega_m}{2} \right)^{1/2} s \right] + b_m \sin \left[\omega_m \hat{\tau} - \left(\frac{\omega_m}{2} \right)^{1/2} s \right] \right\}, \end{aligned} \quad (3.8)$$

where a_m and b_m are the expansion coefficients of the boundary condition

$$\begin{aligned} \bar{C}_{osc}^0(s = 0, \hat{\tau}) &= C_{sb} [p_G^*(\hat{\tau}) - \langle p_G^*(\hat{\tau}) \rangle_{\hat{\tau}}] \\ &= \sum_{m=1}^{\infty} [a_m \cos(\omega_m \hat{\tau}) + b_m \sin(\omega_m \hat{\tau})] \end{aligned}$$

and

$$\omega_m = \frac{2m\pi}{\hat{\tau}(T)}.$$

The long-time rate of mass transport is determined from (3.6). The zeroth order oscillatory problem \bar{C}_{osc}^0 does not contribute to any net bubble growth or dissolution, because the mass transport is a periodic function of time ($\hat{\tau}$) with zero mean.

3.2.2 First order oscillatory problem

The condition for uniform validity of \bar{C}_{osc}^1 (3.5) is not so straightforward to obtain as a consequence of the inhomogeneous term. In Appendix D we show that the condition for uniform validity of the oscillatory problem is

$$\langle C_{osc}^i(s = 0, \hat{\tau}) \rangle_{\hat{\tau}} = \int_0^{\infty} \int_{-\infty}^{s'} \langle F^i(s'') \rangle_{\hat{\tau}} ds'' ds',$$

where F^i is the inhomogeneous term (forcing term) associated with i th order oscillatory problem. The resulting condition for the C_{osc}^1 problem is

$$\langle \bar{C}_{osc}^1(0, \hat{\tau}) \rangle_{\hat{\tau}} = - \left\langle \frac{4}{x^3(\hat{\tau})} \int_0^{\infty} \bar{C}_{osc}^0(s', \hat{\tau}) ds' \right\rangle_{\hat{\tau}}. \quad (3.9)$$

Hence the parts of the total boundary conditions ascribed to C_{osc}^1 and C_{sm}^1 are determined from (3.5) to be

$$C_{osc}^1(s=0, \hat{\tau}) = x^2(\hat{\tau})R_I(\hat{\tau})\frac{\partial\bar{C}_{osc}^0(s=0, \hat{\tau})}{\partial s} - \left(\left\langle x^2(\hat{\tau})R_I(\hat{\tau})\frac{\partial\bar{C}_{osc}^0(s=0, \hat{\tau})}{\partial s} \right\rangle_{\hat{\tau}} + \left\langle \frac{4}{x^3(\hat{\tau})} \int_0^\infty \bar{C}_{osc}^0(s', \hat{\tau})ds' \right\rangle_{\hat{\tau}} \right)$$

and

$$C_{sm}^1(\sigma=0, \tau) = \left\langle x^2(\hat{\tau})R_I(\hat{\tau})\frac{\partial\bar{C}_{osc}^0(s=0, \hat{\tau})}{\partial s} \right\rangle_{\hat{\tau}} + \left\langle \frac{4}{x^3(\hat{\tau})} \int_0^\infty \bar{C}_{osc}^0(s', \hat{\tau})ds' \right\rangle_{\hat{\tau}}, \quad (3.10)$$

respectively. The asymptotic solution \bar{C}_{osc}^1 is not required in the present analysis as our intent is to solve the smooth problem through order $\mathcal{P}^{-1/2}$. The solution can be obtained using Fourier series.

To compute the amount of mass transfer due to the first order oscillatory problem we use (3.6) and recall that the mean part of the long-time asymptotic solution \bar{C}_{osc}^1 decays exponentially as shown in Appendix D. Hence, the first order oscillatory problem contributes very little to the transport, and then only in the initial stages.

3.3 The smooth problem

The *smooth problem* is defined by

$$\frac{\partial C_{sm}}{\partial \tau} = \frac{1}{\mathcal{P}} \frac{\partial}{\partial \sigma} \left((3\sigma + x^3(\tau))^{(4/3)} \frac{\partial C_{sm}}{\partial \sigma} \right), \quad (3.11)$$

with the boundary condition (obtained by the sum of 3.7 and 3.10)

$$\frac{x^2(\tau)R_I(\tau)}{\mathcal{P}} \frac{\partial C_{sm}(\sigma=0, \tau)}{\partial \sigma} = C_{sm}(\sigma=0, \tau) - [C_{sb} \langle p_G^*(\hat{\tau}) \rangle_{\hat{\tau}} - C_\infty] - \frac{1}{\mathcal{P}^{1/2}} \left[\left\langle x^2(\hat{\tau})R_I(\hat{\tau})\frac{\partial\bar{C}_{osc}^0(s=0, \hat{\tau})}{\partial s} \right\rangle_{\hat{\tau}} + \left\langle \frac{4}{x^3(\hat{\tau})} \int_0^\infty \bar{C}_{osc}^0(s', \hat{\tau})ds' \right\rangle_{\hat{\tau}} \right] + \mathcal{O}(\mathcal{P}^{-1}) \quad (3.12)$$

and initial condition

$$C_{sm}(\sigma, \tau=0) = C_{sm}(\sigma \rightarrow \infty, \tau) = 0.$$

The smooth boundary condition (3.12) includes terms of order $\mathcal{P}^{-1/2}$ and represents a higher order correction to our earlier solution in Chapter 2, in the case of a clean surface.

In the clean surface problem ($R_I(\tau) = 0$) the additional term presents a small correction as it is multiplied by $\mathcal{P}^{-1/2}$ which is very small at conditions of practical interest. As we shall demonstrate, the correction is not small in the surfactant-covered surface problem because $R_I(\tau)$ happens to be of the same magnitude as $\mathcal{P}^{1/2}$ in the physical problems of interest.

The smooth problem is treated by the method of multiple scales in time. Similar to section 2.3 we introduce a second time scale $\lambda \equiv \tau/\mathcal{P} = tD/a^2$, which captures the slow diffusive behavior and define a second (conventional) time average with respect to the fast time τ ,

$$\langle f(\sigma, \tau) \rangle_\tau \equiv \frac{1}{T} \int_0^T f(\sigma, \tau) d\tau. \quad (3.13)$$

Equation (3.11) transforms to

$$\frac{\partial C_{sm}}{\partial \tau} + \frac{1}{\mathcal{P}} \frac{\partial C_{sm}}{\partial \lambda} = \frac{1}{\mathcal{P}} \frac{\partial}{\partial \sigma} \left((3\sigma + x^3(\tau))^{(4/3)} \frac{\partial C_{sm}}{\partial \sigma} \right).$$

Next we expand

$$C_{sm}(\sigma, \tau) = C_{sm}^0(\sigma, \lambda, \tau) + \frac{1}{\mathcal{P}^{1/2}} C_{sm}^1(\sigma, \lambda, \tau) + \frac{1}{\mathcal{P}} C_{sm}^2(\sigma, \lambda, \tau) + \frac{1}{\mathcal{P}^{3/2}} C_{sm}^3(\sigma, \lambda, \tau) + \dots$$

Note that we must expand the smooth problem in powers of $\mathcal{P}^{-1/2}$ in view of the asymptotic sequence in the boundary condition (3.12). Upon substituting in our expansion for C_{sm} and equating coefficients of like powers of $\mathcal{P}^{-1/2}$, we obtain a sequence of problems for C_{sm}^i for $i = 0, 1, 2, \dots$. We remark that the $C_{sm}^0 - C_{sm}^2$ problems decouple from $C_{sm}^1 - C_{sm}^3$. To zeroth and first order in the small parameter $\mathcal{P}^{-1/2}$, we have the systems

$$\frac{\partial C_{sm}^i}{\partial \tau} = 0, \quad \text{where } i = 0, 1 \quad (3.14)$$

with boundary and initial conditions

$$\begin{aligned} C_{sm}^0(\sigma = 0, \lambda, \tau) &= C_{sb} \langle p_G^*(\hat{\tau}) \rangle_{\hat{\tau}} - C_\infty, \\ C_{sm}^1(\sigma = 0, \lambda, \tau) &= \left[\left\langle x^2(\hat{\tau}) R_I(\hat{\tau}) \frac{\partial C_{osc}^0(s=0, \hat{\tau})}{\partial s} \right\rangle_{\hat{\tau}} + \left\langle \frac{4}{x^3(\hat{\tau})} \int_0^\infty C_{osc}^0(s', \hat{\tau}) ds' \right\rangle_{\hat{\tau}} \right], \\ C_{sm}^i(\sigma, \lambda = 0, \tau = 0) &= C_{sm}^i(\sigma \rightarrow \infty, \lambda, \tau) = 0, \quad i = 0, 1. \end{aligned}$$

The solution to the zeroth and first order problems (3.14) is simply $C_{sm}^i(\sigma, \lambda, \tau) = C_{sm}^i(\sigma, \lambda)$, $i = 0, 1$. However C_{sm}^i is further determined by ensuring that there is no secular behavior

in C_{sm}^{i+2} , lest the expansion become disordered as τ increases. Hence we force the right-hand side of the second and third order problems to have zero τ -average (defined in (3.13)); this leads to a second equation for C_{sm}^i ($i = 0, 1$)

$$\frac{\partial C_{sm}^i}{\partial \lambda} = \frac{\partial}{\partial \sigma} \left(\left\langle \left(3\sigma + x^3(\tau) \right)^{(4/3)} \right\rangle_{\tau} \frac{\partial C_{sm}^i}{\partial \sigma} \right).$$

The smooth problem has a very straightforward asymptotic solution $\bar{C}_{sm}^i(\sigma)$ (indicated by an overbar) in the limit $\lambda \rightarrow \infty$, developed in section 2.3:

$$\bar{C}_{sm}^i(\sigma) = C_{sm}^i(\sigma = 0) \left[1 - \frac{\int_0^{\sigma} \frac{d\sigma'}{\left\langle \left(3\sigma' + x^3(\tau) \right)^{(4/3)} \right\rangle_{\tau}}}{\int_0^{\infty} \frac{d\sigma}{\left\langle \left(3\sigma + x^3(\tau) \right)^{(4/3)} \right\rangle_{\tau}}} \right], \quad (3.15)$$

which is valid for any nonlinear periodic bubble oscillation. The asymptotic solution for the (smooth) concentration field and for the rate of mass transport up to first order in $\mathcal{P}^{-1/2}$ may be expressed as

$$\bar{C}_{sm}(\sigma) = \bar{C}_{sm}(0) \left[1 - \frac{\int_0^{\sigma} \frac{d\sigma'}{\left\langle \left(3\sigma' + x^3(\tau) \right)^{(4/3)} \right\rangle_{\tau}}}{\int_0^{\infty} \frac{d\sigma}{\left\langle \left(3\sigma + x^3(\tau) \right)^{(4/3)} \right\rangle_{\tau}}} \right] \quad (3.16)$$

and

$$\frac{d\bar{m}_{Gsm}^*(\lambda)}{d\lambda} = -3 \frac{\bar{C}_{sm}(0)}{\int_0^{\infty} \frac{d\sigma}{\left\langle \left(3\sigma + x^3(\tau) \right)^{(4/3)} \right\rangle_{\tau}}}, \quad (3.17)$$

respectively, where $\bar{C}_{sm}(0)$ is the threshold condition for rectified diffusion

$$\bar{C}_{sm}(0) = C_{sb} \langle p_G^*(\hat{\tau}) \rangle_{\hat{\tau}} - C_{\infty} + \frac{1}{\mathcal{P}^{1/2}} \left[\left\langle x^2(\hat{\tau}) R_I(\hat{\tau}) \frac{\partial \bar{C}_{osc}^0(s=0, \hat{\tau})}{\partial s} \right\rangle_{\hat{\tau}} + \left\langle \frac{4}{x^3(\hat{\tau})} \int_0^{\infty} \bar{C}_{osc}^0(s', \hat{\tau}) ds' \right\rangle_{\hat{\tau}} \right] + \mathcal{O}(\mathcal{P}^{-1}) \quad (3.18)$$

and \bar{C}_{osc}^0 is the zeroth order asymptotic solution (3.8) of the oscillatory problem. In section 3.5 we turn to consideration of $R_I(\tau)$ before evaluating these expressions for specific physical problems.

3.4 Effect of surfactants on a still bubble

In the absence of pressure oscillations the bubble is still; the transport problem (3.1) simplifies because $x(\tau) = 1$ and $R_I(\tau)$ is constant. At steady state *i.e.* $\partial C/\partial \tau = 0$, the rate of mass transport is readily determined:

$$\frac{dm_G^*}{d\lambda} = -3 \frac{[C_{sb} - C_\infty]}{(1 + R_I/\mathcal{P})}.$$

Because R_I is a positive number, the effect of a surfactant is to reduce mass transport and hence to suppress both growth or dissolution.

When \mathcal{P} is large the growth rate simplifies to

$$\frac{dm_G^*}{d\lambda} = -3 [C_{sb} - C_\infty] \left(1 - \frac{R_I}{\mathcal{P}}\right), \quad (3.19)$$

which reveals two important differences between a still and an oscillating bubble. For the former, surfactants inhibit mass transport and their effect appears at $\mathcal{O}(\mathcal{P}^{-1})$. In the case of an oscillating bubble however, the effect of a surfactant appears at $\mathcal{O}(\mathcal{P}^{-1/2})$, and, as we show in section 3.6, surfactants might enhance or reduce mass transport depending on the way in which R_I depends on the surface concentration of the surfactant.

3.5 Interfacial Resistance

A surfactant molecule consists of a hydrophobic and a hydrophilic portion; as a consequence surfactant molecules tend to accumulate at a gas-liquid interface. In a set of experiments of great significance to the present work, Crum [11] demonstrated that the addition of small amounts of surfactant to the liquid in which a bubble was suspended had a very significant effect on the growth rate of the bubble by rectified diffusion. These were preliminary experiments; it appears that the intentional addition of surfactants was for the purpose of supporting speculation on the inability of the theory adequately to explain the large growth rates of large bubbles by rectified diffusion. Crum made use of a commercially available surfactant known by the trade name *Photoflo 200* –which is commonly employed

in photographic processing. We are advised that this formulated product contains a number of other, unspecified components in addition to the surfactant ethoxylated octylphenol. Moreover, there are statistical distributions of chain length of the hydrophobic end and of the oxyethylene hydrophilic end of the surfactants. The interfacial resistance properties of this product do not appear to have been characterized. Therefore it does not seem possible to compare the theoretical predictions we can now make regarding bubble growth rates in the presence of surfactants with the experimental results of Crum. Clearly this is an area to pursue in future work.

In the present work, we shall have to content ourselves with the development of theoretical predictions of bubble growth rates for surfactant systems that are well-characterized. We shall show that the theoretical prediction for these surfactant systems yields growth rates of bubbles that are significantly larger than growth rates for clean bubbles.

Therefore, using experimental results by Caskey & Barlage [8, 9], we shall obtain simple expressions that relate surfactant surface concentrations with interfacial resistances and surface tensions for three surfactant systems. The former is needed for the calculation of the mass transport (3.17) and threshold (3.18) and the latter in the model for the dynamical equations for bubble oscillations.

A general treatment for surfactant transport along a deforming interface presents a formidable task. This would require a transport equation for the bulk and surface-excess quantities of surfactant and a constitutive relation for nonequilibrium partitioning of a soluble surfactant between interface and bulk [17].

Assuming insoluble surfactant [50], the resulting equation for the surface concentration yields

$$\rho_i^s(\tau)x(\tau)^2 = \text{const} = \rho_i^s(\tau = 0),$$

where $\rho_i^s(\tau)$ is the surface surfactant concentration, $x(\tau)$ is the dimensionless bubble radius and $\rho_i^s(\tau = 0)$ the initial concentration. Finally, we note that $R_I(\tau)$ is then a function of $\rho_i^s(\tau)$, or equivalently of $\rho_i^s(\tau = 0)/x(\tau)^2$.

We shall make use of experimental results for three surfactants:

- (a) dodecyltrimethylammonium chloride ($C_{12}H_{25}N(CH_3)_3Cl$),
- (b) hexadecyltrimethylammonium chloride ($C_{16}H_{33}N(CH_3)_3Cl$) and
- (c) dodecyl sodium sulfate ($C_{12}H_{25}SO_4Na$).

To obtain an expression for the interfacial resistance as a function of surface concentration we developed straightforward exponential fits to the data in figure 3 of Caskey & Barlage [9]; this procedure seems to yield adequate approximations, as shown in figure 3.1.

Finally, a remark concerning the numerical results we present below is in order. When we make use of the experimental data of Caskey & Barlage, we take great care in remaining within the ranges of surfactant surface concentration at which the interfacial resistance is known. This implies a restriction on the amplitudes of driving pressure that we may consider; however, it is important to base our numerical results on hard evidence rather than on pure extrapolation.

Because interfacial tension does not vary significantly with surfactant surface concentration we use an average value of 60 dynes cm^{-1} obtained from figure 5 of Caskey & Barlage [8].

3.6 Theoretical predictions of bubble growth rates

Now we shall evaluate the expression we have developed for the growth rate of a surfactant-covered bubble via the mechanism of rectified diffusion. The last component required for the evaluation of the growth rate is the periodic bubble motion $R(t)$. There are numerous mathematical models for bubble oscillations as reviewed by Plesset & Prosperetti [40]. For rectified diffusion calculations, polytropic models have been used in the vast majority of studies. However, a comparison in Appendix C showed a dramatic difference near resonance in the solution of the clean surface transport problem between polytropic and a more accurate non-polytropic model. Consequently we shall use the four term Galerkin formulation of Kamath & Prosperetti [30] in which the polytropic assumption for the bubble

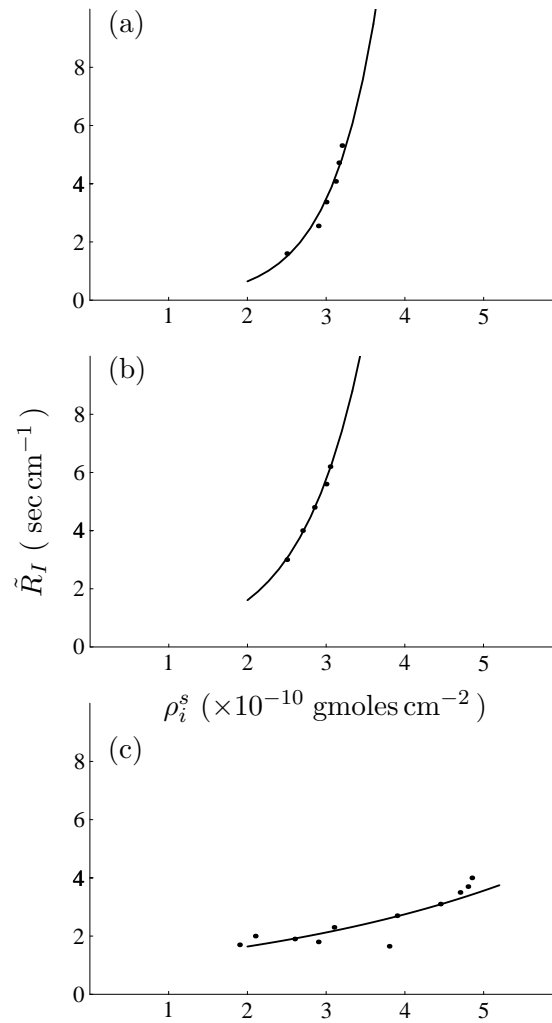


Figure 3.1: Interfacial resistance \tilde{R}_I in sec cm^{-1} versus surfactant surface concentration ρ_i^s in $10^{-10} \text{ gmoles cm}^{-2}$. The points correspond to the experimental data of Caskey & Barlage [9] and the solid line to an exponential curve fit. The surfactants are (a) dodecyltrimethylammonium chloride ($C_{12}H_{25}N(CH_3)_3Cl$), (b) hexadecyltrimethylammonium chloride ($C_{16}H_{33}N(CH_3)_3Cl$) and (c) dodecyl sodium sulfate ($C_{12}H_{25}SO_4Na$). The fits are (a) $\tilde{R}_I = 0.022 \exp(1.68 \rho_i^s)$, (b) $\tilde{R}_I = 0.13 \exp(1.26 \rho_i^s)$, (c) $\tilde{R}_I = 0.72 \exp(0.36 \rho_i^s)$.

internal pressure is relaxed and thermal effects are included. This model, like the polytropic models, assumes that the pressure field within the bubble is uniform. However a spatially non-uniform temperature field is allowed. This spatial nonuniformity requires solution of the energy equation for the gas within the bubble, which is a partial differential equation.

Hence, to the bubble dynamical equations we append four ordinary differential equations for the amplitude coefficients of the Galerkin expansion of the temperature field. The pressure inside the bubble is given explicitly by an equation based on constant mass of gas within the bubble. These equations are given in the appendix of the paper by Kamath & Prosperetti [30]. The bubble dynamical equations are $x_1 \equiv x$,

$$\frac{dx_1}{d\tau} = x_2,$$

and

$$\begin{aligned} \frac{dx_2}{d\tau} = & \left[3 x_2^2 \left(\frac{x_2}{3 c^*} - 1 \right) + \left(1 + \frac{x_2}{c^*} \right) (p_B^* - p^*) + \right. \\ & \left. \frac{x_1}{c^*} \left(\frac{8 x_2}{We x_1^2} + \frac{8 x_2^2}{Re x_1^2} - p_{Gi}^* \frac{dp_G^*(\tau)}{d\tau} \right) \right] \times \left[2 \left(1 - \frac{x_2}{c^*} \right) x_1 + \frac{8}{Re c^*} \right]^{-1} \end{aligned}$$

where

$$\begin{aligned} p_B^* &= p_{Gi}^* p_G^*(\tau) - \frac{8}{We x_1} - \frac{8 x_2}{Re x_1}, \\ p^* &= p_\infty^* \left[1 - \frac{p_A^* \left(\Omega_0^{-1} [\tau + x_1/c^*] \right)}{p_\infty^*} \right], \end{aligned}$$

c^* is the dimensionless sound speed, We denotes the Weber number, and Re the Reynolds number. Finally, we add two more nonlinear ODEs which yield the oscillatory part of the background pressure that drives the bubble oscillation. The details are in section 2.5.1. The system of eight nonlinear ODEs is integrated numerically using the software AUTO [16]. To ensure that the four-term Galerkin expansion is accurate enough we stop the calculation if one of the amplitude coefficients is not at least one order of magnitude less than the preceding one. For the bubble radii used in our calculations, *i.e.* 20, 40 and 60 μm , we had to stop the integration at a dimensionless pressure amplitude of 0.5.

Following Eller [18], the dimensional rate of growth of the equilibrium bubble radius is related to the mass transfer as follows

$$\begin{aligned} \frac{da}{dt} &= a \Omega_0 \frac{R_G T_\infty \rho}{3 M p_0} \frac{1}{\mathcal{P}} \left(1 + \frac{16}{3 We p_0^*}\right)^{-1} \frac{d\bar{m}_{G_{sm}}^*}{d\lambda} \\ &= a \Omega_0 \frac{R_G T_\infty \rho}{M p_0} \frac{1}{\mathcal{P}} \left(1 + \frac{16}{3 We p_0^*}\right)^{-1} \frac{-3\bar{C}_{sm}(0)}{\int_0^\infty \frac{d\sigma}{\langle (3\sigma + x^3(\tau))^{(4/3)} \rangle_\tau}}, \end{aligned} \quad (3.20)$$

where $\bar{C}_{sm}(0)$ is the threshold condition given by equation (3.18); $R_G = 8314$ J/kmol K is the universal gas constant, $T_\infty = 300$ K is the temperature of the liquid at the far field, $\rho = 1.0$ gm cm⁻³ is the liquid density, $M = 29$ kmol/kg is the molecular weight of the gas and $p_0 = 1 \times 10^6$ dynes cm⁻² is the background pressure.

In figures 3.2-3.4 we show plots of predicted bubble growth rates versus dimensionless pressure amplitude for bubbles of radius 20, 40 and 60 μ m respectively. The upper plot in each of these figures consists of a magnification of the vertical axis near zero growth rate (which corresponds to the threshold for rectified diffusion). In all cases, the curves showing bubble growth rates correspond to dynamic surfactant surface concentrations within the ranges over which we know the interfacial resistance from the work of Caskey & Barlage.

The solid curves show the effect of the three different surfactants on the bubble growth rates. As we mentioned previously, surfactants can affect bubble growth rates through two mechanisms: (i) reduction of interfacial tension, and (ii) introduction of interfacial resistance to mass transfer. Of these, the latter is the far more significant effect, as demonstrated in the figures where we plot the growth rates as modified by both mechanisms (solid curves) and by only the reduction in surface tension (long-dashed curves). The clean surface results are shown using the short-dashed curves. Reduction of surface tension contributes only to a small upward shift of the growth rate curve, a result first noted by Crum [11], and cannot justify the high bubble growth rates observed in experiments. This observation suggests that the ‘‘missing physics’’ which accounts for the difference between theoretical predictions and experimental results for growth rates by rectified diffusion is the effect of interfacial resistance on mass transfer. This finding would appear to bear out the speculations of Crum

and of Church, to which we made earlier reference, on the importance of surfactants to the phenomenon of rectified diffusion.

It is also of considerable interest to note that surfactants are not only responsible for higher growth rates but might tend to favor dissolution of bubbles as one can see in figure 3.2 curve c. This fact is further clarified by the following investigation. In figure 3.5 we show the effect of initial surface concentration of the surfactant hexadecyltrimethylammonium chloride ($C_{16}H_{33}N(CH_3)_3Cl$) on bubble growth rates, for a bubble of radius $20 \mu\text{m}$. There is a dramatic effect of a slight increase of initial surface concentration on bubble growth rates. Clearly, higher concentration of surfactant appears to favor growth of bubbles for this surfactant.

The principal effect of changing the initial concentration of surfactant is to move up or down the exponential curve of interfacial resistance. At larger concentrations, the interfacial resistance changes more rapidly with concentration. This behavior leads one to conclude that if the interfacial resistance versus surface concentration curve for one surfactant is steeper than for another, then the first surfactant will tend to promote bubble growth more than the second. These statements are in agreement with the predictions we have made thus far, and with the following.

We shall assume a general form for the interfacial resistance

$$\tilde{R}_I(\tau) = \exp\left(\frac{\alpha}{x^2(\tau)}\right), \quad (3.21)$$

and investigate the effect of interfacial resistance on bubble growth rates for different values of the exponent α and a fixed bubble oscillation. For these calculations we use equation (3.20) but include only the interfacial resistance term in $\bar{C}_{sm}(0)$:

$$\frac{1}{\mathcal{P}^{1/2}} \left[\left\langle x^2(\hat{\tau}) R_I(\hat{\tau}) \frac{\partial \bar{C}_{osc}^0(s=0, \hat{\tau})}{\partial s} \right\rangle_{\hat{\tau}} \right]. \quad (3.22)$$

Figure 3.6 demonstrates that there is a critical exponent α_c for which interfacial resistance does not contribute to bubble growth rate, *i.e.* the bubble surface behaves like a clean surface. The fact that the value of α_c is close to one can be verified by linearization of the interfacial resistance term for small oscillations. Interfacial resistance enhances bubble

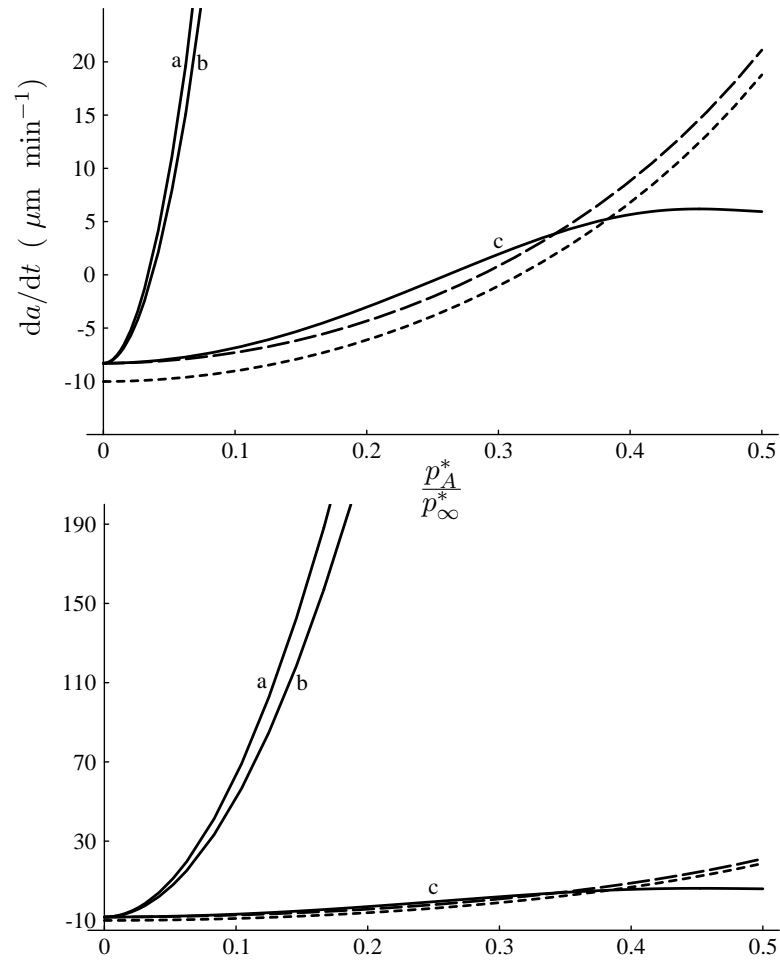


Figure 3.2: The rate of bubble growth in μm per minute versus dimensionless pressure amplitude p_A^*/p_∞^* . The solid curves correspond to (3.20) for the surfactants (a) $C_{12}H_{25}N(CH_3)_3Cl$, (b) $C_{16}H_{33}N(CH_3)_3Cl$ and (c) $C_{12}H_{25}SO_4Na$, each with initial surface concentration 2.9×10^{-10} gmol cm^{-2} . The two dashed curves correspond to (3.20) with R_I set to zero. The diffusivity of the gas in the liquid is 2.0×10^{-5} $\text{cm}^2 \text{sec}^{-1}$. The bubble is of equilibrium radius $20 \mu\text{m}$ and is driven at a frequency of 26.6 kHz. The interfacial tension is 60 dynes cm^{-1} except for the short-dashed curve which corresponds to the clean surface with interfacial tension 73 dynes cm^{-1} . The upper plot consists of a magnification of the vertical axis near zero growth rate which corresponds to the threshold for rectified diffusion. Note that the presence of surfactant is associated with a reduction in the threshold pressure amplitude for rectified diffusion.

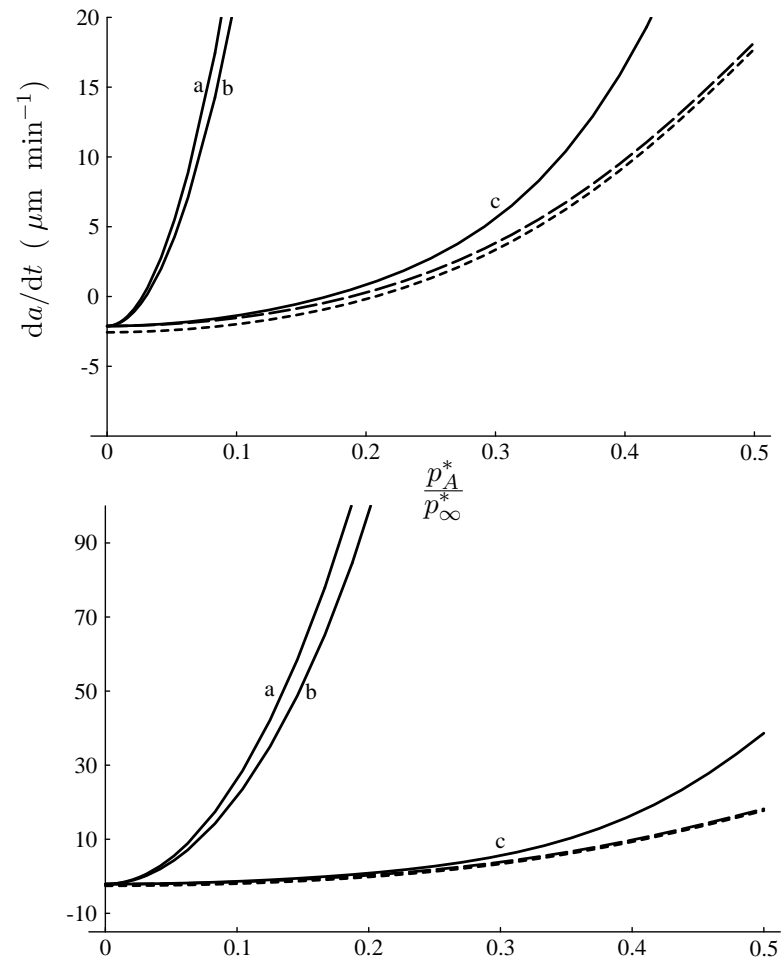


Figure 3.3: The rate of bubble growth in μm per minute versus dimensionless pressure amplitude p_A^*/p_∞^* . The data are the same as for figure 3.2 except the bubble is of equilibrium radius $40 \mu\text{m}$.

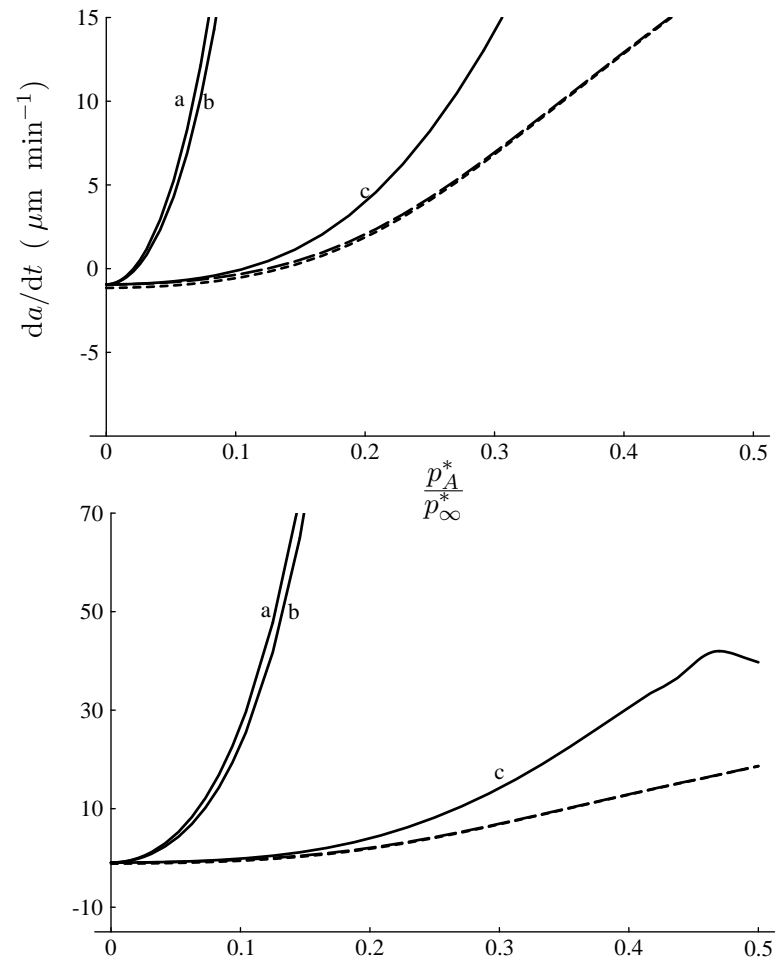


Figure 3.4: The rate of bubble growth in μm per minute versus dimensionless pressure amplitude p_A^*/p_∞^* . The data are the same as for figures 3.2 and 3.3 except the bubble is of equilibrium radius $60 \mu\text{m}$.

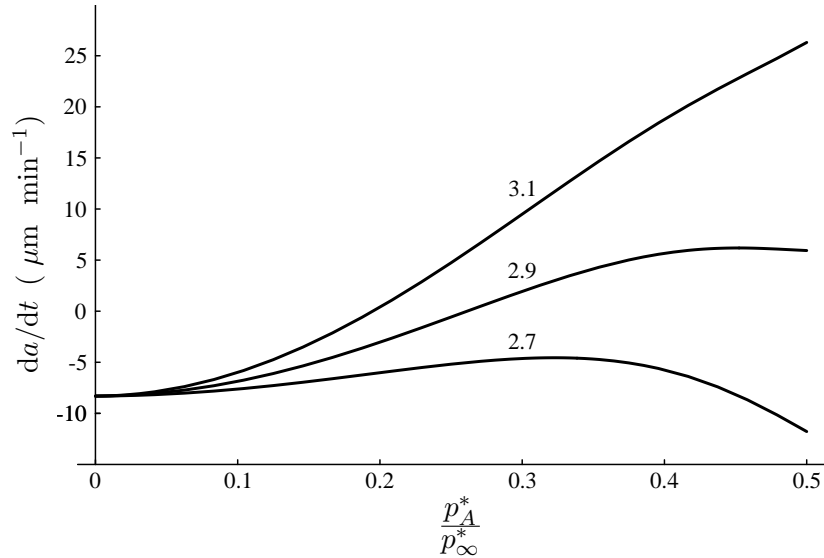


Figure 3.5: The rate of bubble growth in μm per minute versus dimensionless pressure amplitude p_A^*/p_∞^* . The curves correspond to (3.20) for the surfactant $C_{12}H_{25}SO_4Na$ for initial surface concentrations $2.7, 2.9$ and 3.1×10^{-10} gmols cm^{-2} on a $20 \mu\text{m}$ bubble. The other data are the same as for figures 3.2-3.4.

growth rates for $\alpha > \alpha_c$ and inhibits growth rates for $\alpha < \alpha_c$. The mechanism that leads to this transition is the behavior of the term $x^2(\hat{\tau})R_I(\hat{\tau})$ for different values of α . In figure 3.7, we show plots of $x^2(\hat{\tau})R_I(\hat{\tau}) - \langle x^2(\hat{\tau})R_I(\hat{\tau}) \rangle_{\hat{\tau}}$ for $\alpha = 0.6$ (dashed curve) and $\alpha = 1.4$ (solid curve). Notice that the change in behavior of this term is going to lead to a change in sign of the interfacial resistance term (equation 3.22).

A comparison of the magnitude of the terms in $\bar{C}_{sm}(0)$ (3.18) reveals that the interfacial resistance term is the most significant one for bubble oscillations of practical interest. The fact that the first order problem presents a significant correction to the zeroth order problem does not suggest a breakdown of the perturbation scheme, because the expansions remain well-ordered as $\mathcal{P} \rightarrow \infty$. Furthermore, in the second order correction the resistance term, R_I , appears multiplied by \mathcal{P}^{-1} . Since $R_I\mathcal{P}^{-1/2}$ is of order one, then $R_I\mathcal{P}^{-1}$ is of order $\mathcal{P}^{-1/2}$ and presents a small correction to the first order term. In contrast the first order correction to the clean surface problem involves the factor $\mathcal{P}^{-1/2}$ and is therefore very small.

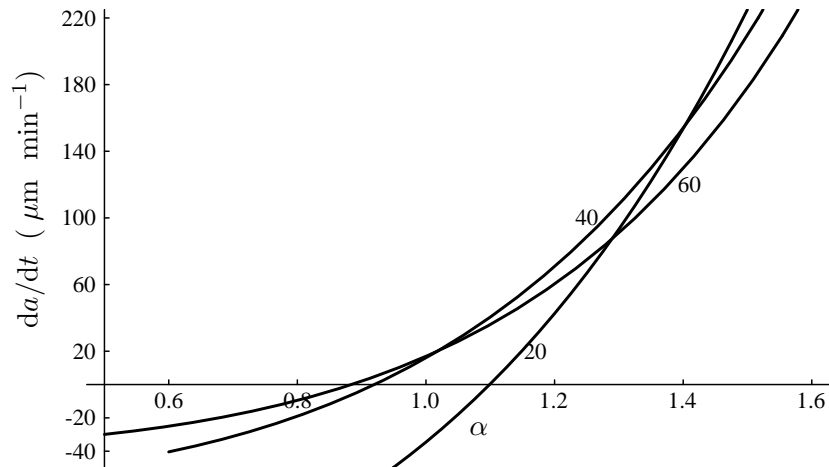


Figure 3.6: The rate of bubble growth in μm per minute versus the exponent α . The curves correspond to (3.20) but include only the effect of interfacial resistance (see text). The bubbles considered are of radius 20, 40 and 60 μm (as shown), forced at a dimensionless pressure amplitude of 0.5. The other data are the same as for figures 3.2-3.4.

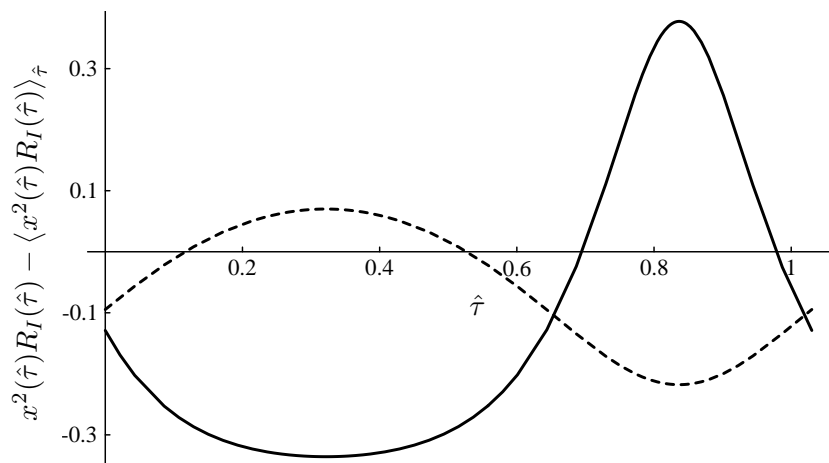


Figure 3.7: The term $x^2 R_I - \langle x^2 R_I \rangle_{\hat{\tau}}$ versus the nonlinear time $\hat{\tau}$ for $\alpha = 0.6$ (dashed curve) and $\alpha = 1.4$ (solid curve). The bubble oscillation and the boundary condition are the same as in figure 2.1.

3.7 Conclusions

We have developed a theory to explain the observed effects of surfactants on the problem of mass transport across the dynamic interface of a soluble spherical gas bubble undergoing volume oscillations in a liquid. The difference between the surfactant problem and the clean surface problem is the boundary condition on the bubble interface. Surfactants present an interfacial barrier to mass transport and the boundary condition of the first kind (Henry's law), used in the clean problem, is replaced by a flux boundary condition of the third kind, where the effect of surfactants appears as an interfacial resistance and Henry's law is the equilibrium state.

The clean surface problem was treated to leading order in Chapter 2 by splitting the problem into two parts; the oscillatory problem and the smooth problem. As in the case of the clean surface, the surfactant-covered surface problem is split into the same two parts. The oscillatory problem is treated using the method of matched asymptotic expansions in a way such that the outer approximation to the oscillatory solution is identically zero. This serves to define the splitting in successive powers in $\mathcal{P}^{-1/2}$. The oscillatory solution is valid everywhere in the liquid but differs from zero only in a thin layer in the neighborhood of the bubble surface. Furthermore it does not contribute to bubble growth or dissolution because it accounts for only a finite amount of mass transfer at initial times. The smooth solution is also valid everywhere in the liquid and evolves via convection-enhanced diffusion which is treated by the singular perturbation method of multiple scales.

To leading order, the clean surface solution is recovered. Continuing to higher order it is shown that the concentration field depends on $R_I \mathcal{P}^{-1/2}$, where R_I is the (dimensionless) interfacial resistance due to the presence of surfactants. Although the influence of surfactants appears at higher order in the small parameter, surfactants are shown to have a large effect on bubble growth rates owing to the fact that the magnitude of R_I is approximately the same as the magnitude of $\mathcal{P}^{1/2}$ at conditions of practical interest. Hence the "corrections" are numerically of the same magnitude as the leading order, clean surface problem.

This is in contrast to the case of a still, surfactant-covered bubble, in which corrections to the bubble growth rate due to surfactants are smaller by $\mathcal{P}^{-1/2}$.

Based on experimental data of Caskey & Barlage [9], an exponential dependence between interfacial resistance and surfactant surface concentration was assumed. For the case of insoluble surfactants, the resistance is of the form $R_I \propto \exp(\alpha/x^2(\tau))$, where α is a constant which depends on the surfactant and the initial concentration, and $x(\tau)$ is the dimensionless bubble radius. It was observed that for a fixed bubble oscillation, there is a critical exponent (α_c), which determines the effect of the surfactant on the growth rate. If $\alpha > \alpha_c$ the bubble grows more quickly (or dissolves more slowly); if $\alpha < \alpha_c$ the bubble grows more slowly (or dissolves more quickly) as a consequence of the presence of surfactants. For small oscillations $\alpha_c = 1$.

For the case of an oscillating bubble the enhancement of bubble growth by rectified diffusion when surfactants are present is predicted to be at least as significant as was observed in the experiments of Crum [11].

Chapter 4

Surfactant Transport Problem

In this Chapter the surfactant transport problem is treated to obtain information about the amount of surfactants on the interface. This amount is required in the calculation of interfacial resistance as mentioned in Chapter 3. Although the governing differential equation is the same as in Chapters 2 and 3, the boundary condition on the bubble interface consists of a differential equation for the surface excess.

4.1 Formulation

In this section we formulate the mass transport problem for a surfactant outside a spherically bubble undergoing radial oscillations ($R(t)$). As presented by Edwards, Brenner & Wasan [17] this formulation requires a transport equation for the bulk

$$\frac{\partial \rho}{\partial t} + \frac{R^2(t)\dot{R}(t)}{r^2} \frac{\partial \rho}{\partial r} = \frac{D_s}{r^2} \frac{\partial}{\partial r} \left(r^2 \frac{\partial \rho}{\partial r} \right), \quad (4.1)$$

an equation for the surface-excess

$$\frac{d\rho^s(t)}{dt} + 2\frac{\dot{R}(t)}{R(t)}\rho^s(t) = \Phi(\rho^s(t), \rho(r = R(t), t)) \quad (4.2)$$

and a constitutive relation for nonequilibrium partitioning of a soluble surfactant between interface and bulk

$$D_s \frac{\partial \rho}{\partial r} (r = R(t), t) = \Phi(\rho^s(t), \rho(r = R(t), t)). \quad (4.3)$$

Thus, equation (4.3) is regarded as the boundary condition for the field equation (4.1); equation (4.2) is an auxiliary equation for the surface-excess concentration of surfactant.

Here Φ is the kinetic rate expression given by

$$\Phi = k_i \exp \left[\frac{A}{2} \left(\frac{\rho^s}{\rho_\infty^s} \right)^2 \right] \left(\rho(r = R(t), t) (\rho_\infty^s - \rho^s) - \frac{\rho^s}{K_a} \exp \left[-A \frac{\rho^s}{\rho_\infty^s} \right] \right), \quad (4.4)$$

where k_i is the forward rate constant in the kinetic rate expression, K_a is the adsorption coefficient, D_s is the diffusivity of the surfactant in the liquid, ρ is the mass of surfactant per unit volume, ρ^s is the surface-excess mass density of the surfactant and ρ_∞^s is the surface-excess saturation density which corresponds to the maximum realizable surface-excess concentration. Parameter A measures the degree of non-ideality of the interface; it is positive if there is an attractive interaction between the solute and solvent and negative if there is a repulsive interaction.

For initial and far field conditions we will assume that the bubble was created in a liquid with initial concentration ρ_∞ , *i.e.*

$$\rho(r \rightarrow \infty, t) = \rho(r, t = 0) = \rho_\infty$$

and

$$\rho^s(t = 0) = 0.$$

In the above equations $R(t)$ may be obtained by integration of the equations of motion of the bubble. We defer any specification of these equations to section 2.5.1.

The problem may be non-dimensionalized with respect to the following natural scales. As a length scale we take a , the radius of the undisturbed bubble; the time scale is Ω_0^{-1} , which is the inverse of the natural frequency of radial oscillation of the bubble about the undisturbed state; the surface excess is non-dimensionalized using ρ_∞^s and the bulk concentration by a/ρ_∞^s . This leads to dimensionless parameters corresponding to the Péclet number for the surfactant transport problem

$$\mathcal{P}_f = \frac{a^2 \Omega_0}{D_s}$$

the affinity of surfactant for interface versus bulk

$$A_f = \frac{\rho_\infty^s K_a}{a}$$

and the adsorption per cycle of bubble oscillation

$$k = \frac{k_i \rho_\infty^s}{\Omega_0 a}.$$

We also define a new dimensionless surfactant bulk concentration

$$\Psi = \frac{a}{\rho_\infty^s} (\rho - \rho_\infty)$$

and surface excess concentration

$$\Psi^s = \frac{\rho^s}{\rho_\infty^s}.$$

Another parameter that will emerge later in our analysis is the product

$$A_f \Psi_\infty = K_a \rho_\infty,$$

which is equal to the dimensionless surface excess concentration on a still interface based on a linearized adsorption isotherm.

Following the analysis in section 2.1.1, we recast the problem in the dimensionless Lagrangian coordinate

$$\sigma \equiv \frac{1}{3a^3} (r^3 - R^3(t))$$

and the nonlinear time

$$\hat{\tau} = \int_0^\tau x^4(\theta) d\theta,$$

where τ is the dimensionless time defined as $\tau \equiv t\Omega_0$. Equations (4.1) and (4.2) take the form

$$\frac{\partial \Psi}{\partial \hat{\tau}} = \frac{1}{\mathcal{P}_f} \frac{\partial}{\partial \sigma} \left(\left(\frac{3\sigma}{x^3(\hat{\tau})} + 1 \right)^{(4/3)} \frac{\partial \Psi}{\partial \sigma} \right) \quad (4.5)$$

and

$$\frac{d(x^2(\hat{\tau})\Psi^s(\hat{\tau}))}{d\hat{\tau}} = \frac{1}{x^2(\hat{\tau})} \Phi(\Psi^s(\hat{\tau}), \Psi(\sigma=0, \hat{\tau})) \quad (4.6)$$

respectively, with boundary and initial conditions for the field equation

$$\frac{x^2(\hat{\tau})}{\mathcal{P}_f} \frac{\partial \Psi(\sigma=0, \hat{\tau})}{\partial \sigma} = \Phi \quad (4.7)$$

$$\Psi(\sigma, \hat{\tau}=0) = \Psi(\sigma \rightarrow \infty, \hat{\tau}) = \Psi^s(\hat{\tau}=0) = 0.$$

Here Φ is the dimensionless kinetic expression (equation 4.4)

$$\Phi = k \exp \left[\frac{A}{2} \Psi^s{}^2 \right] \left((1 - \Psi^s)(\Psi(\sigma=0) + \Psi_\infty) - \frac{\Psi^s}{A_f} \exp[-A\Psi^s] \right).$$

4.2 Analysis

Surfactants, due to the large size of their molecules, are characterized by weak diffusion, hence the Péclet number associated with the surfactant transport process is very large. Similar problems were treated in Chapters 2 and 3 for the gas transport associated with an oscillating bubble. In the present analysis the techniques developed therein will be used. The plan of the analysis is as follows. The bulk problem (4.5) is treated by splitting it into an oscillatory and a smooth problem and expanding each in powers of the small parameter $\mathcal{P}_f^{-1/2}$. By treating the surface excess concentration (Ψ_s) as an arbitrary but known function of time we obtain expressions for the bulk concentration on the interface $\Psi(\sigma = 0, \hat{\tau})$ to each order in $\mathcal{P}_f^{-1/2}$. The surface excess differential equation (4.6) can then be expanded in a perturbation series for large $\mathcal{P}_f^{1/2}$ and solved using the method of multiple scales.

The bulk problem (4.5) can be brought to a form similar to the problem solved in Chapter 3, by rearranging the boundary condition (4.7) in the following form:

$$\frac{G(\hat{\tau})}{\mathcal{P}_f} \frac{\partial \Psi(\sigma = 0, \hat{\tau})}{\partial \sigma} = \Psi(\sigma = 0, \hat{\tau}) - \Psi_e(\hat{\tau}) + (\Psi_{sp}^0 - \Psi_{sp}^0) + \frac{1}{\mathcal{P}_f^{1/2}} (\Psi_{sp}^1 - \Psi_{sp}^1) + \frac{1}{\mathcal{P}_f} (\Psi_{sp}^2 - \Psi_{sp}^2) + \frac{1}{\mathcal{P}_f^{3/2}} (\Psi_{sp}^3 - \Psi_{sp}^3),$$

where

$$G(\hat{\tau}) \equiv \hat{G}(x(\hat{\tau}), N(\hat{\tau})) = \frac{x^4 \exp\left[-\frac{AN^2}{x^4}\right]}{k(x^2 - N)}$$

and

$$\Psi_e(\hat{\tau}) \equiv \hat{\Psi}_e(x(\hat{\tau}), N(\hat{\tau})) = \frac{N \exp\left[-\frac{AN}{x^2}\right]}{A_f(x^2 - N)} - \Psi_\infty.$$

In these equations the surface excess concentration, $\Psi^s(\hat{\tau})$, is transformed by a defining a new dependent variable $N(\hat{\tau}) = x^2(\hat{\tau})\Psi^s(\hat{\tau})$, which is proportional to the (excess) amount of surfactant on the interface. Furthermore, the constants Ψ_{sp}^i were introduced to aid in splitting the problem following the procedure developed in Chapters 2 and 3. An explicit expression for Ψ_{sp}^0 is given in the next section.

4.2.1 Oscillatory Problem

As mentioned in section 2.2 solution of the oscillatory problem is nonzero only in a small region near the bubble and is characterized by the stretched spatial coordinate $s = \mathcal{P}_f^{1/2}\sigma$. The oscillatory problem is:

$$\frac{\partial \Psi_{osc}}{\partial \hat{\tau}} = \frac{\partial}{\partial s} \left(\left(\frac{3s}{x^3(\hat{\tau})\mathcal{P}_f^{1/2}} + 1 \right)^{(4/3)} \frac{\partial \Psi_{osc}}{\partial s} \right),$$

with the boundary condition

$$\frac{G(\hat{\tau})}{\mathcal{P}_f^{1/2}} \frac{\partial \Psi_{osc}(s=0, \hat{\tau})}{\partial s} = \Psi_{osc}(s=0, \hat{\tau}) - \Psi_e(\hat{\tau}) + \Psi_{sp}^0 + \frac{1}{\mathcal{P}_f^{1/2}} \Psi_{sp}^1 + \frac{1}{\mathcal{P}_f} \Psi_{sp}^2 + \frac{1}{\mathcal{P}_f^{3/2}} \Psi_{sp}^3.$$

Next we expand Ψ_{osc} and N in successive powers in $\mathcal{P}_f^{-1/2}$. Consequently $\hat{\Psi}_e(\hat{\tau})$ and $\hat{G}(\hat{\tau})$ can be expanded in successive powers in $\mathcal{P}_f^{-1/2}$ provided the surface excess is sufficiently away from saturation as mentioned in Appendix E.

To zeroth-order we get the problem

$$\frac{\partial \Psi_{osc}^0}{\partial \hat{\tau}} = \frac{\partial^2 \Psi_{osc}^0}{\partial s^2}, \quad (4.8)$$

with the boundary condition

$$\Psi_{osc}^0(s=0, \hat{\tau}) = \Psi_e^0(\hat{\tau}) - \Psi_{sp}^0.$$

As developed in section 2.2 the condition for the splitting to zeroth-order is that the average of the boundary condition with respect to the time $\hat{\tau}$, defined as

$$\langle f(\sigma, \tau) \rangle_{\hat{\tau}} \equiv \frac{1}{\hat{\tau}(T)} \int_0^{\hat{\tau}(T)} f(\sigma, \hat{\tau}) d\hat{\tau} = \frac{1}{\int_0^T x^4(\tau) d\tau} \int_0^T f(\sigma, \tau) x^4(\tau) d\tau, \quad (4.9)$$

should be zero. Here T is the dimensionless bubble period. Hence the splitting constant is given by

$$\Psi_{sp}^0 = \langle \Psi_e^0(\hat{\tau}) \rangle_{\hat{\tau}},$$

where

$$\Psi_e^0(\hat{\tau}) = \frac{N^0 \exp\left[-\frac{AN^0}{x^2(\hat{\tau})}\right]}{A_f(x^2(\hat{\tau}) - N^0)} - \Psi_\infty. \quad (4.10)$$

Higher-order terms in the expansion satisfy the forced heat equation (equation 4.8), where the lower terms in the expansion appear in the forcing and in the boundary conditions. To first and second order the boundary conditions are

$$\begin{aligned} \Psi_{osc}^1(s=0, \hat{\tau}) &= \Psi_e^1(\hat{\tau}) + G^0(\hat{\tau}) \frac{\partial \Psi_{osc}^0(s=0, \hat{\tau})}{\partial s} - \Psi_{sp}^1 \\ \Psi_{osc}^2(s=0, \hat{\tau}) &= \Psi_e^2(\hat{\tau}) + G^0(\hat{\tau}) \frac{\partial \Psi_{osc}^1(s=0, \hat{\tau})}{\partial s} + G^1(\hat{\tau}) \frac{\partial \Psi_{osc}^0(s=0, \hat{\tau})}{\partial s} - \Psi_{sp}^2. \end{aligned}$$

4.2.2 Smooth Problem

The smooth problem is characterized by slow convection-enhanced diffusion. Therefore we introduce a second time scale $\lambda \equiv \hat{\tau}/\mathcal{P}_f$, which captures the slow diffusive behavior.

The smooth problem is

$$\frac{\partial \Psi_{sm}}{\partial \hat{\tau}} + \frac{1}{\mathcal{P}_f} \frac{\partial \Psi_{sm}}{\partial \lambda} = \frac{1}{\mathcal{P}_f} \frac{\partial}{\partial \sigma} \left(\left(\frac{3\sigma}{x^3(\hat{\tau})} + 1 \right)^{(4/3)} \frac{\partial \Psi_{sm}}{\partial \sigma} \right),$$

with the boundary condition

$$\begin{aligned} \frac{G(\hat{\tau})}{\mathcal{P}_f} \frac{\partial \Psi_{sm}(\sigma=0, \hat{\tau}, \lambda)}{\partial \sigma} = \\ \Psi_{sm}(\sigma=0, \hat{\tau}, \lambda) - \Psi_{sp}^0 - \frac{1}{\mathcal{P}_f^{1/2}} \Psi_{sp}^1 - \frac{1}{\mathcal{P}_f} \Psi_{sp}^2 - \frac{1}{\mathcal{P}_f^{3/2}} \Psi_{sp}^3. \end{aligned}$$

As with the oscillatory problem we expand the smooth problem and its boundary condition in successive powers in $\mathcal{P}_f^{-1/2}$. To zeroth and first order the smooth problem admits a solution independent of $\hat{\tau}$. By eliminating secular behavior in the second and third problems (as outlined in section 3.3) we get an additional equation for Ψ_{sm}^0 and Ψ_{sm}^1 :

$$\frac{\partial \Psi_{sm}^i}{\partial \lambda} = \frac{\partial}{\partial \sigma} \left(\left\langle \left(\frac{3\sigma}{x^3(\hat{\tau})} + 1 \right)^{(4/3)} \right\rangle_{\hat{\tau}} \frac{\partial \Psi_{sm}^i}{\partial \sigma} \right),$$

where $i = 0, 1$. The boundary condition that each order should satisfy is

$$\Psi_{sm}^0(\sigma=0, \lambda) = \Psi_{sp}^0,$$

$$\begin{aligned}\Psi_{sm}^1(\sigma = 0, \lambda) &= \Psi_{sp}^1, \\ \Psi_{sm}^2(\sigma = 0, \hat{\tau}, \lambda) &= G^0(\hat{\tau}) \frac{\partial \Psi_{sm}^0(\sigma = 0, \hat{\tau}, \lambda)}{\partial \sigma} + \Psi_{sp}^2.\end{aligned}$$

4.2.3 Surface Excess

Now that we have expressions for the surface concentration of the bulk ($\Psi(\sigma = 0, \hat{\tau}, \lambda)$), we turn to the surface excess problem. The differential equation governing the (excess) amount of surfactant on the interface ($N(\tau)$) is

$$\frac{dN}{d\hat{\tau}} = \frac{1}{\hat{G}(N(\hat{\tau}))} \left[\Psi(\sigma = 0, N(\hat{\tau}), \hat{\tau}, \lambda) - \hat{\Psi}_e(x(\hat{\tau}), N(\hat{\tau})) \right].$$

We substitute the expression for the bulk concentration on the bubble interface (obtained by summing the surface concentration of the smooth and oscillatory problems) derived in the previous sections, and use the expansions for \hat{G} and $\hat{\Psi}_e$ (see Appendix E) in orders of $\mathcal{P}_f^{-1/2}$ to obtain

$$\begin{aligned}\frac{dN}{d\hat{\tau}} &= \frac{1}{\mathcal{P}_f^{1/2}} \frac{\partial \Psi_{osc}^0(s = 0, N^0(\tau), \hat{\tau})}{\partial s} + \\ &\frac{1}{\mathcal{P}_f} \left(\frac{\partial \Psi_{sm}^0(\sigma = 0, N^0(\tau), \lambda)}{\partial \sigma} + \frac{\partial \Psi_{osc}^1(s = 0, N^0(\hat{\tau}), N^1(\hat{\tau}), \hat{\tau})}{\partial s} \right).\end{aligned}$$

The problem is treated by the method of multiple scales by introducing, as in the previous section, the slow time scale $\lambda \equiv \hat{\tau}/\mathcal{P}_f$ to capture the slow diffusion-controlled adsorption. Next we expand N in powers of $\mathcal{P}_f^{-1/2}$:

$$N(\lambda, \hat{\tau}) = N^0(\lambda, \hat{\tau}) + \frac{1}{\mathcal{P}_f^{1/2}} N^1(\lambda, \hat{\tau}) + \frac{1}{\mathcal{P}_f} N^2(\lambda, \hat{\tau}) + \frac{1}{\mathcal{P}_f^{3/2}} N^3(\lambda, \hat{\tau}) + \dots$$

To zeroth order we have

$$\frac{\partial N^0(\lambda, \hat{\tau})}{\partial \hat{\tau}} = 0,$$

which admits a solution independent of $\hat{\tau}$, *i.e.* $N^0(\lambda, \hat{\tau}) = N^0(\lambda)$. However N^0 is further determined by eliminating secular behavior in N^2 . The differential equation for N^2 is

$$\frac{\partial N^2}{\partial \hat{\tau}} = -\frac{dN^0}{d\lambda} + \frac{\partial \Psi_{osc}^1(s = 0, N^0(\lambda), N^1(\lambda, \hat{\tau}), \hat{\tau}, \lambda)}{\partial s} + \frac{\partial \Psi_{sm}^0(\sigma = 0, N^0(\lambda), \lambda)}{\partial \sigma}.$$

To eliminate secular behavior we force N^2 to have zero $\hat{\tau}$ -average. Here we should point out that Ψ_{osc}^0 and Ψ_{osc}^1 depend indirectly on the long time λ through the boundary condition.

Furthermore the oscillatory problem reaches its asymptotic limit after a few bubble oscillations (see Appendix A) and does not contribute to any secular behavior since it is periodic with respect to $\hat{\tau}$ with zero mean. These considerations lead to the following equation for N^0

$$\frac{dN^0}{d\lambda} = \frac{\partial \Psi_{sm}^0(\sigma = 0, N^0(\lambda), \lambda)}{\partial \sigma},$$

with initial condition

$$N^0(\lambda = 0) = 0.$$

Of course, this equation is coupled with

$$\frac{\partial \Psi_{sm}^0}{\partial \lambda} = \frac{\partial}{\partial \sigma} \left(\left\langle \left(\frac{3\sigma}{x^3(\hat{\tau})} + 1 \right)^{(4/3)} \right\rangle_{\hat{\tau}} \frac{\partial \Psi_{sm}^0}{\partial \sigma} \right),$$

with boundary conditions

$$\begin{aligned} \Psi_{sm}^0(\sigma = 0, \lambda) &= \langle \Psi_e^0(\hat{\tau}) \rangle_{\hat{\tau}} = \left\langle \frac{N^0}{A_f(x^2(\hat{\tau}) - N^0)} \exp \left[-\frac{AN^0}{x^2(\hat{\tau})} \right] \right\rangle_{\hat{\tau}} - \Psi_\infty, \\ \Psi_{sm}^0(\sigma \rightarrow \infty, \lambda) &= 0 \end{aligned}$$

and initial condition

$$\Psi_{sm}^0(\sigma, \lambda = 0) = 0.$$

At the asymptotic steady state (indicated by an overbar) we do not expect any λ dependence, *i.e.* $\partial \bar{\Psi}_{sm}^0 / \partial \lambda = d\bar{N}^0 / d\lambda = 0$, which leads to $\bar{\Psi}_{sm}^0 \equiv 0$ and \bar{N}^0 is a constant satisfying the following algebraic equation

$$A_f \langle \Psi_e^0(\hat{\tau}) \rangle_{\hat{\tau}} = \left\langle \frac{\bar{N}^0}{(x^2(\hat{\tau}) - \bar{N}^0)} \exp \left[-\frac{A\bar{N}^0}{x^2(\hat{\tau})} \right] \right\rangle_{\hat{\tau}} - A_f \Psi_\infty = 0. \quad (4.11)$$

The result suggests that the asymptotic limit of the surfactant transport problem is such that the smooth problem is identically zero. This deduction is justified because the smooth problem is the one responsible for any mass flux across the bubble interface. Asymptotically in time the excess amount of surfactant adjusts itself so that over one period of bubble oscillation there is no adsorption or desorption between the interface and the bulk. Another important consequence of this result is that although in this analysis we did not make any assumptions on the solubility of the surfactant the results suggest that asymptotically in time the surfactant behaves as though insoluble. Hence the model used in Chapter 2 in

calculating bubble growth rates is not restricted to insoluble surfactants but applies also to the case of soluble surfactants at large \mathcal{P}_f number. The fact that surfactants, due to the size of their molecules, are characterized by weak diffusion renders those results quite general.

For a dilute solution, equation (4.11) can be linearized for small values of $A_f\Psi_\infty$ to give

$$\bar{N}_l^0 = (A_f\Psi_\infty) \frac{\langle x^4(\tau) \rangle_\tau}{\langle x^2(\tau) \rangle_\tau} + (A_f\Psi_\infty)^2 (A-1) \frac{\langle x^4(\tau) \rangle_\tau^2}{\langle x^2(\tau) \rangle_\tau^3} \quad (4.12)$$

to second order, where equation (4.9) was used to express the averages in the original dimensionless time τ . Here $\langle \rangle_\tau$ is defined as the average over one bubble oscillation with respect to time τ .

Because the smooth problem is zero at steady state the bulk concentration is given by the oscillatory problem. Hence the bulk concentration on the interface is equal to $\bar{\Psi}_e^0$ (equation 4.10) which when expressed in original variables gives for the Frumkin isotherm:

$$\bar{\rho}(\sigma = 0, \tau) = \frac{\bar{\rho}^s(\tau)}{K_a (\rho_\infty^s - \bar{\rho}^s(\tau))} \exp \left[-A \frac{\bar{\rho}^s(\tau)}{\rho_\infty^s} \right], \quad (4.13)$$

where

$$\bar{\rho}^s = \frac{\bar{N}^0 \rho_\infty^s}{x^2(\tau)}.$$

Alternatively, equation (4.13) can be obtained from the surface-excess equation (equation 4.6), assuming a quasi-steady approximation, and can be considered to be the quasi-steady adsorption isotherm.

4.3 Results and Discussion

4.3.1 A still vs an oscillating bubble

As mentioned earlier in the case of a still bubble one can obtain an integral equation for the evolution of $\Psi^s(\tau)$. The asymptotic limit, however, can be easily obtained by setting all

time derivatives equal to zero in equations (4.5) and (4.6) and solving the resulting problem. Then it is easy to obtain an equation for Ψ^s :

$$\frac{\Psi^s}{(1 - \Psi^s)} \exp[-A\Psi^s] = A_f \Psi_\infty. \quad (4.14)$$

For an ideal interface, *i.e.* $A=0$, we can solve for Ψ^s to get

$$\Psi^s = \frac{A_f \Psi_\infty}{1 + A_f \Psi_\infty}.$$

It is important to note that these results for the surface excess are the same in the case of a plane interface. The transient analysis for a plane interface was presented by Borwankar & Wasan [5]. The asymptotic limit as presented in their figures 3 and 4 agrees with (4.14).

Here we should point out that in the case of an oscillating bubble the asymptotic limit for the surface excess satisfies the asymptotic limit of a still bubble (equation 4.14) in the average sense, as equation (4.11) can be written as

$$\left\langle \frac{\bar{\Psi}^s(\hat{\tau})}{(1 - \bar{\Psi}^s(\hat{\tau}))} \exp[-A\bar{\Psi}^s(\hat{\tau})] \right\rangle_{\hat{\tau}} = A_f \Psi_\infty.$$

What is not intuitive is that the average should be taken with respect to the nonlinear time $\hat{\tau}$, rather than with respect to “real” time τ .

To evaluate the expression for \bar{N}^0 we require a model for the bubble oscillation. We shall use the non-polytropic four term Galerkin formulation of Kamath & Prosperetti [30] (see section 2.5.1). This model allows for a spatially non-uniform temperature field inside the bubble and is more accurate near resonances than polytropic models. It consists of eight non-linear ODEs which are integrated numerically using the software AUTO [16]. The details are in section 2.5.1.

Our theoretical bubble model consists of an air bubble created in water and set into oscillation by a sinusoidal sound field. In figure 4.1 we show for comparison the asymptotic results of the dimensionless excess amount of surfactant (\bar{N}^0) versus the dimensionless quantity $A_f\Psi_\infty$ between a still (solid curves) and an oscillating (dashed curves) bubble, and between an ideal ($A = 0$) and a non-ideal ($A = 2$) interface. The bubble is of radius 20 μm and the amplitude of the sound field is 0.5 bars. In this calculation we assumed that

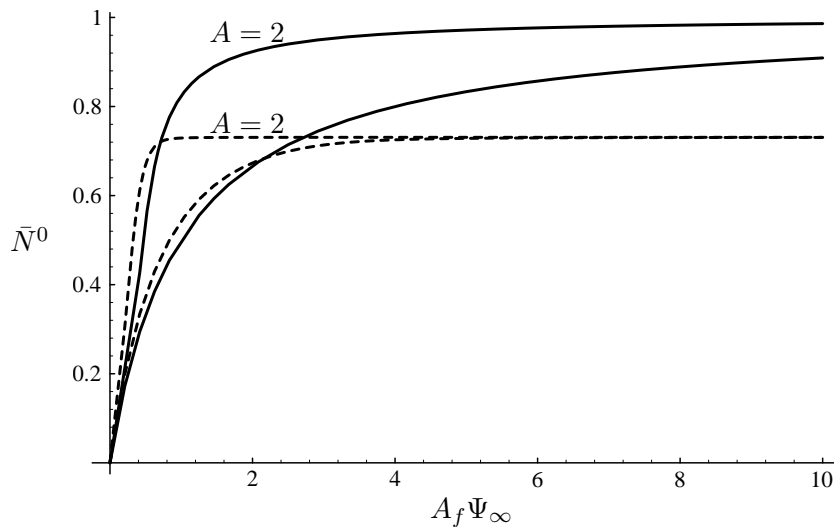


Figure 4.1: The dimensionless excess amount of surfactant versus dimensionless concentration at infinity for a bubble of radius $20 \mu\text{m}$. The solid curves correspond to a still bubble and the dashed curves to an oscillating bubble forced by a pressure amplitude of 0.5 bars.

surfactants do not alter bubble dynamics through surface tension (see section 4.3.2). This is true for dilute to moderate concentrations as mentioned in section 4.3.2.

If one examines figure 4.1 carefully it is clear that oscillations favor the presence of surfactants on the interface for dilute solutions. A perturbation expansion of equation (4.11) for small amounts of surfactant (section 4.3.2) will reveal that the ratio between the fourth and second moment of the bubble oscillation (equation 4.12) is the controlling parameter to first order. If it is greater than one an oscillating bubble would have a greater amount of surfactants on its interface than a still bubble, assuming both are immersed in a liquid with the same far-field bulk concentration of dissolved surfactant. Because this ratio is greater than one for oscillations that linger at large x , the result is intuitively obvious. Another parameter that favors the presence of surfactants on the interface is positive values of the interaction parameter A , which measures the attraction between molecules [5].

The most important result is that oscillations seem to decrease the saturation limit of the interface. A careful analysis of equation (4.11) reveals that the saturation limit is controlled by the minimum bubble radius. The maximum amount of surfactants that can reside on the interface is the one that renders the interface saturated at the minimum

radius (x_{min}). Hence at saturation, \bar{N}^0 is equal to the square of the minimum bubble radius ($\bar{N}^0 = x_{min}^2$). The physical explanation of this dependency is that any amount of surfactant that would yield the interface supersaturated has no time to diffuse to the bubble surface because desorption is instantaneous at such a condition while diffusion is rate-limited. One should be careful though not to generalize these results because, firstly, the present analysis is valid provided $x_{min}^2 - \bar{N}^0 \gg \mathcal{P}_f^{-1/2}$ as mentioned in Appendix E and, secondly, the validity of the kinetic rate expression is questionable very close to saturation due to possible crystallization or collapse of the interface [53].

4.3.2 Equation of State

Because asymptotically in time the interface complies with the Frumkin isotherm (equation 4.13), the surface equation of state is [17]

$$\pi \equiv \gamma_0 - \gamma \equiv -\frac{R_G T}{M} \rho_\infty^s \left(\ln \left[1 - \frac{\bar{N}^0}{x^2(\tau)} \right] + \frac{A}{2} \left(\frac{\bar{N}^0}{x^2(\tau)} \right)^2 \right), \quad (4.15)$$

where R_G is the universal gas constant, T is the temperature, π is the surface pressure and γ is the surface tension (where the subscript 0 corresponds to the surface tension of a clean interface). This equation is valid provided the solution is dilute enough so that the behavior is ideal and the mass concentration is proportional to the mole fraction [23].

Equation (4.15) was used, as a modification of the interfacial surface tension due to the presence of surfactants in the liquid, in the model of bubble dynamics, to compare a clean bubble, *i.e.* $\bar{N}^0 = 0$, with a surfactant-covered bubble. No significant changes were observed in the bubble oscillation even for values of \bar{N}^0 very close to saturation. A comparison of the gas pressure term, $p_{Gi}(a/R(t))^{3\eta}$, and the surface tension term, $2\gamma/R(t)$, in the dynamical equation for bubble oscillations (equation 2.3), reveals that the former is two order of magnitudes larger than the latter for oscillations away from resonance [44].

4.3.3 Bubble growth rates

Asymptotically in time, the present analysis of nearly insoluble surfactants suggests that they behave as being insoluble, with the following expression for the surfactant concentration on the interface

$$\bar{\rho}^s = \frac{\bar{N}^0 \rho_\infty^s}{x^2(\tau)}.$$

Following the analysis in section 3.6 (equation 3.21), we assume an exponential dependence of interfacial resistance on surface concentration

$$\tilde{R}_I(\tau) = \exp(\beta \bar{\rho}^s) = \exp\left(\frac{\alpha}{x^2(\tau)}\right),$$

where β is a constant depending on the surfactant and $\alpha = \beta \bar{N}^0 \rho_\infty^s$. For dilute solutions, α is proportional to $A_f \Psi_\infty$:

$$\alpha = \beta \rho_\infty^s \frac{\langle x^4(\tau) \rangle_\tau}{\langle x^2(\tau) \rangle_\tau} (A_f \Psi_\infty).$$

Hence, figure 3.6 demonstrates that there is a critical bulk concentration for which surfactants do not contribute to bubble growth rates. Higher bulk concentrations favor bubble growth rates while smaller concentrations inhibit growth rates. Explicit calculations for the three surfactants mentioned in Chapter 3 are not possible, due to lack of experimental results on their adsorption isotherms. This is an area for future work.

4.4 Conclusions

Employing the technique of *splitting* developed in the earlier Chapters (Chapters 2 and 3) we were able to find simplified equations for the surfactant transport problem associated with a spherical bubble undergoing arbitrary but periodic volume oscillations in the limit of large but finite Péclet number \mathcal{P}_f . Explicit expressions were obtained for the amount of surfactant on the interface and for the equation of state asymptotically in time.

The surfactant transport problem is governed by the convection-diffusion equation in spherical coordinates and an equation for the surface-excess concentration, where the

barrier to adsorption is based on a diffusion-kinetic model developed by Borwankar & Wasan [5]. The problem was split into two parts. The oscillatory problem differs from zero only in a thin layer in the neighborhood of the bubble surface and is not responsible for any net mass transport. The smooth problem is the one responsible for mass flux across the bubble interface and is identically zero asymptotically in time. It was found that the amount of surfactant adsorbing on the interface is controlled by the diffusion time scale, and asymptotically in time there is no adsorption or desorption. The surfactant behaves as though insoluble, and the amount of surfactants residing on the interface satisfies the corresponding adsorption isotherm in an average sense. For dilute solutions, oscillations favor the adsorption process, and the excess amount of surfactant on an oscillating bubble is higher than that on a still bubble. However, oscillations lower the saturation limit of the interface which is controlled by the minimum bubble radius. The maximum number of surfactants on an oscillating bubble is the one that renders the interface saturated at the minimum radius.

Using Gibb's equation, an expression for the equation of state was developed which was used in the bubble dynamics model as a correction to the surface tension due to the presence of surfactants. No significant changes were observed in the bubble oscillation since the gas pressure term is much more significant than the surface tension term for oscillations away from resonance.

Because asymptotically in time the amount of surfactants on the interface is fixed, the results of Chapter 3 can be extended to sparingly soluble surfactants. Assuming an exponential dependence between interfacial resistance and surfactant surface concentration, it was observed that there is a critical bulk concentration for which surfactants do not contribute to bubble growth rates. Higher concentrations favor bubble growth rates while smaller concentrations inhibit growth rates.

Chapter 5

Conclusions

5.1 Summary of Work

The gas and surfactant transport associated with a rapidly oscillating gas bubble embedded in an infinite liquid was studied theoretically by taking advantage of the weak diffusion process characterizing these problems. Associated with the diffusion process a dimensionless parameter can be introduced, the Péclet number (\mathcal{P}), which is the ratio between the time scales for convection and diffusion and consequently is large. Expressions were obtained for the bubble growth rates; these were compared with experimental results and observations.

For the gas transport problem two cases were considered which differ only in the boundary condition on the bubble surface of the governing convection-diffusion equation: (I) the case of a clean bubble where the concentration on the bubble surface is proportional to the bubble internal pressure, the constant of proportionality being Henry's constant, and (II) the case of a bubble contaminated with surfactants where the Henry's law boundary condition of the first kind is replaced by a flux boundary condition of the third kind that features an interfacial resistance that depends on the concentration of surfactant molecules on the interface. The driving force is the disequilibrium partitioning of the gas between free and dissolved states across the interface. The convection-diffusion equations governing transport of dissolved gas in the liquid were written in Lagrangian coordinates to account for the moving domain. In both cases the boundary condition was split into a constant and an oscillating part, yielding the *smooth* and the *oscillatory* problems respectively. The splitting corresponds in a certain sense to Stoke's first and second problem. The smooth

problem was treated using the method of multiple scales in time and evolves via convection-enhanced diffusion on a slow time scale controlled by the Péclet number. An asymptotic solution to the oscillatory problem, valid in the limit of large Péclet number, was developed using the method of matched asymptotics. By requiring that the outer limit of the inner approximation match zero, the splitting into smooth and oscillatory problems was determined unambiguously in successive powers of $\mathcal{P}^{-1/2}$, where \mathcal{P} is the Péclet number. Hence the solution of the oscillatory problem is valid everywhere in the liquid but differs from zero only in a thin layer of the liquid in the neighborhood of the bubble surface. To leading order, the clean and the surfactant-covered surface problems give the same result. Continuing to higher order it was shown that the latter depends on $R_I \mathcal{P}^{-1/2}$ as well, where R_I is the (dimensionless) interfacial resistance associated with the presence of surfactants. Although the influence of surfactants appears at higher order in the small parameter, surfactants were shown to have a very significant effect on bubble growth rates owing to the fact that the magnitude of R_I is approximately the same as the magnitude of $\mathcal{P}^{1/2}$ at conditions of practical interest. Hence the higher order “corrections” happen numerically to be of the same magnitude as the leading order, clean surface problem. This situation is in contrast to the case of a still, surfactant-covered bubble, in which corrections to the bubble growth rate due to surfactants are smaller by $\mathcal{P}^{-1/2}$.

Based on experimental data of Caskey & Barlage [9], an exponential dependence between interfacial resistance and surfactant surface concentration was assumed. For both insoluble and nearly insoluble surfactants, the resistance is of the form $R_I \propto \exp(\alpha/x^2(\tau))$ where $x(\tau)$ is the dimensionless bubble radius. The exponent coefficient α is proportional to the initial surface concentration for insoluble surfactants and to the bulk concentration, through the adsorption isotherm, for dilute solutions of soluble surfactants. It was observed that for a fixed bubble oscillation, there is a critical exponent (α_c), which determines the effect of the surfactant on the growth rate. If $\alpha > \alpha_c$ the bubble grows more quickly (or dissolves more slowly); if $\alpha < \alpha_c$ the bubble grows more slowly (or dissolves more quickly) as a consequence of the presence of surfactants. The value of α_c was found to be close to one for small oscillations. For the case of an oscillating bubble, the enhancement of bubble

growth by rectified diffusion when surfactants are present is predicted to be at least as significant as was observed in the experiments of Crum [11].

The surfactant transport problem was treated in a similar way. Asymptotically in time there is no adsorption or desorption, and the smooth problem, which is the one responsible for mass flux across the bubble interface, is identically zero. Explicit expressions were obtained for the amount of surfactant on the interface and for the equation of state asymptotically in time. The surfactant behaves as though insoluble, and the amount of surfactants residing on the interface satisfies the corresponding adsorption isotherm in an average sense. For dilute solutions, oscillations favor the adsorption process, and the excess amount of surfactants on an oscillating bubble is higher than that on a still bubble, which agrees with numerical results by Nadim [37]. However, oscillations lower the saturation limit of the interface, which is controlled by the minimum bubble radius. The maximum number of surfactants on an oscillating bubble is the one that renders the interface saturated at the minimum radius.

Using Gibb's equation, an expression for the equation of state was developed which was used in the bubble dynamic model as a correction to the surface tension due to the presence of surfactants. No significant changes were observed in the bubble oscillation since the gas pressure term is much more significant than the surface tension term for oscillations away from resonance.

5.2 Future Work

In the present work the gas transport problem associated with spherically oscillating bubbles was studied theoretically. Expressions were obtained for the bubble growth rates and the threshold of rectified diffusion for the case of a clean and a surfactant-covered bubble. The effect of surfactants on bubble growth rates is predicted to be at least as significant as was observed in experiments. However, direct comparison was not possible, due to lack of either interfacial resistance properties or bubble growth characteristics, for

the surfactants under consideration. Clearly this is an area to pursue in future work by collaboration with experimentalists.

An area that requires further investigation is the assumption of constant properties of the liquid. A preliminary calculation, assuming adiabatic bubble oscillation, leads to the following expression for the temperature: $T = 300/x^{1.2}(t)$ (initial temperature is $300K$). For a dimensionless bubble oscillation between $0.9 - 1.2$, the temperature will fluctuate between $250K - 350K$. Although this calculation is based on a worst case scenario, it leads to appreciable variations in liquid diffusivity and Henry's law constant. A theoretical treatment of this problem requires solving the heat equation in the liquid and in the bubble simultaneously.

Once the present theoretical work is validated, it can be used as an experimental method to calculate interfacial properties for a surfactant. Although the model might need modifications, the mathematical techniques are robust enough and can be extended to more complicated models of interfacial resistance or interfacial rheology.

An assumption that can be relaxed in the present analysis is the assumption of only radial oscillations of the bubble. The techniques developed in the present work can be used to study the gas transport problem associated with a bubble undergoing arbitrary oscillations. Such a theory would be capable of including the effects of acoustic streaming and large-amplitude shape oscillations on bubble growth rates.

References

- [1] R. E. Apfel. Acoustic cavitation prediction. *J. Acoust. Soc. Am.*, 69:1624–1633, 1981.
- [2] G. T. Barnes. The effects of monolayers on the evaporation of liquids. *Advances in Colloid and Interface Science*, 25:89–200, 1986.
- [3] R. B. Bird, W. E. Steward, and E. N. Lightfoot. *Transport phenomena*. John Wiley & Sons, 1960.
- [4] F. G. Blake. *The onset of cavitation in liquids. I. Cavitation threshold sound pressures in water as a function of temperature and hydrostatic pressure*. Harvard University Acoustic Research Laboratory Technical Memorandum, 1949.
- [5] R. P. Borwankar and D. T. Wasan. The kinetics of adsorption of surface active agents at gas-liquid surfaces. *Chem. Eng. Science*, 25:1637–1649, 1983.
- [6] R. P. Borwankar and D. T. Wasan. Effects of surfactants on interphase solute transport. a theory of interfacial resistance. *Ind. Eng. Chem. Fundam.*, 25:662–668, 1986.
- [7] H. Brenner and L. G. Leal. Conservation and constitutive equations for adsorbed species undergoing surface diffusion and convection at a fluid-fluid interface. *J. Coll. Int. Sci.*, 88:136–184, 1982.
- [8] J.A. Caskey and W.B. Barlage. An improved experimental technique for determining dynamic surface tension of water and surfactant solutions. *J. Coll. Int. Sci.*, 35:46–52, 1971.
- [9] J.A. Caskey and W.B. Barlage. A study of the effects of soluble surfactants on gas absorption using liquid laminar jets. *J. Coll. Int. Sci.*, 41:52–62, 1972.
- [10] C. C. Church. Prediction of rectified diffusion during nonlinear bubble pulsations at biomedical frequencies. *J. Acoust. Soc. Am.*, 83:2210–2217, 1988.
- [11] L. A. Crum. Measurements of the growth of air bubbles by rectified diffusion. *J. Acoust. Soc. Am.*, 68:203–211, 1980.
- [12] L. A. Crum. Acoustic cavitation series part five - rectified diffusion. *Ultrasonics*, 22:215–223, 1984.
- [13] L. A. Crum and G. M. Hansen. Generalized equations for rectified diffusion. *J. Acoust. Soc. Am.*, 72:1586–1592, 1982.
- [14] L. A. Crum and G. M. Hansen. Growth of air bubbles in tissue by rectified diffusion. *Phys. Med. Biol.*, 27:413–417, 1982.

- [15] L. A. Crum and Y. Mao. Acoustically enhanced bubble growth at low frequencies and its implications for human diver and marine mammal safety. *J. Acoust. Soc. Am.*, submitted, 1995.
- [16] E. A. Doedel. *AUTO: software for continuation and bifurcation problems in ordinary differential equations, 1986*. Doedel, E. A., 1986.
- [17] D.A. Edwards, H. Brenner, and D.T. Wasan. *Interfacial transport processes and rheology*. Butterworth-Heinemann Series in Chemical Engineering, 1991.
- [18] A. Eller. Growth of bubbles by rectified diffusion. *J. Acoust. Soc. Am.*, 46:1246–1250, 1969.
- [19] A. Eller. Bubble growth by diffusion in an 11-khz sound field. *J. Acoust. Soc. Am.*, 52:1447–1449, 1972.
- [20] A. Eller and H. G. Flynn. Rectified diffusion during nonlinear pulsations of cavitation bubbles. *J. Acoust. Soc. Am.*, 37:493–503, 1965.
- [21] R. E. Emmert and R. L. Pigford. A study of gas absorption in falling liquid films. *Chem. Eng. Prog.*, 50:87–93, 1954.
- [22] A. Fannjiang and G. Papanicolaou. Convection enhanced diffusion for periodic flows. *S.I.A.M. J. Appl. Maths.*, 54:333–408, 1994.
- [23] G. L. Gaines. *Insoluble monolayers at liquid-gas interfaces*. Interscience Publishers, 1966.
- [24] D. F. Gaitan, L. A. Crum, C. C. Church, and R. A. Roy. Sonoluminescence and bubble dynamics for a single stable cavitation bubble. *J. Acoust. Soc. Am.*, 91:3166–3183, 1992.
- [25] G. M. Gottier, N. R. Amundson, and R. W. Flumerfelt. Transient dilation of bubbles and drops: theoretical basis for dynamic interfacial measurements. *J. Coll. Int. Sci.*, 114:106–130, 1986.
- [26] E. J. Hinch. *Perturbation methods*. Cambridge University Press, 1991.
- [27] D.-Y. Hsieh and M. S. Plesset. Theory of rectified diffusion of mass into gas bubbles. *J. Acoust. Soc. Am.*, 33:206–215, 1961.
- [28] D. O. Johnson and K. J. Stebe. Oscillating bubble tensiometry: A method for measuring the surfactant adsorptive-desorptive kinetics and the surface dilatational viscosity. *J. Colloid Interface Sci.*, 168:21–31, 1994.
- [29] P. Joos and M Van Uffelen. Adsorption kinetics with surface dilatation i. desorption of slightly soluble monolayers at constant surface pressure. *J. Colloid Interface Sci.*, 155:271–282, 1993.
- [30] V. Kamath and A. Prosperetti. Numerical integration methods in gas-bubble dynamics. *J. Acoust. Soc. Am.*, 85:1538–1548, 1989.
- [31] V. Kamath and A. Prosperetti. Mass transfer during bubble oscillations. *In Frontiers of nonlinear acoustics: proceedings of the Twelfth Intl. Symp. on Nonlinear Acoustics*, 12:503–508, 1990.

- [32] J. B. Keller and M. Miksis. Bubble oscillations of large amplitude. *J. Acoust. Soc. Am.*, 68:628–633, 1980.
- [33] J. P. Kundu. *Fluid mechanics*. Academic Press, 1990.
- [34] W. Lauterborn. Numerical investigation of nonlinear oscillations of gas bubbles in liquids. *J. Acoust. Soc. Am.*, 59:283–293, 1976.
- [35] L. G. Leal. *Laminar flow and convective transport processes: scaling principles and asymptotic analysis*. Butterworth-Heinemann, 1992.
- [36] P. A. Lewin and L. Bjørnø. Acoustic pressure amplitude thresholds for rectified diffusion in gaseous microbubbles in biological tissues. *J. Acoust. Soc. Am.*, 69:846–852, 1981.
- [37] A. Nadim. Effects of surfactants and interfacial rheology on bubble dynamics. *J. Fluid Mech.*, submitted, 1995.
- [38] F. B. Nagiev and N. S. Khabeev. Dynamics of soluble gas bubbles. *Izvestiya Akademii Nauk SSSR, Mekhanika Zhidkosti i Gaza*, 6:52–59, 1985.
- [39] L. A. Nguyen Ly, R. G. Carbonell, and B. J. McCoy. Diffusion of gases through surfactants films: Interfacial resistance to mass transfer. *AIChE J.*, 25:1015–1024, 1979.
- [40] M. S. Plesset and A. Prosperetti. Bubble dynamics and cavitation. *Ann. Rev. Fluid Mech.*, 9:145–185, 1977.
- [41] M. S. Plesset and S. A. Zwick. A nonsteady heat diffusion problem with spherical symmetry. *J. Appl. Phys.*, 23:95–98, 1952.
- [42] R. E. Plevan and J. A. Quinn. The effect of monomolecular films on the rate of gas absorption into a quiescent liquid. *AIChE J.*, 12:894–902, 1966.
- [43] A. Prosperetti. Acoustic cavitation series part two – bubble phenomena in sound fields: part one. *Ultrasonics*, 22:69–77, 1984.
- [44] A. Prosperetti. Personal communication. 1994.
- [45] Lord Rayleigh. *Phil. Mag.*, 34:94–, 1917.
- [46] L. A. Skinner. Pressure threshold for acoustic cavitation. *J. Acoust. Soc. Am.*, 47:327–331, 1970.
- [47] L. A. Skinner. Acoustically induced gas bubble growth. *J. Acoust. Soc. Am.*, 51:378–382, 1972.
- [48] P. Smereka, B. Birnir, and S. Banerjee. Regular and chaotic bubble oscillations in periodically driven pressure fields. *Phys. Fluids*, 30:3342–3350, 1987.
- [49] G. G. Stokes. On the effect of the internal friction of fluids on the motion of pendulums. *Trans. Camb. Phil. Soc.*, 9:8–106, 1951.
- [50] H.A. Stone. A simple derivation of the time-dependent convective-diffusion equation for the surfactant transport along a deforming interface. *Phys. Fluids A*, 2:111–112, 1990.

- [51] A. J. Szeri and L. G. Leal. The onset of chaotic oscillations and rapid growth of a spherical bubble at subcritical conditions in an incompressible liquid. *Phys. Fluids A*, 3:551–555, 1991.
- [52] M. Valenti. Taming Hansford’s most troublesome nuclear waste tank. *Mechanical Engineering*, 115:68–72, 1993.
- [53] M Van Uffelen and P. Joos. Adsorption kinetics with surface dilatation ii. the steady state dynamic surface tension by compressing an adsorbed soluble monolayer with constant dilatation rate. *J. Colloid Interface Sci.*, 158:452–459, 1993.
- [54] F. Van Voorst Vader, Th. F. Erkelens, and M. Van Den Tempel. Measurements of dilatational surface properties. *Trans. Faraday Soc*, 60:1170–1177, 1964.
- [55] S. Whitaker and R. L. Pigford. Response of a gas-liquid interface to concentration pulses. *AIChE J.*, 3:741–746, 1966.

Appendix A

Transients in the oscillatory problem

Eller & Flynn [20] work out the details of the transient solution to the oscillatory problem (2.16) for the concentration field given any boundary condition at $s = 0$.

$$C_{osc}^0 = \frac{s}{2\pi^{1/2}} \int_0^{\hat{\tau}} \frac{1}{\theta^{3/2}} \exp\left(-\frac{s^2}{4\theta}\right) C_{osc}^0(s=0, \hat{\tau} - \theta) d\theta, \quad (\text{A.1})$$

as an initial step in their analysis. As we have reported, the mass transport associated with the oscillatory problem is zero, after the decay of initial transients. This observation leads naturally to the question, how quickly does the mass transport associated with the transient solution of the oscillatory problem go to zero?

In order to answer this question, we compute the mass transport obtained from the transient solution (A.1). After some manipulation we find

$$m_{G_{osc}}^*(\hat{\tau}) - m_{G_{osc}}^*(0) = -\frac{3}{\mathcal{P}^{1/2}} \int_0^{\hat{\tau}} \frac{C_{osc}^0(s=0, \hat{\tau} - \theta)}{(\theta\pi)^{1/2}} d\theta.$$

Next we make use of the Fourier expansion of the boundary condition (2.17), to obtain the change in bubble mass due to the transient part of the oscillatory problem

$$m_{G_{osc}}^*(\hat{\tau}) - m_{G_{osc}}^*(0) = \frac{3}{\mathcal{P}^{1/2}} \sum_{m=1}^{\infty} \left(\frac{2}{\omega_m}\right)^{1/2} \times \\ \left\{ \left(b_m \text{S} \left[\left(\frac{2 \omega_m \hat{\tau}}{\pi} \right)^{1/2} \right] - a_m \text{C} \left[\left(\frac{2 \omega_m \hat{\tau}}{\pi} \right)^{1/2} \right] \right) \cos [\omega_m \hat{\tau}] - \right. \\ \left. \left(a_m \text{S} \left[\left(\frac{2 \omega_m \hat{\tau}}{\pi} \right)^{1/2} \right] + b_m \text{C} \left[\left(\frac{2 \omega_m \hat{\tau}}{\pi} \right)^{1/2} \right] \right) \sin [\omega_m \hat{\tau}] \right\},$$

where $\text{S}[x]$ and $\text{C}[x]$ are the sine and cosine Fresnel integrals respectively. These functions reach their asymptotic values of $1/2$ in a few periods of the bubble oscillation. Thereafter each term in the Fourier expansion corresponds to an oscillation with zero mean. We

conclude that the oscillatory problem contributes very little to the transport across the bubble surface, and then only in the first few periods of oscillation.

Appendix B

Transients in the smooth problem

We were able to determine in section 2.3 the asymptotic concentration field associated with the smooth problem for any nonlinear periodic bubble oscillation. In order to determine the behavior at finite λ , it is necessary to make an additional assumption so as to obtain a tractable problem. Equation (2.22) simplifies if we make a supposition regarding the size of volume oscillations. The analysis that follows in this section is therefore further restricted to small oscillations about the mean volume.

Under this assumption, the volume of the bubble, which is proportional to $x^3(\tau)$, can be split into a mean and an oscillating part

$$x^3(\tau) \equiv V_0 + \Delta(\tau), \quad V_0 = \langle x^3(\tau) \rangle_\tau, \quad \langle \Delta(\tau) \rangle_\tau = 0, \quad |\Delta(\tau)| \ll 1.$$

Using the binomial theorem, the average within (2.14) may be expanded to yield

$$\begin{aligned} \left\langle \left(3\sigma + x^3(\tau) \right)^{(4/3)} \right\rangle_\tau = \\ (3\sigma + V_0)^{(4/3)} \left(1 + \frac{\frac{4}{3} \left(\frac{4}{3} - 1 \right)}{2!} \frac{\langle \Delta^2(\tau) \rangle_\tau}{(3\sigma + V_0)^2} + \frac{\frac{4}{3} \left(\frac{4}{3} - 1 \right) \left(\frac{4}{3} - 2 \right)}{3!} \frac{\langle \Delta^3(\tau) \rangle_\tau}{(3\sigma + V_0)^3} + \dots \right). \end{aligned}$$

The mean values of the various powers of $\Delta(\tau)$ are identified as the central moments. The first central moment, of course, is zero. For an arbitrary nonlinear bubble oscillation, it is impossible to know *a priori* which of the central moments is most significant. We will therefore combine the remaining terms of the expansion into a single function,

$$\delta f(\sigma) \equiv \frac{\frac{4}{3} \left(\frac{4}{3} - 1 \right)}{2!} \frac{\langle \Delta^2(\tau) \rangle_\tau}{(3\sigma + V_0)^2} + \frac{\frac{4}{3} \left(\frac{4}{3} - 1 \right) \left(\frac{4}{3} - 2 \right)}{3!} \frac{\langle \Delta^3(\tau) \rangle_\tau}{(3\sigma + V_0)^3} + \dots,$$

where δ is a small parameter associated with the bubble oscillation defined by the latter equation and $f(0) = 1$. Furthermore, (2.14) can be brought to a well known form by the

variable transformation

$$\begin{aligned} C_{sm}^0(\sigma, \lambda) &= \frac{n(\sigma, \lambda)}{(3\sigma + V_0)^{(1/3)}} = \frac{n(\sigma, \lambda)}{z + V_0^{(1/3)}}, \\ z &= (3\sigma + V_0)^{(1/3)} - V_0^{(1/3)}. \end{aligned}$$

This transformation leads to

$$\frac{\partial n}{\partial \lambda} = \frac{\partial^2 n}{\partial z^2} + \frac{\delta}{z + V_0^{(1/3)}} \frac{\partial}{\partial z} \left[f(z) \left((z + V_0^{(1/3)}) \frac{\partial n}{\partial z} - n \right) \right],$$

with boundary and initial conditions

$$\begin{aligned} n(z = 0, \lambda) &= V_0^{(1/3)} [C_{sb} \langle p_G^*(\tau) \rangle_{\hat{\tau}} - C_\infty], \\ n(z, \lambda = 0) &= n(z \rightarrow \infty, \lambda) = 0. \end{aligned}$$

This equation may be solved using a regular perturbation in the small parameter δ , of the form

$$n(z, \lambda) = n^0(z, \lambda) + \delta n^1(z, \lambda) + \dots$$

The zeroth order problem is given by

$$\begin{aligned} \frac{\partial n^0}{\partial \lambda} &= \frac{\partial^2 n^0}{\partial z^2} \\ n^0(z = 0, \lambda) &= V_0^{(1/3)} [C_{sb} \langle p_G^*(\tau) \rangle_{\hat{\tau}} - C_\infty], \\ n^0(z, \lambda = 0) &= n^0(z \rightarrow \infty, \lambda) = 0, \end{aligned}$$

and can be solved by Laplace transforms in λ , to yield

$$n^0 = V_0^{(1/3)} [C_{sb} \langle p_G^*(\tau) \rangle_{\hat{\tau}} - C_\infty] \operatorname{erfc} \left[\frac{z}{2\lambda^{(1/2)}} \right].$$

The associated mass transport is

$$\frac{dm_{G_{sm}}^*(\lambda)}{d\lambda} = -3 \langle x^4(\tau) \rangle_\tau V_0^{(1/3)} [C_{sb} \langle p_G^*(\tau) \rangle_{\hat{\tau}} - C_\infty] \left[\frac{1}{V_0(\pi\lambda)^{(1/2)}} + \frac{1}{V_0^{(4/3)}} \right],$$

and for the numerically computed bubble oscillations reported above, we found that the asymptotic form (2.24) is reached by $\lambda \approx 10$.

Appendix C

Comparison between non-polytropic and polytropic bubble models

Finally, we turn to the influence of the bubble dynamical model itself on threshold pressure amplitudes and bubble growth rates one calculates for nonlinear bubble oscillations. The vast majority of studies of rectified diffusion have made use of a polytropic expression for the bubble internal pressure. There is one exception of which we are aware –the numerical study of Kamath & Prosperetti [31]. In the results we presented above, we made use of the non-polytropic expression for the bubble internal pressure due to Kamath & Prosperetti [30]. As we show in what follows, the primary difference in the results for the polytropic model is a large increase in the effect of resonance. It appears that resonances are of lesser importance in the non-polytropic model owing to the greater care with which the model accounts for thermal dissipation of energy.

To see this, we shall recreate figures 2.4 and 2.6, and an expanded version of figure 2.7, but with a polytropic bubble model for the purposes of comparison. We choose here to use a modification due to Prosperetti [43] of the formulation of Keller & Miksis [32]. This formulation accounts for compressibility of the liquid; for thermal, viscous and radiation damping; and makes use of the theoretically estimated polytropic exponent (η) of Prosperetti [43]. The formulation compares well with more sophisticated models in a recent careful study by Gaitan, *et al.* [24].

The governing equations for the bubble sub-system are the same as in the non-polytropic case. The dimensionless bubble internal pressure however, is assumed to have

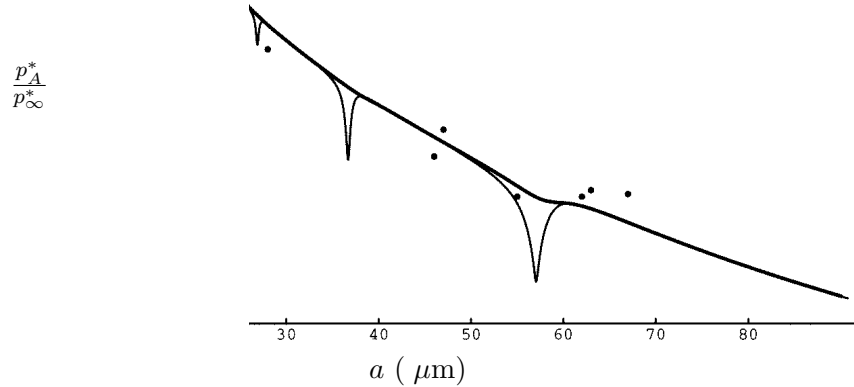


Figure C.1: A plot of the ratio of the threshold pressure amplitude for rectified diffusion to the steady part of the background pressure versus equilibrium bubble radius. This is a comparison between the non-polytropic bubble model (heavy curve) and a polytropic bubble model (fine curve). The heavy curve corresponds to the dashed curve of figure 2.4. The bubbles are driven at a frequency of 26.6 kHz, the liquid saturation is 101.5 % and the interfacial tension is 73 dynes cm^{-1} .

the following form

$$p_G^*(\tau) = \frac{1}{x^{3\eta}(\tau)},$$

which provides an alternative for the energy equation.

Continuation is again used as the basic technique for developing numerical solutions to the bubble dynamical equations, and for testing the threshold criterion. In figure C.1, we show the threshold curves corresponding to the two bubble models for the previously examined case of figure 2.4. The threshold curves in figure C.1 are comparable over the majority of the range in a . However, there are several dips in the fine curve corresponding to the polytropic bubble model. These are dips of variable magnitude, at which the threshold pressure decreases rapidly, and then rises again to nearly the same magnitude. The dips correspond to particularly efficient forcing of the (polytropic) bubble dynamics that occurs near a resonance between some natural frequency of the bubble and the forcing frequency. If one examines, for example, the maximum bubble radius over a period of oscillation versus

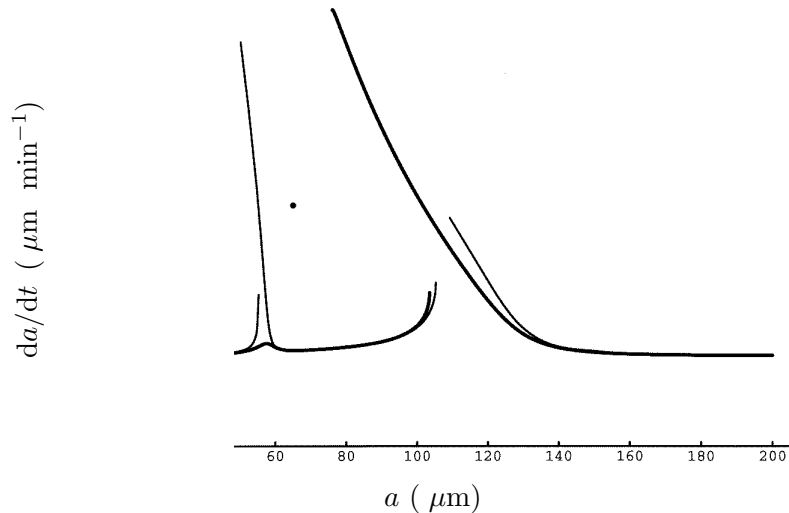


Figure C.2: The rate of bubble growth in μm per minute versus equilibrium bubble radius in μm . This is a comparison between the non-polytropic bubble model (heavy curve) and a polytropic bubble model (fine curve). The bubbles are forced at a pressure amplitude of 0.2 bar. The curves correspond to (2.26), the points correspond to the experimental data of Eller [18]. The diffusivity of the gas in the liquid is $2.0 \times 10^{-5} \text{ cm}^2 \text{ sec}^{-1}$. The bubbles are driven at a frequency of 26.6 kHz, and the interfacial tension is 73 dynes cm^{-1} .

the equilibrium bubble radius, then one observes clearly a jump in maximum bubble radius near these resonant dips in the polytropic bubble model. Clearly, while still present, the effects of resonances in the non-polytropic bubble model are much less.

A second example of the exaggerated importance ascribed to resonance in the polytropic bubble model can be seen in figure C.2. Again we see various large jumps in bubble growth rate, which correspond to resonances of the system by comparison of figures C.2 and C.3. Where the fine curve in figure C.2 is broken, the corresponding bubble oscillation is unstable, as determined by the moduli of the associated eigenvalues of the Poincaré map, computed by AUTO. The non-polytropic bubble model displays only a weak bump at resonance. It is clear that the more sophisticated bubble model would seem to eliminate unusual bubble growth rates near resonances as an explanation of the failure of the theory as it now stands to explain the disagreement of experimental results.

As a third example of the very different behavior of the two bubble models near resonance, we show a bifurcation diagram in figure C.3 which is essentially a reproduction

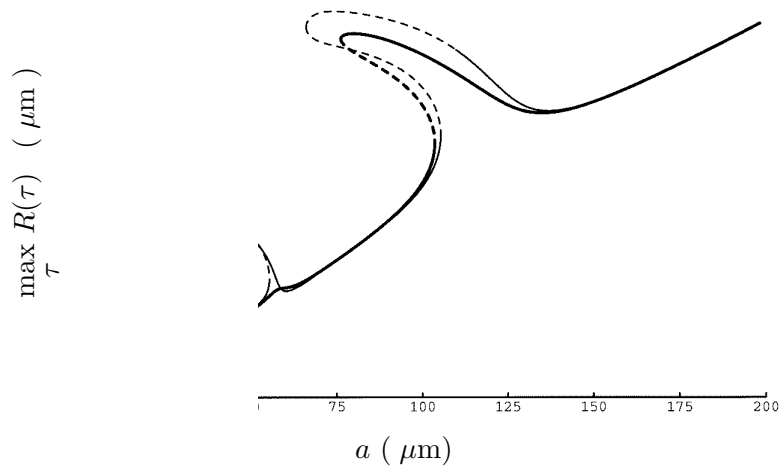


Figure C.3: An expanded view of the bifurcation diagram of figure 2.7. This is a comparison between the non-polytropic bubble model (heavy curve) and a polytropic bubble model (fine curve). On the vertical axis, as a measure of the solution, we take the maximum bubble radius in μm over the period of oscillation. On the horizontal axis is the equilibrium bubble radius. The solid curves indicate stable bubble oscillations; unstable parts of the branch are shown as dashed curves. The bubbles are driven at a frequency of 26.6 kHz, the liquid is saturated and the interfacial tension is 73 dynes cm^{-1} .

of figure 2.7 over a broader parameter range. Note that where there are multiple periodic solutions at the same parameter value, the maxima in the curves $R(\tau)$ (which are taken as the measures of the solutions) may occur at different τ . Where the curve is dashed, the corresponding bubble oscillation is unstable; where it is solid, the bubble oscillation is stable. Although it is not possible to see in figure C.3, there are two small folds for the polytropic response (fine curve) near 27 and $36 \mu\text{m}$, where the branch which comes from the left has a limit point where it reverses direction and becomes unstable, followed very quickly by another limit point where the branch again becomes stable. Hence there is a tiny range of parameters near 27 and $36 \mu\text{m}$ where there are multiple stable attracting periodic bubble oscillations for the same forcing pressure amplitude in the polytropic model. Moreover, both stable branches can be reached by exploiting hysteresis in the standard way.

These remarks are perhaps more clear when one looks at the region around $52 \mu\text{m}$ on the polytropic branch. There is an obvious limit point at $55.3 \mu\text{m}$ where the polytropic branch doubles back and becomes unstable. Following this unstable portion of the

branch, the solution develops very deep cusps that become increasingly difficult to compute. However, AUTO is able to track the cusps and follow the solutions. Continuing on the same branch, there is a bifurcation to an invariant torus (*i.e.* a secondary Hopf bifurcation of the associated fixed point of the Poincaré map that corresponds to quasi-periodic motion), where the periodic branch for the polytropic model becomes stable again when the radius is $50.2 \mu\text{m}$. The important feature to which we wish to draw attention is the rather large overlap, where there are two stable attracting periodic bubble oscillations for the polytropic model. Similar features were described by Lauterborn [34], although his method of integrating through the transients makes it impossible to find unstable solutions or to determine bifurcations or to deduce the overall structure of the solution set. Either attractor may be reached by continuation from below or from above; hence there is hysteresis. Because the two attractors for the polytropic model in the parameter range $50.2\text{-}55.3 \mu\text{m}$ are characterized by bubble oscillations of different shape and magnitude, the growth rates of bubbles following these two attractors are different (figure C.2). In stark contrast, the corresponding resonance in the non-polytropic bubble model appears in the response curve as a small bump.

Finally, in figure C.3, note the large fold that occurs near $105 \mu\text{m}$ in both the polytropic and non-polytropic bubble models. The oscillations are unstable on the reversed part of the branches. In the non-polytropic model (heavy curve), the oscillations stabilize after a second limit point. In the polytropic model (fine curve), the oscillations stabilize after a bifurcation to an invariant torus near $110 \mu\text{m}$. For the polytropic model, this largest fold is similar to the one near $50 \mu\text{m}$, except that instead of a set of equilibrium bubble radii with multiple attracting periodic bubble oscillations, there is now a window of equilibrium bubble radii with no attracting periodic bubble oscillation. The dynamics in this window are most likely characterized by a quasi-periodic attractor corresponding to the invariant torus. Alternately, the dynamics may be chaotic. In either case, we did not pursue intense study of the oscillations of larger bubbles, as Crum [11] has reported that such bubbles are susceptible to visible surface waves upon excitation by the acoustic sound field; this behavior violates the assumption of spherically symmetric motion we made at the outset.

In addition, we note that the amplitude coefficients of the Galerkin expansion of the non-polytropic model decay only slowly for a greater than about $100 \mu\text{m}$. This indicates that some skepticism is in order regarding the results in this parameter range. Increasing the Galerkin approximation to more than four terms would be appropriate for further study.

These comparisons indicate that great care must be taken in studies of rectified diffusion to use an appropriate bubble model, particularly near resonances of the bubble dynamical equations.

Appendix D

Splitting

In general the asymptotic solution to the oscillatory problem to any order $i = 1, 2, \dots$ (\bar{C}_{osc}^i) leads to the following partial differential equation

$$\frac{\partial C_{osc}^i}{\partial \hat{\tau}} - \frac{\partial^2 C_{osc}^i}{\partial s^2} = F^i \left(x(\hat{\tau}), s, C_{osc}^0, \dots, C_{osc}^{i-1} \right) \quad (\text{D.1})$$

with boundary condition

$$C_{osc}^i(s = 0, \hat{\tau}) = B^i \left(x(\hat{\tau}), C_{osc}^{i-1}(s = 0, \hat{\tau}) \right),$$

where F^i is the inhomogeneous term associated with the i th order oscillatory problem. In this appendix, we shall determine restrictions on the boundary conditions necessary for the outer limit of the inner approximation of the oscillatory solution to be zero. In other words, we need to verify that the boundary layer solution of the oscillatory problem decays to zero as $s \rightarrow \infty$.

The asymptotic solution \bar{C}_{osc}^i can be represented as a Fourier series of the form

$$\bar{C}_{osc}^i(s, \hat{\tau}) = \sum_{m=-\infty}^{\infty} c_m(s) \exp[\omega_m i \hat{\tau}],$$

where

$$\omega_m = \frac{2m\pi}{\hat{\tau}(T)}.$$

Similarly F^i and B^i can be expanded in a Fourier series with Fourier coefficients f_m and b_m respectively. This fact can be shown inductively for all $i \geq 0$ beginning from $i = 0$ and (2.18).

Next we substitute these complex Fourier expansions into (D.1); this substitution leads to the following system of ordinary differential equations for $m = -\infty$ to ∞ :

$$\frac{d^2 c_m(s)}{ds^2} - i\omega_m c_m(s) = -f_m(s) \quad (\text{D.2})$$

with boundary condition

$$c_m(s=0) = b_m. \quad (\text{D.3})$$

The general solution of equation (D.2) which is zero as $s \rightarrow \infty$ is

$$c_m(s) = A_m \exp \left[- \left(\frac{\omega_m}{2} \right)^{1/2} s \right] \exp \left[-i \left(\frac{\omega_m}{2} \right)^{1/2} s \right] - \frac{1}{(1+i)(\omega_m/2)^{1/2}} \int_s^\infty f_m(s') \sinh \left[(1+i) \left(\frac{\omega_m}{2} \right)^{1/2} (s-s') \right] ds'. \quad (\text{D.4})$$

Note the exponential decay for large s of $f_m(s')$ ameliorates the exponential growth of the sinh in the integrand. Finally, we use the boundary condition at $s=0$ (D.3) to obtain an expression for A_m :

$$A_m = b_m + \frac{1}{(1+i)(\omega_m/2)^{1/2}} \int_0^\infty f_m(s') \sinh \left[-(1+i) \left(\frac{\omega_m}{2} \right)^{1/2} s' \right] ds'. \quad (\text{D.5})$$

Equations (D.4,D.5) give the expression for the Fourier coefficients of the asymptotic oscillatory problem to any order.

The differential equation for $m=0$, however, is somewhat different in view of $\omega_0=0$:

$$\frac{d^2 c_0(s)}{ds^2} = -f_0(s)$$

with boundary condition

$$c_0(s=0) = b_0.$$

The solution that is zero as $s \rightarrow \infty$ is

$$c_0(s) = \int_s^\infty \int_\infty^{s'} f_0(s'') ds'' ds'.$$

If we try to implement the boundary condition at $s=0$ we get

$$b_0 = \int_0^\infty \int_\infty^{s'} f_0(s'') ds'' ds'.$$

In other words the inhomogeneous term of the $m=0$ equation restricts the boundary condition that can be satisfied in order to have a solution of the oscillatory problem which differs from zero only near the bubble. Recognizing that b_0 and f_0 are just the averages (with respect to $\hat{\tau}$) of the boundary condition and the inhomogeneous term, we have developed the following condition, which actually defines the splitting

$$\langle C_{osc}^i(s=0, \hat{\tau}) \rangle_{\hat{\tau}} = \int_0^\infty \int_\infty^{s'} \langle F^i(s'') \rangle_{\hat{\tau}} ds'' ds'. \quad (\text{D.6})$$

Appendix E

Expansions for G and Ψ_e

Expanding N in successive powers of $\mathcal{P}_f^{-1/2}$, *i.e.*

$$N = N^0 + \frac{1}{\mathcal{P}_f^{1/2}} N^1 + \mathcal{O}(\mathcal{P}_f^{-1})$$

leads to the following expressions for G and Ψ_e to zeroth order

$$G^0(\hat{\tau}) = \frac{x^4 \exp\left[-\frac{AN^{02}}{x^4}\right]}{k(x^2 - N^0)}$$

$$\Psi_e^0(\hat{\tau}) = \frac{N^0 \exp\left[-\frac{AN^0}{x^2(\hat{\tau})}\right]}{A_f(x^2(\hat{\tau}) - N^0)} - \Psi_\infty,$$

respectively. Higher-order terms are not required explicitly in the present analysis.

In section 4.2, when treating the zeroth order oscillatory and smooth problems, the term involving G^0 appears divided $\mathcal{P}_f^{1/2}$ and \mathcal{P}_f respectively, and was dropped because it is of higher order. However, a more careful treatment is required because the expression for G^0 has $(x^2 - N^0)$ on the denominator. This term, which is proportional to $(1 - \Psi^s)$, is very close to zero when the surface concentration is close to saturation, and can be omitted provided that

$$(x^2(\tau) - N^0(\lambda)) \gg \mathcal{P}_f^{-1/2}.$$

This condition can be expressed more precisely using the asymptotic value of N^0 and the fact that the value of \bar{N}^0 is always less than the square of the minimum bubble radius (x_{min}^2):

$$x_{min}^2 - \bar{N}^0 \gg \mathcal{P}_f^{-1/2}.$$

For a given a bubble oscillation, use of figure 4.1 can give us an idea of the maximum value of $A_f\Psi_\infty$ so that this condition is satisfied.